

HIGH FREQUENCY PULSED ELECTROMIGRATION

By

DAVID WAYNE MALONE

A DISSERTATION PRESENTED TO THE GRADUATE SCHOOL  
OF THE UNIVERSITY OF FLORIDA IN PARTIAL FULFILLMENT  
OF THE REQUIREMENTS FOR THE DEGREE OF  
DOCTOR OF PHILOSOPHY

UNIVERSITY OF FLORIDA

1997

## ACKNOWLEDGMENTS

First and foremost, I must thank my wife, Ming Rong. I have relied upon her support and sacrifice above all else over the past four years, while our family life has been on hold. Together with our daughter, Lili, we can finally proceed.

I thank my mother, Judy, and my father, Wayne, for their endless support. It was my fortune to have, in addition to great parents, a father who is an expert in rf design. His help in the design and construction of the electromigration test apparatus was invaluable, as was the generosity of Skydata, Inc.

Dr. Rolf Hummel has been a consistent source of confidence. It was my contact with him as an undergraduate that led to my return to the University of Florida for graduate work, and many of his philosophies will go with me after I leave. I thank him for his guidance and for his belief in me.

Funding for this work was provided by Motorola, Inc., through their Advanced Products Research and Development Laboratory at Austin, TX. I gratefully acknowledge their support. Several people at Motorola should be mentioned by name. At the top of the list is H. Kawasaki, who directed our relationship with Motorola. Test samples were provided by M. Fernandes, C. Lee, M. Gall, and R. Hernandez. R. Hernandez also performed SEM work.

Finally, I acknowledge Drs. R. T. DeHoff, R. M. Park, R. K. Singh, and T. J. Anderson for their service on my faculty committee.

## TABLE OF CONTENTS

ACKNOWLEDGMENTS .....	ii
ABSTRACT .....	v
INTRODUCTION .....	1
Overview .....	1
The Integrated Circuit and Electromigration .....	4
Motivation .....	11
BACKGROUND .....	13
Foundations .....	13
Groundwork and Prior Research .....	34
Modern Implications .....	60
Pulsed Electromigration .....	61
Summary .....	77
SETUP AND PROCEDURE .....	79
Overview .....	79
Test Apparatus Performance Goals .....	79
Design Issues .....	81
Summary of Test Apparatus .....	84
Test Stripes .....	88
Test Procedure .....	90
Data Gathering and Analysis .....	90
Test Conditions .....	92
RESULTS AND DISCUSSION .....	94
Overview .....	94
Resistance Plots and Optical Micrographs .....	95
Lifetime Data .....	126
Relationships Between Lifetime, Pulse Frequency and Duty Cycle ..	147
Further Discussion .....	157
SUMMARY AND CONCLUSION .....	165

SUGGESTIONS FOR FUTURE WORK .....	169
APPENDIX .....	171
Test Apparatus .....	171
Further Discussion of Design and Procedure .....	183
REFERENCES .....	186
BIOGRAPHICAL SKETCH .....	194

Abstract of Dissertation Presented to the Graduate School  
of the University of Florida in Partial Fulfillment of the  
Requirements for the Degree of Doctor of Philosophy

## HIGH FREQUENCY PULSED ELECTROMIGRATION

By

DAVID WAYNE MALONE

May, 1997

Chairman: Dr. Rolf E. Hummel

Major Department: Materials Science and Engineering

Electromigration life tests were performed on copper-alloyed aluminum test structures that were representative of modern CMOS metallization schemes, complete with Ti/TiN cladding layers and a tungsten-plug contact at the cathode. A total of 18 electrical stress treatments were applied. One was a DC current of 15 mA. The other 17 were pulsed currents, varied according to duty cycle and frequency. The pulse amplitude was 15 mA ( $\sim 2.7 \times 10^6 \text{ A/cm}^2$ ) for all treatments. Duty cycles ranged from 33.3% to 80%, and frequencies fell into three rough ranges – 100 KHz, 1 MHz, and 100 MHz. The ambient test temperature was 200 °C in all experiments. Six to 9 samples were subjected to each treatment.

Experimental data were gathered in the form of test stripe resistance versus time,  $R(t)$ . For purposes of lifetime analysis, "failure" was defined by the criterion  $R(t)/R(0) = 1.10$ , and the median time to failure,  $t_{50}$ , was used as the primary basis of comparison between test groups.

It was found that the dependence of  $t_{50}$  on pulse duty cycle conformed rather well to the so-called "average current density model" for duty cycles of 50% and higher. Lifetimes were less enhanced for a duty cycle of 33.3%, but they were still considerably longer than an "on-time" model would predict. No specific dependence of  $t_{50}$  on pulse frequency was revealed by the data, that is, reasonably good predictions of  $t_{50}$  could be made by recognizing the dominant influence of duty cycle.

These findings confirm that IC miniaturization can be more aggressively pursued than an on-time prediction would allow. It is significant that this was found to be true for frequencies on the order of 100 MHz, where many present day digital applications operate.

Post-test optical micrographs were obtained for each test subject in order to determine the location of electromigration damage. The pulse duty cycle was found to influence the location. Most damage occurred at the cathode contact, regardless of treatment conditions, but there was an increased incidence of damage farther downwind with decreasing duty cycle. This tendency and the deviation from the average current density model for small duty cycles were explained in terms of the Blech length, its dependence on microstructure and duty cycle, and its impact on the relative rates of damage and recovery.

## INTRODUCTION

### Overview

Electromigration, a process whereby an electric current “erodes” the conductor that carries it, is commonly recognized as a failure mechanism in integrated circuits. The on-chip interconnections of an integrated circuit are particularly vulnerable to such a process because they are microscopic in size, and failure occurs if one of them becomes excessively resistive or discontinuous at some point because of localized thinning or voiding. Although it was not immediately identified as electromigration, this mode of failure was discovered shortly after the inception of the integrated circuit (IC) in the early 1960s, and it has continued to be a reliability issue with IC manufacturers ever since.

Recent interest in electromigration research is closely related to the incessant drive to place more circuit functions on a chip. This drive, which seeks to increase device packing densities, has been carried out largely by reducing the sizes of circuit features. For example, it has been a common practice to reduce the widths of interconnections whenever process technologies allow it. Such practice often endangers reliability, though, because when the widths of interconnections are scaled down, it is not always possible to scale the current down in proportion. Those interconnections must then carry a larger amount of current per unit of interconnect cross section, that is, they must carry a larger

current density. Electromigration is then more likely. Future battles with electromigration are likely to be a by-product of IC miniaturization.

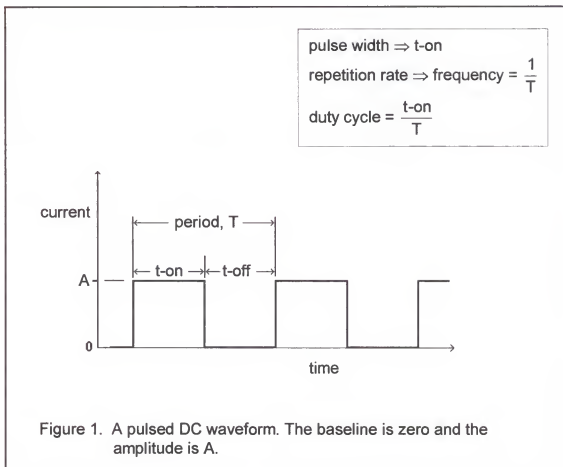
In practice, the ability of a particular IC interconnect structure to resist electromigration is predicted by performing experiments on specially prepared test structures. A group of test structures is subjected to some steady DC current, and the temperature is elevated in order to accelerate the damage process. Some measure of electromigration damage is monitored and is reported for all appropriate variations of conditions.

The traditional reliability test employs a steady DC current as the primary treatment variable. It is important, however, to realize that a steady DC current may not be particularly relevant. Many of the interconnections on a typical integrated circuit might, in actual operation, carry pulsed currents, alternating currents, or other less destructive current waveforms. The reliability of these interconnections will be underestimated if no adjustment is made to the DC test or its interpretation. This is acceptable if the prediction falls within specifications anyway, but if it does not, the true reliability of these interconnections must be further investigated.

Such an investigation is the subject of this dissertation, which reports work directed specifically toward pulsed DC current. Figure 1 provides an illustration of a pulsed current waveform. The features of interest -- pulse width, repetition rate, and duty cycle -- are defined in the figure. The goal was to determine how interconnect degradation and reliability depend on pulse width and repetition rate or, equivalently, on frequency and duty cycle. Emphasis was placed on



high and very high frequencies, which have received less attention from other workers, despite their practical significance to modern applications.



Although it might be a reasonable first guess, it is generally not true, for a given amplitude, that the rate of interconnect degradation is directly proportional to the duty cycle. The improvement in reliability with decreasing duty cycle is usually found to be larger than such a relation would predict. The reliability is said to be “enhanced” when the current is pulsed. The reason that the reliability is enhanced, and even more so, the degree to which the reliability should be enhanced, are both matters of debate and play a central role in this work.

### The Integrated Circuit and Electromigration

An integrated circuit (IC) is that special type of electronic circuit commonly known as a "microchip." The computer chip is a familiar example. True to its name, an IC is, in fact, an electronic circuit that is consolidated (integrated) onto a thin substrate such that it appears to be a small piece (chip) of solid material. The circuitry on a chip is microscopic, a feat which is made possible by the thin film techniques that are used to fabricate it. Although it is this microscopic size that makes an IC such a marvel of computing power, it is also responsible for the vulnerability of an IC to the effects of electromigration.

The microscopic thin film "wires" that connect the components on a chip are usually called "interconnections" or "interconnects." Sometimes, the term "metallization" is used, not only in reference to the interconnections themselves, but also in reference to the process of fabricating them. Most interconnections are, in fact, made of metallic alloys or compounds, and any metal film that is deposited during the course of IC fabrication is likely done so for this purpose. Copper-alloyed aluminum is the predominant material used for interconnections, but other metals, primarily titanium and tungsten, serve important supplementary roles in most metallization schemes.

Electromigration can be viewed roughly as an electronic form of erosion, because it takes place when the current running through any particular part of a circuit is large enough to push atoms down the length of an interconnect. Just as wind blows sand from one portion of a beach and piles it up in other locations downwind, the flowing electrons that comprise an electric current may push

material away from some portions of an IC interconnect and pile it up in other regions "downwind." The rough nature of this analogy does not detract from the introductory picture that it provides, but it will need some clarification later.

Nonetheless, a segment of interconnect may be broken open at a spot upwind, where material is depleted by the current. Conduction is lost, and the result is failure of the circuit. Downwind accumulation of material can be a problem, as well. It often appears as a mound called a "hillock." Sometimes, when enough compression is built up downwind, material may be extruded out from the bulk of the interconnect, to form what is called an "extrusion" or a "whisker." If a hillock or whisker is large enough that it makes contact with an adjacent interconnect line, then the resulting electrical short will likely constitute a failure of the circuit.

A depiction of electromigration damage is presented in Figure 2. The figure depicts a conductor with a (-) terminal, a (+) terminal, and the resulting direction of electron flow. It could be taken to be an IC interconnect or a test structure. An electromigration-induced void is shown at the upwind end of the conducting strip, and hillocks are shown at the downwind end.

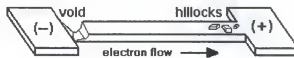


Figure 2. Electromigration-induced degradation of an interconnect.

Because of the analogy to erosion, and because the electric current is a flow of electrons, the force that causes electromigration is sometimes called the "electron wind" force. An electron wind force is present, and electromigration is possible, in any wire or material that is made to pass an electric current. For example, it has been observed in DC-powered light bulb filaments, and it has been observed in liquid metals. In fact, it is a potentially useful phenomenon for purifying metals. In the microelectronics industry, electromigration is a detriment to business, and its prevention has been an issue for about three decades.

Even though it is just one of many reliability issues associated with integrated circuits, electromigration is particularly relevant with regard to long term reliability. This "electronic erosion" process is normally quite slow, and it is usually noticed only after years of device operation. Electromigration failure cannot be screened-out by inspection or burn-in before delivery the way that some processing defects can. The only way to avoid electromigration-related failures in the field is to eliminate the occurrence of electromigration or to slow it down enough that its effects are not likely to be seen before the product is discarded. This effort starts with an understanding of why electromigration occurs and how its occurrence depends on the materials properties of a given interconnection and the conditions to which the interconnection is subjected. Research has placed special emphasis on the following variables:

1. Current density
2. Temperature
3. Chemical composition
4. Microstructure
5. Macrostructure

The first two of these variables, current density and temperature, are the conditions to which the interconnect may be subjected. They are the true "variables" per se. Since electric current is the erosive agent responsible for electromigration, it is certainly the critical variable. The rate of electromigration is expected to increase as the magnitude of the current density increases. The temperature should be important, as well, because it determines how vigorous the atomic vibrations are, and therefore how mobile the atoms are, in a solid. Higher temperatures should encourage faster migration rates.

The final three variables in the above list are chemical composition, microstructure, and macrostructure, which are those physical attributes of the interconnect that influence the manner and extent of atom migration, given some current density and temperature. The effort to produce reliable interconnects has been concentrated largely on these factors.

Chemical composition is important presumably because such properties as density, atomic weight, and bond strength determine how well the atoms of a material resist displacement from their positions. The more dense and strongly bound a material is, the more resistant one might expect it to be to disruption by the electron wind force.

The rate at which atoms are pushed by the electron wind should, it seems, be determined by the degree to which the given chemical composition can oppose the active influences of current density and temperature. This is essentially correct, but the rate of migration, by itself, does not determine the rate of damage. It was stated earlier that the electron wind damages an

interconnect by pushing material away from some regions upwind and by piling material up in other regions downwind. So, damage shows itself as localized depletions or accumulations of material. In order for material to be depleted from or accumulated at a particular location, there must be a discontinuity or divergence in the migration rate at that location. Such a divergence could be caused by a local variation of the current density or temperature. Even when the current density and temperature are uniform, however, rate divergences will certainly exist, because virtually all materials have a microstructure, which is the fourth variable in the above list.

The microstructure of a material is derived from such structural features as grain size, grain size distribution, and phase distribution, which affect the interior uniformity of a piece of material. If a microstructure contains some distribution of a second phase, for example, then it is not uniform chemically. Migration should proceed more readily in the less dense, less strongly bound phase than it does in the other, so long as the current density is uniform throughout. The resulting variation in migration rate from one phase to the next requires that material be depleted from or accumulated at the boundary between those differing regions. That boundary thus becomes a site of electromigration damage. Voids may be formed at boundaries where material is depleted, and hillocks or whiskers may be formed where material is accumulated. Another microstructural feature, the grain boundary, is not such an obvious example of chemical inhomogeneity as is a second phase, but it is chemically different from the interior of a grain. A grain boundary is less dense and less strongly bound. So, electromigration should

occur more readily in a grain boundary than it does within the grains that it separates. Localized depletion or accumulation is again the likely result. In practice, grain boundary migration is the primary mode of damage.

So, if an interconnect does not contain such microstructural nonuniformities as second phases or grain boundaries, no damage is expected, so long as the current density and temperature are uniform. According to this reasoning, no damage should occur within a single crystal interconnect, regardless of the migration rate. Of course, there must be an infinite source of atoms at the upwind end and an infinite sink at the downwind end in order to maintain the steady state migration over time.

Normally, an interconnect configuration provides neither an infinite upwind source of atoms nor an infinite downwind sink. This reality is related to the final item in the above list -- macrostructure. The macrostructure of an interconnect includes such factors as size and shape, as well as the composite structure and composition of the entire metallization scheme. For example, any interconnect, on both ends, will ultimately make contact to a dissimilar material, such as an electrode, or some kind of a splice along the way. There will always be at least two sites, then, at which the migration rate is discontinuous, even when the interconnect itself happens to be a single crystal.

The size and shape of an interconnect may also influence its susceptibility to electromigration damage. For example, a void of some given size should be more detrimental to a narrow, thin interconnect than it is to a wide, thick interconnect. This is just a statistical effect, but geometry can also influence

damage kinetics by affecting the uniformity of current density and temperature. For a given current, if the cross-sectional area is not uniform over the length of an interconnect, then the current density is not uniform, either. A divergence in current density produces a local divergence in migration rate. In addition, a nonuniform current density is likely to produce a local temperature gradient, which aggravates the rate divergence even further.

Studies of electromigration generally involve a systematic variation of some or all of these five variables, where each variation is applied to a small group of identical samples. Each sample is a specially designed test structure that is chemically and structurally similar to an actual segment of interconnect. Even though special considerations do go into the design of a test structure, it is usually not much more than a microscopic strip of metal built onto a chip. It is often called a "test stripe."

In order to monitor the electromigration behavior of a group of test stripes, some appropriate measure is needed. A commonly utilized *in situ* measure is electrical resistance. As material is redistributed during the course of electromigration, the electrical resistance of a given test stripe will probably change. If the stripe becomes thinner, or if it experiences localized depletions of material, the resistance will increase. If the stripe ultimately breaks completely open, then conduction is completely lost, and the resistance becomes infinite.

It has been mentioned that reliability tests must be accelerated by subjecting test stripes to current densities and temperatures that are higher than normal. The first order of business, then, in early work, was to determine the



dependence of electromigration on current density and temperature. A model was needed to extrapolate test results for application in the field. With such a model in hand, the other three variables -- chemical composition, microstructure, and macrostructure -- could be more easily evaluated, as well.

### Motivation

With the miniaturization afforded by recent IC metallization technologies, electromigration is increasingly a significant reliability issue. The emerging relevance of electromigration is mostly due to falling interconnection linewidths and the elimination of contact overlap, in conjunction with the continued use of aluminum-based interconnections. A key feature of present technologies, the tungsten-filled contact via, seems to be an open invitation to electromigration damage. Interconnect reliability is determined conclusively at this structural discontinuity by the ability of the aluminum-copper alloy to endure an electron wind. It seems advisable to avoid the use of such a structure, but the "tungsten plug" is a key to producing "ultra high" levels of integration. In addition, it is not possible to eliminate all similarly unfavorable structural features, anyway. A compositional discontinuity is always present at the end of an interconnect, whether that end is contacted to a tungsten plug or to a silicon device. This vulnerability is unavoidable, so the adoption of sufficiently robust interconnect materials is the surest way to minimize concerns about electromigration.

Industry is hesitant or unprepared to abandon copper-alloyed aluminum as the primary constituent of IC interconnections. It is not certain when this fact will

become the downfall of efforts for miniaturization, but significant ground may be gained in the meantime by ensuring that test models are as realistic as possible. Specifically, it is preferable to utilize electromigration models that are tailored for AC operation or pulsed DC operation whenever these more accurately represent true circuit conditions. With regard to pulsed DC applications, such an effort is based upon the dependence of interconnect reliability on pulse length and pulse repetition rate. The accurate determination of this dependence will give circuit engineers the opportunity to more fully utilize the limits of present metallization schemes. Given the limitation of aluminum-copper alloys, the need for such knowledge is great.

This study is most significant from a technological viewpoint, because the information that it reveals is particularly relevant for IC designers who need to predict the reliability of circuits that will carry pulsed currents. The practical need for such information has been discussed.

The dependence of the rate of electromigration damage on the pulse duty cycle and frequency is a reflection of the time-dependences of the associated diffusion processes. This is fundamentally a scientific consideration, but it is also inherently relevant in light of the computer industry's constant push for faster processing speeds. As such, the high frequency regime is of particular interest, but little work is reported in the literature for pulse frequencies greater than 1 MHz. These issues were motivation for the present work.

## BACKGROUND

### Foundations

An introduction to the integrated circuit and electromigration was presented in the previous chapter. The discussion included, in addition to basic introductory remarks, a rather complete qualitative description of the significant variables that determine electromigration behavior. Quantitative discussion is saved for later. Further, the motivation for this work was revealed by identifying the challenges associated with IC miniaturization and the resulting need for accurate models when assessing the reliability of circuits that will carry pulsed currents. Next is a discussion of the scientific basis for electromigration.

As a start to understanding why electromigration might occur in the first place, it is helpful to consider the process of electrical conduction. This is a reasonable starting point for revealing why electromigration is possible, and it provides a basis for speculating on the form of any fundamental model that might describe the process.

When an electric current is made to flow through a conductive material under the force of an applied voltage, the charge carriers of which the current is composed cannot avoid interaction with the atoms of the conducting material. This interaction causes some resistance to the flow of current, and the magnitude of the resistance determines the amount of current that can flow.

Electrical resistance can be viewed as a frictional force that opposes the motion of electrons as they try to accelerate through a metal conductor under the force of an applied voltage. At steady state, the accelerating force imposed by the voltage and the resistive frictional force are equal in magnitude and opposite in direction. There is no net acceleration of the conduction electrons as they appear to attain some uniform terminal velocity similar to the manner in which a skydiver reaches a terminal velocity when the force of the wind resistance becomes equal to the force of gravity. This analogy appears to be reasonable, but it works only when the electrons are viewed for their average motion. Taken individually, the motions of electrons within a conductor, even those participating in conduction, cannot be considered to be so uniform or so laminar as the motion of a skydiver. Any given free electron can be moving in any direction, and, according to the wave theory for electrons, the manner in which it interacts with nearby atoms depends, at any moment, on the instantaneous positioning and periodicity of those atoms. This much is true regardless of the external conditions to which the conducting material is subjected. The electrons and nearby atoms interact constantly in a random give and take fashion, and, at thermal equilibrium, there is no net velocity displayed by either component in the homogeneous system. The sum of all the individual electron velocities resolved in any given direction is balanced by an equal sum resolved in the opposite direction, so long as no voltage or other external force is imposed.

The effect of an applied voltage and the associated electrical force field is just to divert the path of some electrons very slightly toward the direction of the

electrical force. This diversion is very small compared to the otherwise random motions of electrons, but it represents, nonetheless, some net component of velocity directed down the conductor. This is the apparent terminal velocity mentioned earlier for steady state. The term "apparent" is used because this velocity consists only of the small drift component that is superimposed on the total electron velocity field, and, even though the magnitude of the drift velocity of any particular electron is actually several orders of magnitude smaller than its total speed, it is only the drift component that is observable. It is observed as an electric current, and it delivers the electron wind force.

The friction-like resistance is not so uniform on the atomic scale, either. It is associated not only with the simple physical impediment that the atoms of the conductor present by their presence in the path of electron flow, but also with the vibrational thermal energy that is distributed among the atoms. In fact, quantum theory says that the simple physical barrier that the atoms seem to present will not exist if the atoms remain stationary in a perfectly periodic arrangement. The fact that the atoms of a solid are not stationary, but rather vibrate about some equilibrium lattice position, in addition to the fact that they probably would not be perfectly periodic even if they were stationary, accounts for the failure of an electric current to flow unimpeded. The distribution of possible electron/atom interactions is determined by the temperature-dependent distribution of lattice vibrational energies.

Because of electrical resistance, then, a conduction electron cannot reach the same drift speed in a piece of matter as it can if it is accelerated through the

same voltage in a vacuum. This deficit in speed shows up as a quantity of energy dissipated among those interfering atoms that cause the deficit. That is, if atoms exert an interference force on conduction electrons, then it must be that those electrons exert a force on the atoms -- the electron wind force. The drift velocity represents a balance of these forces.

It is clear that the electron wind force delivers energy to the atoms of a conducting medium. In fact, it can deliver enough energy to heat the material considerably, even to its melting point. A more important consideration in the present context, however, is what happens when the current is not so large as to cause extreme heating, and the temperature is therefore far below the melting point. Can atoms be pushed down the conductor by the electron wind at normal circuit operating conditions? The answer is certainly "yes," but a consideration of some quantitative facts might lead one to initially doubt such a claim. For this purpose, consider the following quantities for an aluminum conductor, held at a temperature of 100 °C and carrying a current density of  $1 \times 10^6$  A/cm<sup>2</sup>:

- |   |                         |
|---|-------------------------|
| 1. Energy required to move an atom:             | ~ 0.2 to 1 eV           |
| 2. Thermal energy of an average atom:           | ~ 0.04 eV               |
| 3. "Wind" energy per electron/atom interaction: | < $1 \times 10^{-5}$ eV |

It does not seem that there is any chance for a conduction electron to push an aluminum atom to a new position in the crystal. The typical drift content of a conduction electron carries less than  $1 \times 10^{-5}$  eV of energy into an electron/atom interaction, and it takes about 0.2 eV to 1 eV to move an atom to an adjacent position, depending on the nature of that position.

So, how can electromigration occur? The answer lies in the knowledge that atoms already contain some quantity of thermal energy anyway, and they may migrate through bulk crystals quite readily by the process of diffusion. At first glance, this also appears to be questionable, because the average thermal energy per aluminum atom in this example is only about 0.04 eV. It is not the average atom, however, that moves by diffusion. The thermally induced vibrational energy in a crystal is distributed quite broadly among the atoms, and, although the average atom possesses an energy of only 0.04 eV, there is some fraction of atoms whose energy will equal or exceed 1 eV. So, this fraction, at any moment, can move to adjacent locations if those locations are vacant.

The primary requirements for an atom to move to a neighboring location within a piece of matter are that it obtain the appropriate energy and that there be a space for it there. Within the bulk of a crystal grain, such a space may be provided by a lattice vacancy. There is also space on free surfaces, interfaces, and boundaries between individual crystal grains. When the moving species is substantially smaller than the atoms of the host lattice, room may be available between regular lattice sites. There is always some quantity of vacant lattice sites, there is always some number of interfaces or free surfaces, and there is almost always an ample number of grain boundaries within a piece of matter. This is certainly true of the aluminum thin films of which integrated circuit interconnect is composed.

At normal temperatures, then, diffusion always occurs. Any given atom, or even more assuredly, any given vacancy, may move a considerable distance

through the lattice over time. This movement has no real effect on the apparent condition of a piece of material, however, if the material is homogeneous and there is no other influence, because for whatever direction and distance any particular atom migrates through a crystal, there will be, on average, another atom that migrates an equal distance in the opposite direction. Diffusion causes some net change in the arrangement of atoms only if there is some bias imposed on the apparent direction of the diffusive process. That is, there must be some so-called "driving force."

The most commonly treated driving force results from a concentration gradient, on which the traditional study of diffusion is based. For example, the science of diffusion and simple intuition will predict that if a piece of material is somehow made to have most of its vacancies located toward one of its ends at a given moment, then over time the vacancies will redistribute toward a more uniform arrangement. The influence that causes this rearrangement is not really a force in the physical sense, rather it is derived from the statistical bias associated with the vacancy concentration gradient that was set up. The end with most of the vacancies can "send" more vacancies to the other end than the other end can "give" back. So, the vacancy concentration tends to even out. The effect of the concentration gradient is equivalent to a driving force, so it is considered as such.

Other driving forces are commonly encountered as well. A temperature gradient provides a kind of directional bias in which atoms tend to move from hotter regions toward cooler regions. A stress gradient will assist migration



away from regions of compression and toward regions of tension. The driving force for electromigration is provided by the electron wind. It is important to stress, however, that none of these driving forces cause diffusion, they only impose a bias on the apparent direction of the basic diffusive process. They only influence the direction toward which the net change will occur. Diffusion is caused by "thermal activation." This distinction requires that the comparison made earlier between electromigration and erosion not be taken too literally.

The thermal content of a piece of material causes each of its atoms to vibrate about some average position, its lattice position, at a frequency between  $10^{12}$  and  $10^{13}$  per second. The period of a lattice vibration is thus  $10^{-13}$  to  $10^{-12}$  seconds, and the smallest moment during which a thermally induced event may occur is about this length of time. For example, an atom that hops from its lattice position to a vacant position next to it does so because it has gained sufficient kinetic energy to make such a hop, and it has gained that energy during a moment that is roughly  $10^{-13}$  to  $10^{-12}$  seconds long. Each successive interval of time of this approximate length provides a new chance for an atom to obtain the kinetic energy to engage in some process, such as lattice hopping or chemical reaction. Since it is this period of time during which an atom "attempts" to do something, the reciprocal of this time period is sometimes called the attempt frequency. In mathematical terms, the fraction of attempts that are successful is equivalent to the probability that any given attempt is successful. There is also an equivalence between probability and concentration. For example, the probability that some lattice position is vacant will be reflected directly by the

concentration of vacant lattice sites in the material. The terms "fraction," "concentration," and "probability" are interchangeable concepts.

A discussion of thermal activation can be attempted with reference to Figure 3. This figure is a two-dimensional depiction of several atoms in a close-packed arrangement. Atom A is chosen as a candidate to move to the adjacent vacant site of Figure 3(a). In order for this atom to move to the vacant site, it must push past the repulsion of the two shaded atoms and escape the attraction of the other three neighbors. The inherent thermal content of the material may, at some moment, randomly provide the required kinetic energy. If the atom, on some given attempt, gains just enough momentarily directed thermal energy that it just reaches the so-called "saddle point" halfway between its starting position and the vacant position, as depicted in Figure 3(b), it is said to be "thermally activated" for diffusion. The quantity of energy required for this activation is called the "activation energy." If this quantity of energy, this quantity exactly, is gained by the atom, so that it just reaches the saddle point, then it has a 50% chance of dropping back to where it was and a 50% chance of continuing

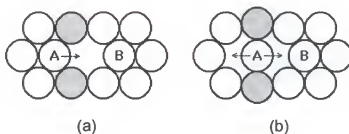
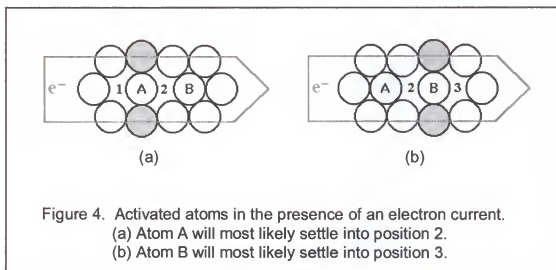


Figure 3. Activation of an atom for diffusion.  
 (a) Atoms surrounding a vacancy.  
 (b) Atom A is activated and sits at the saddle point.

forward into the originally vacant site if there is no other driving influence. The same type of consideration applies to atom B and all other atoms next to the vacancy if any happen to reach the activated state at any moment. With no other influence, the average vacancy has an equally good chance of exchanging positions with any one of its neighbor atoms as it does with any other.

When an electric current is passed through the material, there is another influence -- the electron wind. There is some chance that while an atom is in the saddle position a conduction electron will deliver a push. As small as this push is, the atom is nonetheless rendered more likely to move parallel to the electron flow than it is to move the opposite way. For example, the activated atom A in Figure 4(a) is biased slightly toward position 2. Likewise, the activated atom B in Figure 4(b) is biased toward position 3.



The activated atom is apparently the focus of directionally biased diffusive processes such as electromigration. In fact, it is the focus of the basic diffusion mechanism itself. This is so because an atom that receives more than the

activation energy as it approaches the saddle point will pass through that point and into the associated vacancy. An atom that receives less than the activation energy will drop back into its starting position. The activated state is the pivotal condition for an atom. This is true with or without an electron wind, but the electron wind influences the outcome.

The rate of electromigration (or any diffusive process) is thus related to the quantity of activated atoms at any moment, because this quantity determines how many pivotal candidates there are for migration at that moment. It is widely accepted that the fraction of atoms that possesses the energy required for activation is proportional to  $\exp(-E_a/kT)$ , where  $E_a$  is the activation energy,  $T$  is the temperature, and  $k$  is a constant known as Boltzmann's constant.

Implicit in the discussion so far has been the assumption that there is a vacancy adjacent to the candidate atom. For most atoms in the bulk, however, there is not a neighboring vacancy. An atom can be activated for diffusion only if it gains sufficient energy and there is room for it to move, so the concentration of vacancies is important in this analysis. This concentration is proportional to  $\exp(-H_v/kT)$ , where  $H_v$  is the enthalpy for the formation of a vacancy. The probability that an atom will gain sufficient energy for activation and have a neighboring vacancy is the product of the probabilities for each condition alone. This probability,  $r_A$ , thus follows the proportionality given by

$$r_A \propto \exp\left(\frac{-E_a}{kT}\right) \cdot \exp\left(\frac{-H_v}{kT}\right) \Rightarrow r_A \propto \exp\left[\frac{-(E_a + H_v)}{kT}\right]. \quad (1)$$

The quantity ( $E_a + H_v$ ) is usually given a new symbol,  $Q$ , which is taken as the activation energy for diffusion that accounts for both the energy requirement and the neighboring vacancy requirement. The rate at which atoms are activated for diffusion is thus proportional to  $\exp(-Q/kT)$ . The activation energy,  $Q$ , depends on the material.

With respect to electromigration, the rate of activation is just part of the story. Another part is related to the degree of directional bias, that is, the driving force, imposed by the electron wind. The probability that a conduction electron will interact with an atom while it is activated is expected to be proportional to the rate at which electrons are conducted past any given point in the material, which is equivalent to saying that this probability is proportional to the magnitude of the electric current. The rate of electromigration should then be proportional to the magnitude of the current for a specific piece of material and proportional to the amount of current per unit of cross-sectional area (the current density) in the general case.

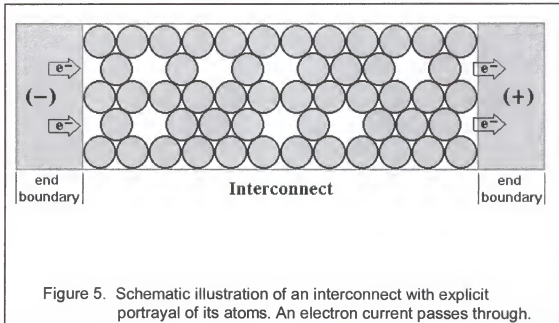
An expression that relates current density and temperature to the rate of electromigration can be proposed with the results of the preceding discussion. The probability that a particular atom will become activated for migration at a particular moment and will receive a push from a conduction electron while it is activated, is given by the product of the probabilities for each event alone. The probability of the former, as already mentioned, is proportional to  $\exp(-Q/kT)$ . The probability of the latter is proportional to the current density,  $j$ . So, the total

probability that an atom migrates by an electron wind-assisted mechanism,  $r_{em}$ , is given by the proportionality

$$r_{em} \propto j \cdot \exp\left(\frac{-Q}{kT}\right). \quad (2)$$

The rate of atomic migration should be directly proportional to  $r_{em}$ , so this expression is likely to be present, in some form, in any model that predicts the rate of electromigration as a function of temperature and current density.

Some basics about the electron wind force, diffusion, and how the two combine to create the phenomenon known as electromigration have now been addressed. The next step is to demonstrate how electromigration exhibits itself. Figure 5 depicts, in two dimensions, a close-packed arrangement of atoms that happens to be heavily concentrated with vacant lattice sites. It can be imagined, for the moment, that this is the top view of a nanosized, single-layered integrated circuit interconnection composed of only several atoms. A typical interconnect is

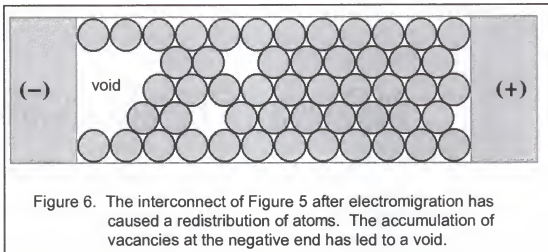


really about one micrometer wide, one micrometer thick, and many micrometers long, so this overly small picture is used only for demonstration.

The gray area on each end of the interconnect in Figure 5 can represent some kind of a terminal, such as a contact pad, a contact to a device, or a splice of some type. It may or may not be composed of the same material as the interconnect. The atoms are not explicitly depicted in these regions because the specific nature of the boundaries is left unknown for the moment. Various types of boundaries can be considered. The interconnect itself is assumed to be any good conductor. It is also indicated in the diagram that an electron current flows from the negative contact toward the positive contact. The figure represents an atom arrangement at time zero, when current has just been applied and no electromigration has yet taken place.

Electromigration damage, we know, is not caused so much by the atomic migration itself as it is by the presence of some nonuniformity or divergence in the rate of migration. If the rate of migration varies from one region to the next, then material will either be accumulated or depleted at a point between the two regions. This is what produces the observable damage. So, in the situation depicted by Figure 5, the electromigration behavior of the interconnect is dependent to a large extent on whether the end boundaries are good sources and/or sinks for atoms and vacancies. If they happen to be highly resistant to electron wind-induced migration, then they act neither as sources nor sinks. The interconnect can then be treated as an isolated entity, because its atoms and vacancies are confined to the area between the two boundaries. If the

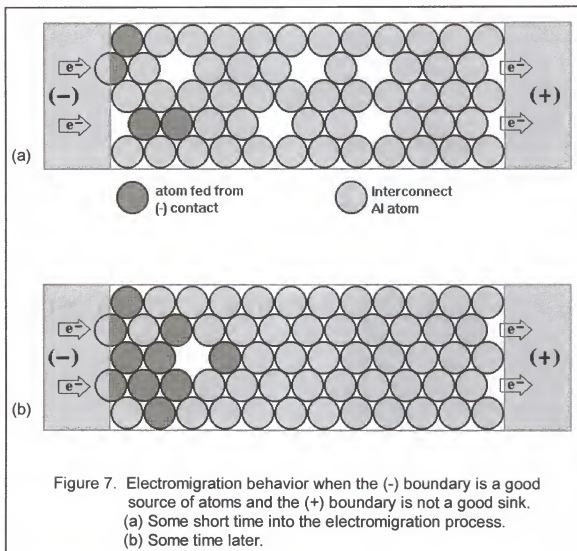
interconnect itself is not so resistant to electromigration, then the atoms will tend to drift toward the positive end, and the vacancies will drift toward the negative end. Since atoms cannot pass into the positive end boundary and vacancies cannot pass into the negative end boundary for this particular scenario, the drifting vacancies accumulate at the negative end and atoms accumulate at the positive end of the interconnect. The accumulation of vacancies will likely produce a void. Figure 6, depicts such a result.



When either or both of the end boundaries are good sinks or sources for atoms and/or vacancies, then the behavior of the interconnect may be different. The susceptibility of the end boundaries to electromigration, relative to that for the interconnect, will ultimately determine the outcome. Suppose that the negative boundary region is some type of contact area that happens to be reasonably susceptible to electromigration, which may be the case, for example, if it is made of aluminum or copper. If the positive end boundary is still resistant to electromigration and therefore does not accept atoms or provide vacancies,



then atoms will still accumulate at that end, but there will now be an additional supply of atoms fed from the negative contact region by the electron wind. This is depicted in Figure 7(a) for some intermediate arrangement of atoms after a short time into the course of electromigration. Figure 7(b) shows a possible arrangement at a later time. The darker shaded atoms are those that have been fed in from the negative end boundary. So long as this region provides atoms



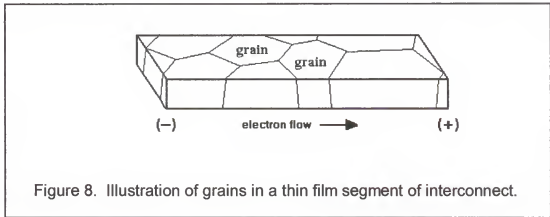
and accepts vacancies as fast as these species drift through the interconnect, the result is quite different from the behavior shown in Figure 6. The vacancies

will eventually be swept out through the left end as they are replaced by atoms drifting to the right. There is no atom depletion, so the interconnect may show no apparent damage, even though there has been significant migration of material. This says nothing, of course, about what is occurring farther upstream. There is probably not an infinite source of atoms there. Further, in this and all cases that involve an accumulation of material at the positive end, it is possible, although it has not been depicted here, that the accumulation there will take the form of hillocks or extrusions.

The discussions that accompany Figures 6 and 7 make reference to the rate divergence that results when electromigration proceeds in one or both of the end boundaries at a rate that is different from the rate in the interconnect itself. This type of discontinuity is present, for example, when the boundary is made of one material and the interconnect is made of another material. Contacts are sometimes made of tungsten and interconnects are often made of aluminum or some other composite composition, so such situations are common in practice.

The interfaces between dissimilar materials are blatant examples of structural discontinuities that can lead to divergences in the atomic migration rate. Such extremes are not necessary, however, to promote electromigration damage. A typical piece of material, we know, even for a pure element, is not perfectly homogeneous. It is normally a heterogeneous mix of crystal grains and grain boundaries. This is certainly true for the typical interconnect. As a result, rate divergences are likely to exist not only at such structural features as contact interfaces, but also just about anywhere within the interconnect itself. An

illustration of a segment of polycrystalline thin film interconnect that includes the explicit portrayal of grains and grain boundaries is given in Figure 8. The



segment contains several grains. Each grain can be seen to run the full thickness of the film, which is typical in reality, because interconnects are quite thin. The thickness is usually 0.5 to 1  $\mu\text{m}$ .

Every grain boundary is a potential site for hillock and/or void formation because it produces a discontinuity in the atom/vacancy migration rate. The activation energy for diffusion is lower on a grain boundary than it is within the bulk of a grain, so the atom migration rate should be higher on the boundary. Aluminum, for example, has an activation energy of about 0.5 eV on a boundary and 1 eV inside a grain. This difference presumably arises because a boundary is more loosely packed than is the interior of a grain, so its atoms may be less strongly bound to their positions. Also, there is more space for migration to take place. The extra space acts as a source for the generation of vacancies. The interfaces between grains and their boundaries will therefore be potential sites for atom accumulation or atom depletion. Figure 9 can be used to see that a

grain/grain boundary discontinuity is equivalent to the contact/interconnect discontinuity discussed previously. The upper part of the figure shows an interconnect with two end boundaries that can be taken to be contacts of some kind, and below that is a magnified view of a small region of the interconnect that includes part of grain 1, part of grain 2, and the boundary between them. Since electromigration occurs more readily in the grain boundary than it does in grain 1 and grain 2, a migration rate divergence is expected. It can be reasoned that grain 1, the grain boundary, and grain 2 are analogous to the negative contact, the interconnect, and the positive contact, respectively. Figure 9(b) depicts the material depletion that might result. The figure does not necessarily give an

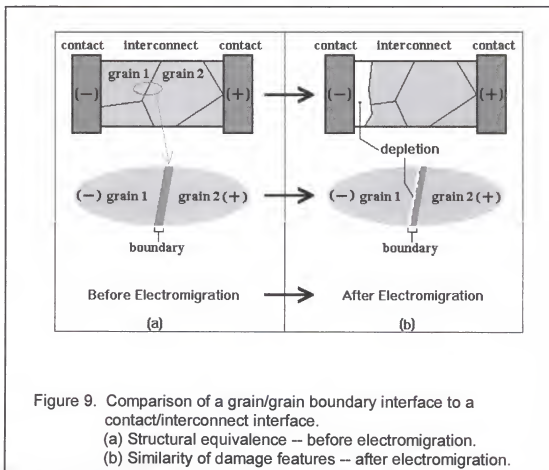
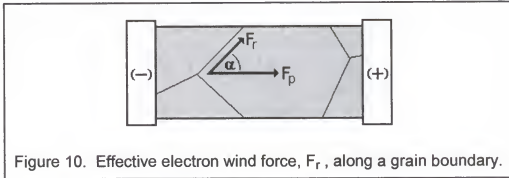


Figure 9. Comparison of a grain/grain boundary interface to a contact/interconnect interface.  
 (a) Structural equivalence -- before electromigration.  
 (b) Similarity of damage features -- after electromigration.

accurate portrayal of the relative amounts of depletion (or the absolute amounts, either). It only illustrates the equivalence of the structural discontinuities and the similar damage behavior that might be expected.

It would appear then, simply because a grain boundary is so small, that less depletion is possible there than is possible in the bulk of the interconnect. The effect of grain boundaries would seem to be relatively insignificant. This might be true if the electron wind force were exerted only in the direction parallel to the length of the interconnect, which has apparently been the assumption so far. It is true that the drift current is directed parallel to the length of the interconnect, and the electron wind force will certainly be maximum in this direction. Also, the relatively isotropic nature of a grain renders no need to consider any other direction. A grain boundary is different. It is relatively anisotropic, so it would be natural to consider the component of the electron wind force resolved in its plane. This is especially true in light of the lower activation energy that is associated with a grain boundary. If the plane of a boundary is seen as a directed pathway for atom migration, then the lower activation energy and the vacancy-generating nature of boundaries may more than negate the apparent insignificance of the boundary size. The extent to which this is true depends on just how much lower the activation energy is and on the magnitude of the appropriately resolved component of the electron wind force. The effective wind force along a grain boundary depends on the angle at which the boundary is inclined to the downwind direction. The activation energy for migration on the grain boundary depends on chemical composition and the

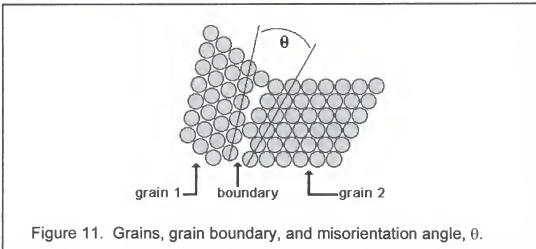
degree of lattice misorientation between the grains that the boundary separates. Figure 10 illustrates the way that the electron wind force can be projected onto a grain boundary to determine the effective force along it. If the length of the vector  $F_p$  represents the magnitude of the wind force parallel to the interconnect length, then the vector  $F_r$  represents the force that is directed along a grain



boundary inclined at an angle,  $\alpha$ , and

$$F_r = F_p \cos(\alpha) . \quad (3)$$

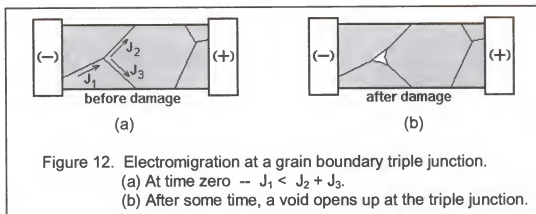
The force  $F_r$  is the effective driving force for electromigration along the boundary. Figure 11 illustrates what is meant by the "degree of misorientation" between grains. The figure depicts a two-dimensional arrangement of atoms for



which there appears to be two distinct grain-like domains whose rows are misaligned by an angle of  $\theta$  degrees. The angle,  $\theta$ , is the misorientation angle for this two-dimensional case. The transitional region between the ordered domains illustrates the nature of a grain boundary. It is less ordered and has extra space. The degree of order and the amount of extra space depend, somewhat, on the angle,  $\theta$ . It follows, then, that the activation energy for migration on this boundary also depends on the value of  $\theta$ .

Since diffusion, as we have said, occurs more readily on grain boundaries than it does within the bulk of a grain, and since some component of the electron wind force acts down the plane of any grain boundary whose angle of inclination is not 90 degrees, most electromigration damage is, in fact, associated with grain boundaries. Exceptions to this generality may arise when an interconnect has very few grains, especially when the associated grain boundaries lay perpendicular to the length of the interconnect, and when the upwind terminal of the interconnect is highly resistant to electromigration. In such cases, damage may occur primarily at the upwind terminal/interconnect interface, similar to that portrayed in Figure 6, or it may occur at the top and bottom surfaces or the edges of the interconnect, where the activation energy for diffusion is also relatively low compared to that for the bulk.

Grain boundary-related damage is frequently associated with so-called "triple junctions." Figure 12 provides a view of this. The symbols  $J_1$ ,  $J_2$ , and  $J_3$  are the atom flux rates that the electron wind force induces on the respectively indicated grain boundaries. If  $J_1$  is smaller than the sum of  $J_2$  and  $J_3$ , then



material is depleted at the junction of the three boundaries. A void will open. This is a common way for electromigration damage to show itself when an interconnect is small-grained and thus has many grain boundaries.

### Groundwork and Prior Research

The preceding discussions have dealt with the founding principles of electromigration -- why it occurs and how it exhibits itself. The groundwork laid by past researchers in this field has been directed toward these two questions. To reveal why it occurs, theorists have developed descriptions of the electron wind driving force. To determine how it exhibits itself, work has been devoted to experimental studies that reveal the importance of certain variables on atomic migration rate, damage rate, and damage morphology.

There have been several review articles written over the years [1-7]. Some early works are devoted heavily to theory, especially with regard to the nature of the electromigration driving force [1-3]. In more recent works, attention is paid primarily, but not entirely, to experimental findings [4-7].



The pure nature of the electromigration driving force can never be truly determined. But, knowing something of electrical conduction and the actions of charged particles in an electric field, a reasonable description of the force can be formulated. A simple treatment in this regard [1] begins by asserting that a metal is a lattice of positively charged ions that is host to a "gas" of negatively charged, freely roaming electrons. On average, there is no net charge on a piece of metal, so the total negative charge associated with the electrons is equal to the total positive charge of the ions. If an electric field is applied to such a system of charged particles, represented by a piece of pure, unalloyed metal, the resultant force,  $F$ , on that system can be expressed as

$$F = n_i e Z_i E - n_e e E , \quad (4)$$

where

- $n_i$  is the number density of ions on the lattice,
- $e$  is the unit electronic charge,
- $Z_i$  is the valence of an ion,
- $E$  is the magnitude of the electric field,
- $n_e$  is the number density of free electrons.

The electric field should exert a force on the ions, expressed by the first term of Equation (4), and on the electrons, expressed by the second term. The resulting steady state drift of free electrons -- the electric current -- is moderated by a resistance, or friction-like drag force, associated with the interfering ion matrix. The drag force,  $F_{\text{drag}}$ , associated with the average ion can be expressed as

$$F_{\text{drag}} = \delta \cdot E , \quad (5)$$

where  $\delta$  is a coefficient of friction, and the drag force is assumed to be proportional to the electric field,  $E$ . If the drag arises solely as a reaction force

associated with the collisions of drifting electrons with the ion matrix, then it is equal to the force exerted on the ion matrix by the electrons. At steady state, the total drag force is equal to the total force exerted on the conduction electrons by the electric field, so it can be resolved that

$$n_e e E = \sum_{k=1}^{n_i} \delta_k \cdot E = n_i \delta \cdot E. \quad (6)$$

The summation is included in Equation (6) in appreciation for the fact that every ion does not contribute equally, at any moment, to the frictional drag. It may be expected that an activated ion presents a different interference cross section to a conduction electron than does a normally positioned ion. So, at any moment, a migrating ion likely makes a different, perhaps larger, contribution to the drag. The electron wind driving force is associated strictly with the activated ion, so it should be the center of attention with regard to electromigration. This being the case, a different symbol,  $\delta_d$ , will be designated as the friction coefficient to be associated strictly with migrating ions.

The net force on a migrating ion,  $F_1$ , is the sum of the electric field force and the drag force, that is,

$$F_1 = e Z_i E - \delta_d E = e E \left( Z_i - \frac{\delta_d}{e} \right). \quad (7)$$

In addition to  $F_1$ , this equation contains two quantities which are not known -- the valence of the ion,  $Z_i$ , and the friction coefficient,  $\delta_d$ . Since an experiment could be conceived in which the electromigration-related ion velocity is measured, it

would be useful to relate the ion velocity to Equation (7). This is possible through a quantity called mobility,  $B_i$ , which is defined as

$$B_i = \frac{v_i}{F_i} \Rightarrow v_i = B_i F_i, \quad (8)$$

where  $v_i$  is the measured ion velocity. According to the Einstein relation,

$$B_i = \frac{D_i}{kT}, \quad (9)$$

where  $D_i$  is the ion diffusion coefficient,  $k$  is the Boltzmann constant and  $T$  is the absolute temperature. Now,

$$v_i = B_i F_i = \frac{D_i}{kT} eE \left( Z_i - \frac{\delta_d}{e} \right). \quad (10)$$

Since  $v_i$  and  $D_i$  can be determined, knowledge of the value for either  $Z_i$  or  $\delta_d$  will reveal the value of the other. But, neither one of these values can be found independently through experiment, so a theoretical estimate must be developed for one or the other. Any such estimate is unlikely to capture the true physics involved, and this belief accounts for the earlier statement that the pure nature of the electromigration driving force cannot be determined. Nonetheless, several theoretical treatments have been developed. One relatively straightforward and often-quoted estimate [8] for  $\delta_d$  gives

$$\delta_d = \frac{1}{2} e Z_i \left( \frac{\rho_d}{N_d} \right) \left( \frac{N_i}{\rho_i} \right) \left( \frac{m^*}{m} \right), \quad (11)$$

where

$\left( \frac{\rho_d}{N_d} \right)$  is the specific "resistivity" of the migrating ions,

$\left( \frac{\rho_i}{N_i} \right)$  is the specific "resistivity" of the normal lattice ions,

$m^*$  is the effective mass of the current carriers.

Equation (11) implies that the magnitude of the electron wind force,  $\delta_d E$ , can be represented as a multiple of the electrostatic force,  $eE Z_i$ , where the factor of multiplication includes the ratio of the "resistivity" contributed by the migrating ions to the "resistivity" contributed by normally positioned ions. The term "resistivity" is given in quotes because, in true terms, resistivity is a concept developed for crystals, not individual atoms. The ratio  $|m^*|/m^*$  is included so that the direction of the force will be correctly indicated whether the current carriers happen to be electrons or holes.

For convenience, the quantity  $\left( Z_i - \frac{\delta_d}{e} \right)$  is assigned its own name. This name is "effective valence," and it is given the symbol  $Z^*$ . The value of  $Z^*$  can be determined by experiment and the use of Equation (10). Since  $Z_i$  is part of the electric field force term and  $\delta_d/e$  is part of the electron wind force (drag force) term in Equation (7), the sign of  $Z^*$  indicates which component is larger. If  $Z^*$  is positive, then the electric field force is larger than the electron wind force. Ions will migrate toward the negative terminal. If  $Z^*$  is negative, then the electron wind force dominates. Ions will migrate toward the positive terminal. Usually,  $Z^*$  is negative. For good metallic conductors, such as the aluminum interconnects that are the subject here,  $Z^*$  is negative, and its magnitude is greater than 10. As such, the electrostatic force is considered a negligible component of the total electromigration driving force. Electron shielding is probably the cause of its weak role. This is the reason that the introductory discussion leading up to Equation (2) conveniently made no mention of the electrostatic force.

Another way of presenting the electromigration-induced ion velocity starts by inserting  $Z^*$  back into Equation (10). The result is

$$v_i = \frac{D_i}{kT} eEZ^* = \frac{D_i}{kT} F_i . \quad (12)$$

The diffusion coefficient,  $D_i$ , can be expressed as

$$D_i = D_o \exp\left(\frac{-Q}{kT}\right), \quad (13)$$

where  $D_o$  is a constant and  $Q$  is the self-diffusion activation energy. Putting this into Equation (12) yields

$$v_i = \frac{F_i}{kT} D_o \exp\left(\frac{-Q}{kT}\right). \quad (14)$$

In practice, it is customary to express a migration rate as a flux rather than a velocity, where flux is defined as the quantity of material that passes a plane of unit cross section per unit time. The ion flux,  $\phi_i$ , is then

$$\phi_i = \frac{N_i F_i}{kT} D_o \exp\left(\frac{-Q}{kT}\right), \quad (15)$$

where  $N_i$  is the number of ions per unit volume. Equation (15) is a form of the Nernst-Einstein equation. Equations (12) and (14) are equivalent expressions, as well. Whatever the form, this relationship is presented in almost any introductory description of electromigration.

Equation (15) is reminiscent of the relation expressed by Equation (2). This can be revealed by substituting  $F_i = eEZ^*$  back into Equation (15) and replacing  $E$  with  $\rho j$ , where  $\rho$  is the resistivity of the conductor and  $j$  is the current density. The result is

$$\phi_i = \frac{N_i e p j Z^*}{kT} D_o \exp\left(\frac{-Q}{kT}\right). \quad (16)$$

The ratio of the resistivity to the absolute temperature,  $\frac{\rho}{T}$ , is approximately constant for a given piece of material over normal temperature ranges. If it is reasonable to take  $\frac{N_i e Z^* D_o}{k}$  as a constant also, then the two can be combined into one constant called A. Then, Equation (16) becomes

$$\phi_i = A \cdot j \cdot \exp\left(\frac{-Q}{kT}\right), \quad (17)$$

which is effectively the same as Equation (2). The relationship of Equation (17) was shown, early on, to be quite valid [8]. This suggests that the consolidation of quantities that led to the constant, A, was not unreasonable.

The primary detriment that electromigration poses to IC interconnects is the formation of voids or some other type of material depletion. So, ion flux is not itself the quantity of most concern. This has been discussed in some detail. Most measurements of electromigration, in engineering practice, are aimed at damage rate, not ion flux rate. The two should be related, but they are not one and the same. A standard engineering test for electromigration is the lifetime test. This is an accelerated test in which a group of test structures is powered until all of the specimens "fail," where "failure" is identified as a complete loss of conduction, or, short of such complete failure, some critical increase in electrical resistance. The distribution of times to failure for the group is examined and the estimated median of these times is the measure of interest. The median time to

failure becomes, then, the measure by which the electromigration reliability of a particular metallization scheme is compared to another for a given set of test conditions, or, conversely, the dependence of electromigration reliability on test conditions is determined for a given metallization scheme. The test conditions of interest are current density and temperature. The important characteristics of a given metallization scheme are chemical composition, microstructure, and macrostructure. These factors were stressed on page 6 in the INTRODUCTION.

It is reasonable to guess that the median time to failure is inversely related to the rate of damage inflicted by the electron wind. Although ion flux rate and damage rate are not one and the same, a commonly used model for the median time to failure,  $t_{50}$ , is

$$t_{50} = \frac{A}{j^n} \cdot \exp\left(\frac{Q}{kT}\right), \quad (18)$$

which, except for the exponent  $n$ , is effectively the reciprocal of Equation (17).

Equation (18) is a generalized form of what has become known as "Black's Equation." Black popularized the use of such a model in electromigration work, and he supported a value of  $n = 2$  in an early paper [9].

Equation (18) includes  $j$  and  $T$  in explicit form. The other major factors -- chemical composition, microstructure, and macrostructure -- are implicit in the quantities  $A$  and  $Q$ . The activation energy,  $Q$ , is of particular interest, because, being in the exponential, it exerts a heavy influence on  $t_{50}$ . The following review will address each of the primary factors in turn.

### Current Density

The exponent,  $n$ , of Equation (18), is usually the center of discussion regarding the role of current density. An early study on bulk metals suggested that a value of  $n = 1$  is quite appropriate [8], and most have agreed that this is the correct theoretical value. Studies on thin films, however, have not yielded a consistent result. Early experimental work [9-12] revealed values of  $n$  between 2 and 3, and a value of 1.5 was found in a later attempt to clarify the matter [13]. Theoretical arguments have given support to  $n=1$  [14,15] and  $n=2$  [9,16,17]. The dependence of energy dissipation on  $j^2$  is one possible basis for believing  $n=2$ , but the energy that is actually dissipated per electron/ion interaction is negligible compared to the activation energy. The electric current, in its role as a driving force for migration, should be viewed only as a biasing influence on the basic diffusion process. In this view, such bias should be proportional to  $j$ . Support for  $n=1$  is generally accompanied by arguments that an apparent value of  $n$  larger than 1 arises when the temperature is not accurately characterized throughout the test. This is believable, because it is practically impossible to follow the temperature throughout the entire failure process. As electromigration damage proceeds, the current density and temperature increase at the damage site. Such a phenomenon is difficult to account for experimentally. When a test is run with the smallest practical initial current density and the test structure makes use of good thermal management,  $n$  is probably between 1 and 2. It is very common to see the use of  $n=2$ .



### Temperature

There is apparently no questioning the placement of  $T$  in an exponential term, as presented in Equation (18). This so-called Arrhenius dependence is well entrenched as a part of all models that incorporate thermal activation. The variable,  $T$ , is sometimes placed as a pre-exponential component, as well. This is apparently done in appreciation for the fact that it may not be strictly correct to consider the pre-exponential quantity of Equation (16), especially the factor  $Z^*$ , to be independent of temperature [4]. So, a slightly modified expression for  $t_{50}$  may appear as

$$t_{50} = \frac{AT}{j^n} \cdot \exp\left(\frac{Q}{kT}\right). \quad (19)$$

And, an equation of the form

$$t_{50} = \frac{AT^3}{j^3} \cdot \exp\left(\frac{Q}{kT}\right) \quad (20)$$

has been offered as an appropriate option when temperature gradients contribute heavily to the driving force for damage [18]. In any case, the dominance of the exponential factor makes the choice of including or excluding the extra  $T$  factor in Equations (19) and (20) somewhat moot in light of normal experimental error. Equation (18) is usually acceptable.

### Chemical Composition

Such physical properties as atomic mass and inter-atom bond strength, which vary with chemical identity, determine how well any atom in a given piece of material resists a diffusive hop from its position. This barrier is essentially a

measure of the activation energy,  $Q$ . So, chemical composition affects  $t_{50}$  largely through  $Q$ . It also has a strong role in determining  $A$ , but again, the exponential factor exerts a dominant influence.

Much of the early work on electromigration was directed at determining  $Q$  for various metals and alloys. Heavy attention was placed on gold [8,12,19-22], silver [19], copper [23], and especially aluminum [10,24-29]. Determination of  $Q$  usually involves the measurement of  $t_{50}$  or ion velocity for several different test temperatures with other conditions held constant. An Arrhenius plot is made, that is,  $\log(t_{50})$ ,  $\log(v_i)$  or  $\log(v_i/j)$  is plotted versus  $1/T$ , and  $Q$  is extracted from the slope of the resulting straight line fit.

The activation energy that is commonly observed for pure aluminum is about 0.5 eV [10,24,25]. For gold, it is about 0.9 eV [19-22], and for copper it is about 0.8 eV [23]. The importance of knowing these values lies in the huge effect that they have on  $t_{50}$ . At a temperature of 350 K, the value of  $\exp(Q/kT)$  for aluminum ( $Q = 0.5$  eV) is  $1.6 \times 10^7$ . The value of  $\exp(Q/kT)$  for gold ( $Q = 0.9$  eV) is  $9.7 \times 10^{12}$  at the same temperature. The choice of material is certainly a pivotal issue, but before making any conclusions, it is important to note that the  $Q$  values quoted here happen to be those for migration on grain boundaries. This detail will be addressed in the next section.

### Microstructure

The chemical identity of a conductor is not all that determines  $Q$ . Just as important is its microstructure, because atomic migration may proceed not only through the bulk, but it may also follow an easier course on free surfaces, grain

boundaries and other types of interfaces, the presence of which help to define the "microstructure" of a given piece of material. The values of  $Q$  quoted in the last section were found under conditions for which grain boundary migration was dominant. This is a critical detail. Using aluminum as an example, and staying with  $T = 350$  K, the activation energy for lattice migration (which is about 1.1 eV) leads to a value for  $\exp(Q/kT)$  of  $7.4 \times 10^{15}$ , which is far different from the value of  $1.6 \times 10^7$  that was obtained above for migration on grain boundaries. The value of  $Q$  on grain boundaries is smaller than it is on the lattice presumably because atoms are less densely packed on grain boundaries and less strongly bound. A similar reasoning leads to the conclusion that  $Q$  on free surfaces is even smaller than it is on grain boundaries.

The apparent activation energy will depend on the temperature and the availability of the various types of migration pathways. At high temperatures, perhaps 350 °C and above, lattice migration occurs readily, and the apparent activation energy will be that for bulk migration. At intermediate temperatures, perhaps 150 °C to 350 °C, the lattice may not contribute much as a pathway. The apparent activation energy will likely be that for grain boundary migration if grain boundaries are available in sufficient quantity. At lower temperatures, it might be that even grain boundaries do not provide a good means of migration. In these cases the apparent activation energy may be that for migration on a free surface if one or more is available. The transitions between these cases need not be abrupt, that is, a mixture of diffusion modes may be apparent whenever the temperature and the availability of a particular pathway are marginal. For

example, in an experiment on aluminum [24] it was found that films with a small grain size displayed a  $Q$  of 0.51 eV, whereas films with a larger grain size displayed a  $Q$  of 0.73 eV. The films with small grains presumably contained a plentiful supply of grain boundaries and therefore showed an activation energy that is accepted to be that for grain boundary migration. The large-grained films had fewer grain boundaries, perhaps a marginal quantity, such that a relevant fraction of the damage occurred by lattice migration. So, in the temperature range used for that particular test, the large-grained films appeared to have an activation energy between that for grain boundary migration ( $\sim 0.5$  eV) and lattice migration ( $\sim 1.1$  eV).

The traditionally heavy attention paid to grain boundaries as pathways for electromigration is fueled by the reality that, until recently, any particular IC interconnection was likely to have a plentiful supply of them. The tendency for damage to occur along grain boundaries was observed *in situ* during an early TEM experiment [27]. Observations were made on large-grained samples and small-grained samples of Al. It was particularly revealing that the voids which formed on the small-grained samples were irregular in shape, whereas those formed on the large-grained samples consistently had straight edges. This was taken as evidence that voids propagate on the boundaries rather than through the grains.

Evidence that grain boundary triple junctions provide natural sites for the formation of voids was also obtained early on in another *in situ* TEM study [28]. This study, performed on Al, showed not only that voids form preferentially at

triple junctions, but also showed that the propagation of a given void will proceed down the outgoing grain boundary that is most favorably oriented relative to the electron wind. That is, the boundary with the largest resolved force component becomes the preferred pathway for propagation beyond the triple junction. See Figure 10 in this regard. A grain boundary triple junction is a natural site for void formation when two of its three associated grain boundaries are arranged as outgoing pathways and the other is arranged as an incoming pathway. In such a configuration, the outgoing grain boundaries, in combination, will likely (but not necessarily) carry material away from the junction at a faster rate than material can be brought in by the single incoming grain boundary. This scenario was illustrated in Figure 12. Of course, the converse arrangement of boundaries should encourage hillock formation at the junction.

Certainly, the number of grain boundaries that will be found in a given width of interconnect is inversely related to the average size of its grains, so it is not surprising to find consistent results in studies of  $t_{50}$  versus grain size. The median time to failure invariably increases as grain size is increased. Some have reported this dependence to be nearly linear [30-33]. The observation that an increase in grain size may be accompanied by an apparent increase in activation energy [10,24,34] suggests that a reduction in the number of grain boundaries available for migration sometimes allows lattice migration to play a noticeable role.

The effect of the grain size distribution on  $t_{50}$  is based on a principle similar to that applied in explaining why triple junctions are prone to damage.

With a mixture of grain sizes, there are bound to be some regions in which the number of grain boundaries is different from the number in adjoining regions. The transitional zone between each region is equivalent, on a larger scale, to a grain boundary triple junction, and damage may occur preferentially in such a zone. Such a structural gradient represents a vulnerability beyond that which is already contributed by the triple junctions themselves. So,  $t_{50}$  should decrease as the standard deviation of the grain size is increased. Experiments have confirmed that it does [35]. A large standard deviation in the grain size may, itself, magnify the vulnerability to void formation, even if there is no bias in the location of any given grain according to its size. It could happen, however, that there is such a bias. For example, if the larger grains are all located more toward the upwind end, and the smaller grains are all located more toward the downwind end of the interconnect, then void formation should be encouraged most strongly where the transition in grain size is the sharpest. Again, such behavior has been verified by experiment [24,36].

It was mentioned, in connection with the two-dimensional illustration of Figure 11, that the activation energy for migration on a grain boundary is related to the angle of misorientation between the grains that it separates. A universally applicable characterization of such a dependence in three dimensions is difficult. At least one effect associated with crystallographic orientation has been clearly demonstrated, though. Thin films with a large degree of  $\{111\}$  fiber texture have been shown to exhibit larger median times to failure [24,34,37-42]. Presumably, when the  $\{111\}$  plane of all grains is aligned parallel to the substrate surface, the

resulting grain boundaries are largely tilt boundaries. Cohesion may be stronger on these boundaries than it is on randomly obtained boundaries. The superior mechanical strength displayed by the {111} plane relative to other planes [43] lends support to this view. In addition, tilt boundaries are composed of steps and ledges, where the steps are essentially dislocations whose lengths are aligned normal to the film plane. With this alignment, the steps might act as blockades against in-plane migration [37]. It seems, then, that the activation energy on such grain boundaries should be larger than it is for boundaries between randomly oriented grains.

An empirical relationship has been proposed for the dependence of  $t_{50}$  on the microstructural characteristics just discussed -- grain size, grain size distribution, and {111} texture [42]. It is given as

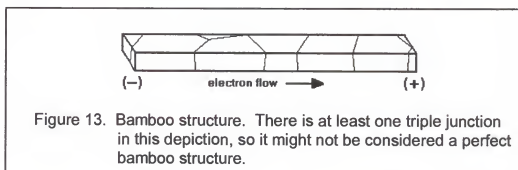
$$t_{50} \propto \frac{S}{\sigma^2} \left( \frac{I_{(111)}}{I_{(200)}} \right)^3, \quad (21)$$

where

$S$  is the median grain size,  
 $\sigma$  is the standard deviation of the grain size distribution,  
 $\left( \frac{I_{(111)}}{I_{(200)}} \right)$  is a measure of the {111} texture based on x-ray intensities.

The ratio of x-ray intensities,  $I_{(111)}/I_{(200)}$ , is obtained from an x-ray diffractometer measurement. According to the JCPDS files for Al, this ratio is about 2 for a powder sample, which is assumed to have randomly oriented grains. If the ratio measured for a thin film is much larger than 2, then, it is considered to display a {111} texture. Films deposited by some techniques, particularly ion-assisted techniques, can be so highly textured that  $I_{(200)}$  is almost unmeasurable [34].

The emphasis on grain boundary migration and its contribution to electromigration damage commands that attention be placed on the grain boundary network. So, the tacit assumption has been that there is a grain boundary network, complete with triple junctions, that provides a continuous pathway for migrating ions to follow down the length of the interconnect. This was assumed, certainly, in explaining the increase of  $t_{50}$  with increasing grain size, but it was not mentioned that there is a natural limit to the reported trend. There is a threshold grain size beyond which the continuity of grain boundaries cannot be maintained. When an interconnect is patterned from a film whose grain size is larger than the intended interconnect width, the result will likely look similar to a chain of single-grained segments. Such an arrangement is referred to as a "bamboo" structure. In a perfect bamboo structure there are no triple junctions and there is no continuous pathway provided down the interconnect by the occasional grain boundaries that are present. Figure 13 illustrates a segment of interconnect which could be called a "bamboo" structure, or, because there is at least one triple junction, a "near-bamboo" structure. The



boundaries will typically be found to run transversely, side-to-side, across the width of the interconnect. The angle at which they traverse this span is of



importance. If the traversing boundary is inclined at any angle other than 90 degrees with respect to the downwind direction, then there will likely be some migration on that boundary. A void may form on the edge of the interconnect at the upwind end of that grain boundary segment. The tendency for this to happen will be greater the smaller the inclination angle and the longer the traversing grain boundary, because the resolved component of the electron wind force is larger with decreasing angle and there is more downwind room, that is, a larger sink, for migrating atoms on longer segments. In any case, the absence or near absence of triple junctions and the lack of a continuous network of pathways should lead to larger  $t_{50}$  values for interconnections with bamboo and near-bamboo grain structures. It might also be estimated that the location and mode of failure is more unpredictable with these structures, and especially with near-bamboo structures, because those interconnects that just happen to contain a triple junction might fail long before those that do not. Concern for this complication was expressed quite early on [44], but the predicted increase in  $t_{50}$  has indeed been confirmed by experiment [45,46].

The idea of reducing the number of grain boundaries can certainly be taken to the extreme case by considering their total elimination. Single crystal interconnects should be the most reliable of all. Indeed, they were observed to be nearly immune to electromigration damage [47], but the production of single crystal interconnects as routine procedure has not been possible. It is routinely possible to obtain bamboo structures, however.

Another structure absent of grain boundaries is the amorphous structure. Prompted by the knowledge that amorphous alloys often make good diffusion barriers, an experimental comparison of electromigration lifetime was made between films composed of an amorphous Cu-Ti alloy and crystallized films of the same composition [48]. The amorphous films showed about a ten-fold improvement in lifetime. There was no comment made on the resistivity of the amorphous films compared to that of the crystalline films.

In unalloyed metals, grains and grain boundaries are certainly the most significant microstructural features with regard to electromigration. This can probably be said for alloys as well, but the addition of alloying elements does bring on an additional set of considerations. These considerations consist, at least, of the migration behavior of the solute, the effect of the solute on the migration behavior of the solvent, and the effect of any additional phases that precipitate out.

Aluminum has enjoyed the most attention as a base metal in the study of alloying effects, since it is the predominant interconnect material. The most heavily considered alloying additions have probably been silicon and copper. Both improve the electromigration resistance of aluminum [11,49-51], but copper is especially effective and has made the biggest impact. The addition of copper has proved to be one of the most significant defenses against electromigration.

The mechanism by which copper additions improve the reliability of Al interconnections was vigorously debated and studied early on. New doubts are raised on occasion, but an integral part of most explanations is related to the

precipitation of  $\text{CuAl}_2$  on grain boundaries. Copper moves quite well on Al grain boundaries, but the self-diffusion of Al on those same boundaries seems to be inhibited by the presence of the Cu [11,37,52-54]. If the copper is eventually depleted, void formation follows quickly, but such depletion is prevented or significantly slowed so long as  $\text{CuAl}_2$  particles are present. Presumably, the precipitates are a replenishing source of Cu atoms.

The measured activation energy for the failure of Al(Cu) thin films is sometimes as high as 0.8 eV [55]. Since failure seems to depend on the depletion of Cu atoms from Al grain boundaries, the activation energy should be associated not only with the diffusion of Cu on those boundaries, but also with the mechanism by which the boundaries are replenished with Cu atoms in the presence of  $\text{CuAl}_2$ . Such quantities as the heat of solution of Cu atoms in Al and the heat of adsorption of Cu atoms on Al grain boundaries should play a role in determining the overall activation energy [55].

Of course, copper and silicon are not the only alloying additions that have been considered. Gold, silver, magnesium, and nickel (to name a few) have also been investigated. Magnesium [56] and nickel [57] are beneficial additions. Gold and silver are not [11].

### Macrostructure

The term "macrostructure," as it is meant here, may encompass just about any defining characteristic of an interconnection that is not an inherent part of the microscopic world. It includes size, shape, and other macroscopic features of construction.

Although macrostructure is a property that is inherently independent of microstructure, the reverse is not strictly true. For example, the grain boundary network that happens to be captured when an interconnect is patterned from a thin film depends on the length and width of the pattern taken. A larger number of unfavorable structural features, such as triple junctions, is captured along the length of a patterned interconnect as that length is increased. Also, the chance that such unfavorable sites will turn up in the "upwind portion" of the interconnect is better with increasing line length. It is not very surprising, then, that  $t_{50}$  has been found to decrease with increasing interconnect line length [58-60].

A similar reasoning can be applied when considering the interconnect width. With increasing width, the probability of capturing damage prone structural features should increase. With this reasoning alone, it appears that  $t_{50}$  should decrease with increasing linewidth. It is important to realize, however, that the length of an interconnect is usually much greater than the width, so void propagation across the width is usually the ultimate cause of failure. As the width is increased, then, a given void must expand farther to cause failure. Also, with linewidths that are large enough to capture several triple junctions, it is less likely with increasing linewidth that all of the triple junctions in a randomly chosen side-to-side span will void and link together. Apparently, then, it may also be reasoned that  $t_{50}$  should increase as linewidth is increased. The two lines of reasoning are in contradiction, but experimentation has shown the second approach to be more appropriate. That is,  $t_{50}$  increases with increasing

linewidth [58]. An empirical relationship was constructed for  $t_{50}$  versus line length and linewidth [58]. It was reported as

$$t_{50} = A \cdot w \cdot \exp\left(\frac{\alpha}{\ell}\right), \quad (22)$$

where

A	is a constant,
w	is the linewidth,
$\alpha$	is a constant that depends on w,
$\ell$	is the line length.

This equation indicates that  $t_{50}$  increases linearly with linewidth. The dependence on length is one in which  $t_{50}$  first decreases rather quickly with increasing line length, but eventually appears to level out as the rate of decrease becomes negligibly small.

It should be noted that the smallest linewidth tested in the experimental determination of Equation (22) was 5  $\mu\text{m}$ , and the grain size was reported to be equal to or less than 2  $\mu\text{m}$ . Equation (22) indicates that  $t_{50}$  decreases linearly as linewidth is decreased, but, if a linewidth of, say 1  $\mu\text{m}$ , had been tested, it is likely that the  $t_{50}$  for that line would have been larger than the  $t_{50}$  for the 5  $\mu\text{m}$  line. This is because a 1  $\mu\text{m}$  line would likely have a bamboo structure. This effect was mentioned earlier in the context of increasing grain size. There are two ways, then, to arrive at a bamboo structure. One way is to increase the grain size until the average grain is larger than the interconnect is wide. The other way is to reduce the linewidth until it is smaller than the size of the average grain. Now, an increase in  $t_{50}$  was reported [45,46] in the context of increasing grain size, so a similar increase is reported [61-65] in the context of decreasing

linewidth. The critical width below which  $t_{50}$  increases depends, of course, on the grain size of the film from which the interconnect is patterned. The critical width appears to be 1-2  $\mu\text{m}$  in practice.

In addition to size, the macrostructure of an interconnect is defined by its terminations and the other purposeful or incidental types of contact that it makes with other materials on the chip. Certainly, an interconnection must lay on top of another material, and it is also routine that other materials are placed over it. For example, it is standard practice to "passivate" IC chips, that is, encapsulate them with a protective coating. If any particular passivation coating might improve electromigration lifetime, all the better. Of course, this is mentioned because some coatings do seem to be beneficial.

Early reports on the effect of coatings claimed that the activation energy of 0.84 eV for large-grained, uncoated Al films was increased to 1.2 eV when the films were coated with  $\text{SiO}_2$  glass [9,10]. Another study showed an improvement in lifetime for aluminum films that were coated with an alumina-silicate glass [26]. The explanation by the authors in both cases was that surface diffusion was inhibited by the coatings. This explanation was challenged [66] by pointing to a study [47] that had shown films of uncoated, single-crystal Al to be essentially immune to electromigration. In addition, it was noted that the native oxide that forms on the surface of Al should inhibit surface migration just as well as any additional coating would, anyway. An alternative proposal was that coatings might be capable of suppressing the formation of hillocks, which in turn, it was thought, should prevent the formation of voids. Calculations of the strengths of

coatings and the forces that might be produced by electromigration led to the conclusion that coatings would have to be very strong to be effective, possibly stronger than can practically be obtained [66]. It was suggested that the proposed mechanism could be effective only for very thin films and relatively thick coatings.

Later work, in which aluminum films were coated with silicon nitride, indicated again that the coating slows the drift of atoms [67]. It was commented, in addition, that the strength of a coating does not have to be so high as was calculated in the earlier work. This statement was based on the notion that electromigration-induced compressive stresses are built up locally across each point of atom depletion and its associated point of accumulation just downwind, and this source-sink distance is often quite small compared to the total length of long conductors. Back-diffusion is encouraged by the local stress gradient between the source and sink.

Overcoatings of doped glass and/or silicon nitride are, in fact, commonly used in the construction of an IC. Also, being that IC circuitry is built up in a multilayered arrangement, dielectric materials are necessary between each layer. These may be composed of  $\text{SiO}_2$ , as well.

In addition to passivations and dielectrics, it is also fairly routine to find the use of interconnect cladding layers, which are used for various purposes, such as the prevention of interdiffusion or the promotion of adhesion between layers. Materials commonly found in these roles are Ti, TiN, W, and TiW. Such claddings are usually significantly thinner than the interconnect itself, so any

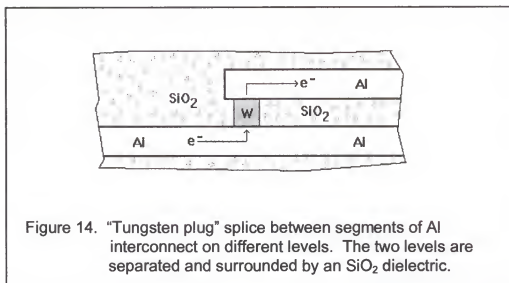
influence that they exert on electromigration behavior is associated with interdiffusion or crystallographic effects on the deposition of the aluminum film.

Finally, any segment of interconnect must eventually make contact to a silicon device or an interlevel splice of some kind. Being that the sole purpose of an interconnection is to make connections between silicon-based devices on a chip, the Al/Si contact interface has a long research history. The reliability concerns associated with this interface are largely related to its metallurgy and the interdiffusion of Si and Al. With respect to electromigration specifically, a silicon device can essentially be disassembled one atom at a time by an electron wind. Even when barrier materials are successfully introduced to avoid the loss of silicon and the invasion of aluminum, the macrostructural discontinuity that must inherently be associated with the interface is sure to be a favorable site for aluminum depletion when the interconnect carries a sufficiently large current. Such a scenario was discussed in connection with Figures 5 and 6.

Another type of contact concern is a more recent arrival. The multilevel arrangement of today's IC designs requires a means of connecting the circuitry on any given level to that on other levels. Such connections are made through small openings etched through the dielectric that separates the layers. An illustration of such a contact arrangement is given in Figure 14. The figure depicts a portion of two metallization layers. The two segments of aluminum interconnect, one on the lower layer and the other on the next layer up, are connected by way of a small segment of tungsten. The surrounding matrix area



is taken to be an  $\text{SiO}_2$  dielectric, and the so-called "tungsten plug" fills a hole that was etched through the dielectric during a previous processing step.



Tungsten is used for this splice instead of aluminum because tungsten can be deposited into very narrow, deep via holes more readily than aluminum can. This opens the door for the use of very narrow interconnections ( $< 0.3 \mu\text{m}$ ). The tungsten process also allows for a more planarized arrangement of levels.

Again, as with the silicon contact, a severe macrostructural discontinuity is associated with the tungsten plug splice. With a flow of electrons in the direction indicated by Figure 14, the interface between the top of the W plug and the upper level Al interconnect will be a prime location for aluminum depletion and void formation [68]. The tungsten is very resistant to the electron wind and stays intact, but aluminum atoms are readily swept away from the interface. It is not surprising, then, that electromigration failures are frequently associated with this interface when it is present [69-73].

### Modern Implications

The preceding discussion of fundamentals and founding research is all pertinent and contributory to the state of the art applications of today. That is, the description of electromigration and the characterization of its effects are essentially no different today than they were after the first decade or so of research. Challenges of recent years are largely associated with the drive for increased IC packing density, which has led to the use of multilevel structures and very small interconnect linewidths. The following list summarizes the most pertinent features of modern IC interconnects:

1. Composition: alloy of aluminum (1- 4% Cu). Claddings may be included.
2. Local operating temperature: may approach 100 °C.
3. Current density: may approach  $1 \times 10^6$  A/cm<sup>2</sup>.
4. Linewidth: < 1  $\mu$ m.
5. Thickness: < 1  $\mu$ m.
6. Grain structure: near-bamboo or bamboo.
7. Interconnect architecture: multileveled, with W plug interlevel splices.

It might be estimated, in light of previous discussions, that an interconnect with these specifications is reasonably resistant to electromigration. Although the tungsten plug is unfavorable, the bamboo or near-bamboo grain structure and the copper alloying should prevent the electron wind from sweeping copper and aluminum away from the plug.

In reality, a temperature of 100 °C and a current density of  $1 \times 10^6 \text{ A/cm}^2$  are quite severe by traditional standards, so the advantage that is gained from the bamboo or near-bamboo grain structure is minimized. Interestingly, the reduction in linewidths that brought in the bamboo structure is also the reason that current densities are increasingly severe. Ultimately, the absence or near absence of grain boundaries does not preclude the migration of Cu and Al along other paths. In traditional polycrystalline interconnects, these alternate routes were relatively insignificant compared to the plentiful supply of grain boundaries that was typically present, but with increasingly narrow interconnects ( $0.25 \mu\text{m}$  ?) and more severe current densities, they can no longer be ignored. Recent studies have revealed, for example, that significant degradation can result from lattice migration and edge migration, in addition to grain boundary migration within the polycrystalline segments that sometimes appear alongside the single crystal segments in near-bamboo interconnects [70-72,74,75].

#### Pulsed Electromigration

Black's equation was introduced earlier as the most popular model of electromigration lifetime. It is repeated now for further consideration.

$$t_{50} = \frac{A}{j^n} \cdot \exp\left(\frac{Q}{kT}\right) \quad (18)$$

The current density,  $j$ , is apparently taken to be constant during the course of an experiment, but if a time varying current is employed, some modification should be made to the equation.

Any ordinary current variation could be considered, but, in keeping with the subject of this work, let us consider a unidirectional pulsed current of the type that was depicted in Figure 1. Assume, for the moment, that  $t_{50}$  is known for a group of test stripes that was subjected to a constant current of magnitude  $A$ . If a second group of identical test stripes is subjected to a pulsed current, where the amplitude is  $A$  and the duty cycle is 50%, what is the expected  $t_{50}$  for this group? Of course, the temperature is assumed to be the same for both tests.

As a first estimate, it might be assumed that normal electromigration occurs for the duration of each pulse and that nothing happens between pulses. If this is true,  $t_{50}$  for the second group is expected to be twice the known  $t_{50}$  of the first group. That is, Black's equation might be modified to read

$$t_{50} = \frac{A}{d \cdot j^n} \cdot \exp\left(\frac{Q}{kT}\right), \quad (23)$$

where  $d$  is the duty cycle expressed as a fraction and  $j$  is the pulse amplitude. Another way to state this relationship, if it is correct, is to say that the median number of on-time hours to failure for the second group is equal to the median number of hours to failure for the first group. Equation (23) is therefore said to express an "on-time" dependence.

Another approach may be to consider the existence of an effective dc current density that might be equivalent to the given pulsed current density. The first obvious candidate for such a quantity is the average of the pulsed current density waveform, which is just  $d \cdot j$  for the square pulses considered. So, if  $j$  is replaced by  $d \cdot j$ , then Black's equation would become

$$t_{50} = \frac{A}{(d \cdot j)^n} \cdot \exp\left(\frac{Q}{kT}\right). \quad (24)$$

This relation is known as the "average current density" model.

Recall, from earlier discussions, that the "correct" value of  $n$  in Black's equation is not known. Estimates generally fall between 1 and 3, but much larger values (as high as 15) have been reported. So, it may be useful to separate the duty cycle dependence from the uncertainty associated with the value of  $n$ . The result might be

$$t_{50} = \frac{A}{d^m \cdot j^n} \cdot \exp\left(\frac{Q}{kT}\right). \quad (25)$$

Of course, this expression represents an average current density dependence only when  $m = n$ .

A value of  $m = 1$  produces the on-time model. A larger value indicates a larger  $t_{50}$ , and in such a case the lifetime is said to be "enhanced." The average current density model predicts enhanced lifetimes, because it is defined by  $m=n$ , and  $n$  is normally taken to be 2.

Neither the on-time model nor the average current density model makes explicit mention of the pulse repetition rate (frequency). The assumption that leads to an on-time model is that "normal" electromigration begins immediately at the start of a pulse, proceeds in the same way that it would for a constant DC current of the same magnitude, then ceases immediately at the end of the pulse. In addition, the time between pulses is treated as though it has no effect on the process. Such an assumption seems to exclude any consideration of frequency

from the start. However, implicit in the average current density model must be an assumption that something does happen between pulses or a pulse is not equivalent to an equal interval of time in a DC experiment or both. This is an implicit recognition that additional transients might exist, just none that are altered according to frequency. In the end, the role of frequency is not so easy to speculate on, but it is quite apparent that duty cycle should affect  $t_{50}$ .

No wide range, continuous dependence of  $t_{50}$  on pulse frequency has been identified with any conclusive experimental evidence or by any compelling theoretical argument. Any observed dependence on frequency has been limited to a low frequency critical point transition that is apparently associated with the response times of thermal transients. Except for this, the frequency seems to be a minor influence compared to duty cycle. Nonetheless, frequency is given continued consideration, in view of the possibility that another critical point or perhaps a continuous dependence of some sort exists at high frequencies. In addition, even the dominant influence of duty cycle has been difficult to characterize. There is considerable disagreement about how it should be incorporated into a quantitative model. Although it is common to see use of a model like Equation (25), the fitted value of  $m$  is not consistent.

The first experimental study of electromigration under pulsed current conditions was carried out by English, Tai, and Turner on Ti-Au thin films [76]. They compared the effects of several different sets of pulse conditions, ranging in frequency from  $10^{-4}$  Hz to  $10^4$  Hz, and in duty cycle from 10% to 70%. Each pulse treatment was applied for 100 on-time hours, that is, the total "exposure"

was the same for every test. The post-test condition of the films was observed by SEM, and it was found that the samples exhibited heavy damage, moderate damage, or no damage, depending on the pulse frequency and duty cycle that had been applied.

The authors' explanation began with the common assumption that electromigration damage is the ultimate result of a local buildup of vacancy concentration at some point of flux divergence. The buildup was assumed to take place rapidly at first, but to eventually slow down while approaching some maximum level of local supersaturation. Under pulsed powering, it was figured that this level of supersaturation might be reachable during the time span of a sufficiently long pulse, but the level was expected to decay somewhat during the off time between pulses. The idea was then introduced that some critical level of supersaturation had to be maintained or exceeded for a sufficient length of time, called the "incubation" time, in order for damage to nucleate in the form of voids. Unlike the vacancy supersaturation, voids were considered to be stable against any relaxation effects associated with the time between pulses.

This reasoning appeared to be particularly effective in the analysis of low frequency behavior, where the pulses were presumed to be long enough that stable voids may be formed within the duration of one pulse. In such a regime, the off time between pulses would be of little significance, and the duty cycle would be unimportant, except to lengthen the total time to failure. An on-time dependence would then be exhibited. Some critical pulse length should define the edge of this regime, but its exact value is difficult to predict. It was estimated

by Rosenberg and Ohring [77] that the supersaturation rise time is on the order of 100 seconds in aluminum ( $T = 125\text{ }^{\circ}\text{C}$  and  $J = 10^6\text{ A/cm}^2$ ), but they did not offer any estimate of an incubation time.

The analysis was continued by considering the possible response to pulse lengths that happen to be shorter than the critical time period for void nucleation, but long enough to produce a large supersaturation of vacancies on one pulse cycle. It was reasoned that the build up of vacancy supersaturation, because it would be large enough to produce a considerable driving force for recovery, could be nearly eliminated during the off time if it was about equal to the on time. Very long, highly enhanced lifetimes could then be the result. The actual response in this intermediate regime was expected to be a function of the pulse duty cycle and frequency.

The likely response to very short on times and off times was said to be different. For such conditions, each pulse was assumed to produce a relatively small increase in the vacancy supersaturation, and each following off time was assumed to allow little recovery. The supersaturation was expected to increase in small increments with each pulse cycle, to eventually reach the critical level, and to stay above that level for a sufficient length of time for void nucleation. According to the authors, the required number of cycles would depend mostly on the duty cycle and not so much on the frequency. They contended that the rise and fall of supersaturation could each be adequately approximated as a linear function of time for arbitrarily small pulse lengths and pulse separations, so the



relative lengths of the on times and off times would determine the behavior, not the individual times themselves.

The concept of vacancy supersaturation has remained a commonly used tool in modeling and/or explaining pulsed electromigration behavior. However, instead of requiring a void incubation period, many treatments just follow the assumption that the time to failure is inversely proportional to the threshold level of supersaturation. In any event, the electromigration damage mechanism is probably more complicated than either approach implies. In addition to excess vacancies, other types of defects probably form along the way, and these may have different implications regarding the kinetics of damage formation and the enhancement of lifetime. In addition, it is known that a downwind compressive stress may be built up during the course of electromigration [67,78]. When this is the case, lifetime enhancement should be associated somewhat with stress driven recovery of damage between pulses. Finally, if it happens that the pulse length is too short for the temperature of the test stripe to attain its steady state DC level, then lifetime should be enhanced. In fact, this consideration received heavy attention in the earliest studies. These issues have been considered in various forms [15,79-117] since the initial study of English, Tai, and Turner.

The first treatment of temperature and thermal response effects was offered by Sigsbee [15]. He considered the electromigration-induced growth of a crack across the width of a test stripe in conjunction with the pulsating Joule heat dissipated by a pulsed current. He attributed lifetime enhancement to the lower average temperature that results when the current is pulsed. He noted, in

addition, that there is some minimum frequency (around 1 KHz in his modeled system) below which the pulse length is long enough that the temperature is able to reach its steady state DC value for much of the pulse duration and the off time is long enough for the temperature to return to ambient for much of the time between pulses. An on-time dependence was then expected.

Davis [79] also presented a thermal treatment, but he contended that the average temperature is not a useful quantity and that the temperature has to be followed over the whole course of a pulse cycle. He demonstrated a variation in the degree of lifetime enhancement with frequency for fixed duty cycle over the range 4 KHz to 300 KHz, even though the average stripe temperature was the same in each case.

Miller [80] found that the duty cycle was the primary factor in a range of frequencies from 20 KHz to 250 KHz. He made a temperature correction to his data and concluded that lifetime enhancement was caused largely by some type of damage relaxation process, and not only by thermal enhancement of the type treated by Sigsbee and Davis. The lifetime with a 50% duty cycle was found to be 20 times larger than the DC lifetime. Miller's data followed the empirical relationship

$$t_{50} = B \cdot \exp(-M \cdot d), \quad (26)$$

where  $t_{50}$  was given in on-time hours, B and M were constants, and d was the duty cycle. He attempted to justify this relationship by invoking the concept of excess vacancy concentration and by postulating that this concentration rises during each pulse and falls during each off time between pulses according to an

exponential time dependence. Schoen [82] also developed a model that was based on an exponential decay of damage between pulses, in addition to a decrease in temperature, and found that Miller's data could be readily explained. These findings caused excitement in the research community, but such highly enhanced lifetimes have not been found by others without the presence of severe thermal effects.

Wu and McNutt [84] confirmed the role of thermal effects in producing extremely large lifetime enhancements, by extending the work of Miller. Their analysis was based on a quantity, similar to the vacancy supersaturation, which they called the "microscopic damage concentration." This quantity was assumed to attain some asymptotic value, which was said to depend on the pulse duty cycle and on the temperature-dependent characteristic rise and fall times of the damage concentration. By requiring that  $t_{50}$  be inversely proportional to the asymptotic damage concentration, the following expression was developed:

$$t_{50}(\text{pulsed}) = \left( \frac{F_r}{d} \right) \cdot t_{50}(\text{DC}), \quad (27)$$

where  $d$  is the duty cycle and  $F_r$  was called the "damage relaxation factor." The damage relaxation factor was defined as

$$F_r = 1 + \left( \frac{\tau_d}{\tau_r} \right) \cdot \left( \frac{1}{d} - 1 \right), \quad (28)$$

where  $\tau_d$  is the damage generation time constant and  $\tau_r$  is the damage relaxation time constant. These expressions were later re-examined by Suehle and Schafft and were found to be useful in explaining the current density dependences of pulsed electromigration [97].

In an attempt to clear up what they perceived as confusion in the research community over the roles of duty cycle and damage relaxation, English and Kinsbron [85] carried out a study in which the electromigration ion velocity was measured as a function of pulse duty cycle and frequency. They sought to avoid temperature excursions by keeping current densities below  $2 \times 10^6 \text{ A/cm}^2$ , and they employed test frequencies from 0.01 Hz to 100 KHz and duty cycles from 1.5% to 100%. Their test temperature was 362 °C. Oddly enough, their results indicated that the ion velocity, in terms of on-time, was the same regardless of frequency and duty cycle. They concluded that there was no damage recovery associated with the time between pulses.

It was already mentioned that some critical frequency might exist, below which the behavior observed by English and Kinsbron should occur. That is, an on-time dependence may be exhibited when the duration of each pulse exceeds the time necessary to produce unrecoverable damage. The transition frequency should be well below 100 KHz. An on-time dependence might also be favored whenever Joule heating is a factor and the pulse width is much larger than the thermal time constant of the test structure. The transition frequency in this case could be as high as 100 KHz, but English and Kinsbron conducted their study with the specific intention of avoiding thermal influences. The implications of their results are unclear.

The first demonstration of an average current density dependence was reported by Towner and van de Ven [86], who observed such a relationship at a frequency of 1 KHz with duty cycles of 25%, 50%, and 75%. They offered the

explanation that the aluminum atoms “experienced” only an average of the pulsed waveform rather than the individual pulses. Brooke [87] supported this view and also found an average current density dependence for aluminum alloy films stressed with a pulse frequency of 500 KHz.

It is not common to find explicit support of the idea that atoms do not experience each individual pulse, but the average current density model is widely supported by theoretical and experimental work. The research group headed by Cheung and Hu has published several papers [92,96,98,99,103,109,115,116] on electromigration under conditions of pulsed current, AC current, and arbitrary current waveforms. They have developed a model based on vacancy generation and recombination, which predicts a  $1/d^2$  dependence for pulsed stress currents. Of course, a  $1/d^2$  dependence is essentially an average current density dependence if the current exponent,  $n$ , in Black’s equation is equal to 2, as it is normally assumed to be. Their experimental data was in agreement with such a dependence, as well. Others who have developed theoretical predictions of a  $1/d^2$  dependence are Maiz [93], Clement [101,102], and Dwyer [117]. Maiz also presented supporting experimental data for a frequency around 1 MHz.

Hatanaka et al. also sought to use a relation like Equation (25). They obtained pulsed electromigration data for a frequency of 1 KHz, a current density of  $7.5 \times 10^5 \text{ A/cm}^2$ , and variable duty cycle. They compared their data with that of other researchers, who had utilized different current densities, and concluded that the exponent,  $m$ , in Equation (25) is a function of current density,  $j$ . Their own data yielded an  $m$  value of about 1.5, and they extracted  $m$  values from the

data of others as follows:  $m = 2$  for  $j = 1.7 \times 10^6 \text{ A/cm}^2$  (Wu and McNutt),  $m = 2$  for  $j = 2 \times 10^6 \text{ A/cm}^2$  (Towner and van de Ven),  $m = 3$  for  $j = 4 \times 10^6 \text{ A/cm}^2$  (Miller), and  $m = 7.5$  for  $j = 1 \times 10^7 \text{ A/cm}^2$  (Miller). The authors did not indicate whether they believed the current density dependence arose from thermal effects or damage recovery between pulses.

A numerical simulation was developed by Harrison [90]. He validated the simulation by comparing the results that it produced for various DC tests to those from well known experimental studies. Finding that the agreement was quite good, he then ran the simulation for pulsed current stressing. The simulation was run to generate resistance versus time plots for various combinations of duty cycle ( $d$ ) and peak pulse current density ( $j_p$ ) such that  $j_p = j_{dc}/d$ , where  $j_{dc}$  was equal to  $1 \times 10^6 \text{ A/cm}^2$ . The pulse frequency was not included explicitly in the model, but other factors, such as the thermal response, were formulated with the assumption that the frequency was higher than 1 MHz. Since the duty cycles and pulse amplitudes were chosen such that  $j_p = j_{dc}/d$ , the simulation would have been expected to produce resistance curves that fell on top of one another if the predicted behavior happened to follow an average current density dependence. This was not the case, however. Although the curve for a 50% duty cycle was quite nearly the same as the DC curve, an increasing deviation toward shorter lifetime was found with decreasing duty cycle below 50%. The implication of the results was that a pulsed current cannot be adequately represented by a DC current equal to the pulsed waveform average, especially for small duty cycles less than 50%.

Hummel and Hoang [95] chose to modify Black's equation in a manner that was different from that attempted by most others. Instead of looking for an appropriate value for  $m$  in Equation (25), they added a second term to account for damage relaxation between pulses. The resulting equation therefore had two terms, one for damage generation during on times and the other for damage recovery during off times. They assumed that damage recovery took place by normal diffusion of vacancies. The expression appeared as

$$t_{50} = \frac{A}{d \cdot J^n} \exp\left(\frac{Q}{kT_0 \exp(\beta d)}\right) + BD \frac{1-d}{f}, \quad (29)$$

where

- $T_0$  is the ambient temperature,
- $\beta$  is a constant which is determined from a DC experiment,
- $B$  is an adjustable constant,
- $D$  is the diffusion coefficient for the given material,
- $f$  is the pulse repetition rate or frequency,

and the other quantities have their usual meaning. The quantity  $T_0 \exp(\beta d)$  was supposed to approximate the test stripe temperature in view of possible Joule heating. It is instructive to realize that the quantity  $(1-d)/f$  is just the off time between pulses. Hummel and Hoang were able to demonstrate that this model approximated their data quite well for a frequency of 10 KHz and duty cycles of 50% and 75%, but the proposed frequency dependence was not investigated.

The idea that "damage" can be partially recovered during the off times between pulses is not universally accepted. Whether those differing opinions are based on the belief that an on-time dependence is followed exclusively and any lifetime enhancement is due to reduced Joule heating or the belief that the atoms only experience an average of the pulsed waveform is not always clear.

Disputes may sometimes be due simply to a lack of agreement on the language to be used. For example, it is common to hear interchangeable use of the terms "recovery," "relaxation," and "healing," even though these may be thought of as different concepts by some researchers. Also, a vacancy concentration gradient may not be called "damage" by some. Several papers have appeared with the primary goal of revealing just what types of recovery, relaxation, and/or healing may actually occur [88,89,104,105,107,111,114]. Typically, such studies have involved the observation of test stripe resistance after the removal of a stress current which had previously induced some level of resistance increase.

Lloyd and Koch [88,89] performed a study of resistance increase and decay. They found that the resistance increase during current stressing was essentially linear in time, and, when the current was interrupted, the resistance was seen to decrease exponentially. This decrease seemed to reflect more than one time constant -- one on the order of seconds or minutes and several others on the order of hours. Lloyd and Koch offered a qualitative explanation for the behavior. They contended that the resistance increase was due to the formation of various defects at a rate proportional to the level of vacancy supersaturation. The damage kinetics were said to depend only on this supersaturation. The resistance decrease, however, was said to be more complex. They attributed the small time constant to the decay of vacancy supersaturation and the other, longer time constants, to various processes, such as void coalescence and the relaxation of dislocation loops.



Li et al. [104] also performed resistance studies. They based their analysis on the mechanical stresses which are known to arise during current stressing. They maintained that the resistance increases as a result of the voids that must form when mechanical stresses rise above the yield stress of the given material (aluminum alloy in their study). Some portion of the resistance increase was said to be recovered by stress relaxation when the stressing current was interrupted, and, if the resistance increase was very small (on the order of 0.1%) the resistance could return completely to its pre-stress value. An interesting conclusion posed by the authors was that the speed of these stress related processes are such that "healing" behavior would not be exhibited during pulsed current stressing unless the frequencies were quite low (about  $10^{-3}$  Hz). They said that any apparent healing effects at higher frequencies must be due to "unusual microstructural conditions."

Hinode et al. [105] reported an exponential decay of resistance upon removal of the stressing current, just as Lloyd and Koch had, and also noted that the decay appeared to contain more than one characteristic time. The authors discounted the concept of vacancy supersaturation, however, and attributed the resistance decay to stress relaxation.

Baldini et al. [107] addressed the concept that only an increase in the residual resistivity can decay upon removal of the stressing current. Any resistance increases that happened to be related to geometrical changes were said to be permanent. They assumed that the decay of residual resistivity was driven by stress relaxation.

Experiments performed by Ohfuji and Tsukada [111] revealed that resistance decay was the result of several processes, whose activation energies ranged from 0.5 to 1.1 eV. They cited, in addition to the decay of vacancy supersaturation, such processes as the relief of mechanical stress, the motion of dislocations, and the dissociation of vacancy-hydrogen complexes.

An interesting study related to stress driven recovery was performed by Frankovic et al. [112,113]. Their work was based on the critical length - current density concept originated by Blech [67,78]. Blech demonstrated experimentally that compressive stresses are built up by the accumulation of material in the downwind portion of an interconnect during the course of electromigration. This stress is the driving force for a backflow of material. It was determined, for a given length of conductor, that there is some minimum current density below which the backflow will prevent any net forward flow. The shorter the conductor length the larger is this critical current density. In fact, it was found that the product of the length and the critical current density was a constant, other things being equal. Of course, it is equivalent to say, for a given current density,  $j$ , that there is some critical length below which a net flow does not occur. This critical length,  $l_c$ , has become known as the "Blech length." The work of Frankovic et al. revealed, for a pulse frequency of 100 KHz, that the  $j l_c$  product increases as the pulse duty cycle is decreased. That is, for a given current density, the Blech length becomes larger with decreasing duty cycle. It was suggested that this renders more of the interconnects of an IC immune to electromigration damage.

Studies of pulsed electromigration have generally been performed for frequencies no higher than 1 MHz, and most have not exceeded 100 KHz. There are two exceptions to this rule. Kwok et al. [100] investigated frequencies up to 200 MHz, and Pierce et al. [110] employed frequencies up to 500 MHz. Both investigations were performed on aluminum test structures. The work of Kwok et al. covered only a narrow range of frequencies from 50 to 200 MHz. They found no clear dependence of  $t_{50}$  on frequency in this range. In the range from 50 to 100 MHz, they found that  $t_{50}$  increased as  $(t\text{-off})^{2.2}$  and decreased as  $(t\text{-on})^{-0.7}$ . At a fixed frequency of 50 MHz,  $t_{50}$  exhibited a  $1/d^{2.7}$  dependence. Pierce et al. investigated the frequency dependence from DC to 500 MHz for a duty cycle of 50%. The temperature for their test was 412 °C and the peak current density was  $4 \times 10^6$  A/cm<sup>2</sup>. They observed a transition from an on-time dependence to an average current density dependence at a frequency of about 1 to 10 MHz. The behavior was attributed to anomalous thermal effects rather than a characteristic vacancy relaxation time. They also studied duty cycle effects for two frequencies -- 10 KHz and 200 MHz. The data at 200 MHz followed a  $1/d^2$  dependence down to the lowest duty cycle tested, which was 25%. At 10 KHz, an on-time dependence was exhibited down to a duty cycle of 50%, but some enhancement (less than that at 200 MHz) was observed at lower duty cycles. The difference in the results for 200 MHz and 10 KHz were again attributed to anomalous thermal effects.

### Summary

A foundation has been laid in this chapter, which serves as a reference for the remainder of the dissertation. The essential principles of electromigration were discussed, and, in that context, a comprehensive review of prior research was presented.

The unfinished nature of pulsed electromigration research has been revealed. The duty cycle dependence, in particular, is not consistently reported in the literature. The interpretation of many studies is probably complicated by the difficulty in discerning the effects of damage recovery processes and thermal effects. Dependences on duty cycle, reported in the literature, range from  $1/d$  to  $1/d^{7.5}$ . In addition, most studies have been limited to pulse frequencies no higher than 1 MHz. Today's digital circuits are pushing into the hundreds of megahertz range, so there is a technological need to investigate such frequencies. Two previous studies have been devoted to very high frequencies, but the study of Kwok et al. was limited to a narrow range of frequencies, and the study of Pierce et al. was affected by thermal anomalies. Further, the results of the two studies were not in agreement. Kwok et al. reported a  $1/d^{2.7}$  dependence on duty cycle, and Pierce et al. reported a  $1/d^2$  dependence.

The present study was performed to clarify the effects of frequency and duty cycle on pulsed current electromigration. The intention was to contribute to the body of scientific knowledge and to meet a technological need. The next chapter proceeds with a discussion of the experimental setup and procedure.

## SETUP AND PROCEDURE

### Overview

This work was performed to expand the understanding of pulsed current electromigration in the regime of very high frequency. Experimentation toward this end required the selection of appropriate methods to induce and measure the electromigration process, the construction and use of appropriate test samples, and the selection of useful means to analyze the results.

### Test Apparatus Performance Goals

The first stage of the work was the design and construction of an apparatus for subjecting test samples to the desired range of treatments. Since the goal was to conduct accelerated lifetests, the apparatus had to be capable of subjecting samples to very high current densities at elevated temperatures. The most important aspect of the design process was the need for delivering currents pulsed at very high frequencies and small duty cycles. Consideration of these requirements led to the following design goals:

1. Pulse current density: up to  $1 \times 10^7$  A/cm<sup>2</sup>
2. Pulse repetition rate: DC to 200 MHz
3. Pulse duty cycle: 15% to 85%, 100%
4. Stripe temperature: up to 220 °C

It was found that these goals are not trivial. The design and construction of the apparatus was a significant task.

For any set of treatment conditions, it was necessary to measure the response of each sample. The test apparatus had to provide for any such measurements to be made *in situ*. Other post-test measurements or analyses could be considered separately. The *in situ* response of the following sample properties was monitored:

1. Electrical resistance
2. Life status (has the sample "failed"?)

Again, the type of reliability test that was used in this work was essentially a life test. In this context, the electrical resistance was monitored as a measure of electromigration damage, and "failure" could be identified by any agreed upon increase in resistance.

Electromigration-induced damage morphology was also a measurement of interest. The test apparatus provided no means of making such observations *in situ*, but they could be made at some later time, after the test samples were removed from the apparatus.

The test apparatus required, therefore, a means for generating a pulsed current waveform whose attributes (frequency, amplitude, etc.) could be varied across the desired test range. The waveform had to be transmitted to and distributed among multiple test samples, each sample being held at an elevated temperature. An *in situ* measurement of the electrical resistance of each sample was required, and, for purposes of lifetime analysis, it was necessary to provide some means for identifying and recording failures. A full description of the test apparatus circuitry is deferred to the APPENDIX, but some comments about the design philosophy are presented in the next section.

### Design Issues

One of the most basic requirements in RF/microwave circuit design is good impedance matching. This demands that the load impedance seen along all branches of the circuit, including the input/output impedance of any pulse generators, amplifiers or other active devices in the wave path, be the same as the characteristic impedance of the transmission lines comprising those branches. If any load seen by the waveform is not impedance-matched to the transmission line, then the pulse power is not fully dissipated in the load and a reflection is sent back up the line. In addition to the partial loss of power delivered to the load, this will often cause a distortion of the waveform along the line as multiply reflected waves interfere. A standing wave is set up on the transmission line, and the measured waveform will depend on the position of the measurement along the line. This latter point is especially critical in the present application because the test stripes must be held at an elevated temperature inside a furnace, so the waveform cannot be measured directly at the stripe. A measurement has to be taken somewhere along the transmission line outside the oven, and the only condition for which this remote measurement will provide an accurate account of the waveform across the test stripe itself is if reflections are avoided.

The characteristic impedance for an ideal transmission line is normally taken to be real, even though, in general, impedance is a complex quantity composed of a resistive part (real) and a reactive part (imaginary). The reactive quantity (composed of inductance and capacitance) is frequency-dependent, but

the resistive quantity is not. The simplest case to handle, therefore, is that in which the load is purely resistive, with the resistance being equal to the characteristic impedance of the transmission line. For this case, frequency is not an issue. In real cases, however, the load is not perfectly resistive. It will always have some inductance associated with its length, for example, and the resulting frequency-dependent reactance becomes more significant with increasing frequency. This increasingly significant reactance leads to increasing mismatch, so it is more difficult to faithfully distribute a waveform the higher its frequency.

Because of this frequency-sensitive matching issue, the task of delivering, to a load, a current waveform pulsed at repetition rates as high as 200 MHz, with duty cycles down to 15%, is not a simple task. Microwave design techniques must be employed. This generally involves laying circuits out on good printed wiring boards and paying close attention to all inductance, capacitance and resistance which will affect the accurate delivery of the waveform to the load. Signals are carried on printed wiring boards by microstrip distribution lines and between boards by good coaxial cable. Surface mount components are employed in order to keep lead lengths short.

Impedance matching can generally be accomplished if, in addition to good circuit design, the appropriate components are available and sufficient care is given to the layout to reduce stray effects. The primary impediment to achieving a matched system in this work was the load, that is, the test sample itself. The sample consists of a patterned thin film metal stripe, called a test



stripe, which is integrated onto a silicon chip using standard IC lithography techniques. When the test chip was mounted in a standard dual-in-line package (DIP) and wired-up with bondwires of typical length, the series inductance due to the bondwires introduced enough of a reactive component to cause a significant mismatch for frequencies on the order of 100 MHz. Lower frequency waveforms, perhaps less than 10 MHz, were not seriously affected. It was eventually found that when the chip was mounted in a special power DIP as close as possible to the lead-outs, so that the bondwires could be very short, then the waveform was acceptable even at 100 MHz, so long as the DC resistance was close to  $50\ \Omega$  at test temperature, which corresponds to the characteristic impedance of the transmission cables. The problem of sample-induced mismatch is noted here, because a different sample packaging scheme will probably be required if test frequencies approaching 1 GHz are eventually desired. An alternative route is to put the pulse generating circuitry on the chip with the test stripe. This has been tried by others, but with erratic success.

Keeping the pervasive requirement of impedance-matching in mind, it was then possible to select a strategy for producing a current pulse, delivering it to several samples held at high temperature, and monitoring the response of those samples. It was decided that the current waveforms would be generated with a commercial function generator and that the test samples would be held inside a temperature-regulated furnace. The methods of waveform distribution and test stripe monitoring are the heart of the design. The next section summarizes the essential features of this design, and full details are provided in the APPENDIX.

### Summary of Test Apparatus

The test apparatus was designed to run 24 samples at a time. The flow chart of Figure 15 depicts, in basic form, the major functional blocks comprising the circuitry for one sample. It is shown that the test current waveform originates from a pulse generator and is then divided into N branches (channels) with a resistive power divider. In the case that all 24 samples are run off of one pulse generator, N is equal to 24. The system makes use of three pulse generators, however, so the samples were placed in groups of 9, 9, and 6. Only one of the groups is depicted in Figure 15, but the flow chart is applicable to any of the three groups. After the power divider breaks the signal into the appropriate number of branches, the pulse amplitude is adjusted on each individual channel with a voltage variable attenuator. The power lost in the divider and attenuator is recovered through one or more amplifiers before the pulse is delivered to the test stripe fixture. Since the pulse path is AC coupled to the test stripe, a DC offset circuit must be included if anything other than a bidirectional pulse is desired. For example, when the duty cycle is 50%, a positive DC voltage equal to one-half the peak-to-peak AC voltage must be added in order to produce a positive pulse train. A computer-based data acquisition system monitors the resistance (actually it monitors a pair of voltages which are used to calculate the resistance) and life status of the test stripes. This system was added as a second generation modification, and the original method of monitoring the samples was kept in place. This method relies on a comparator-switched elapsed time indicator circuit which senses the DC voltage across the test stripe.

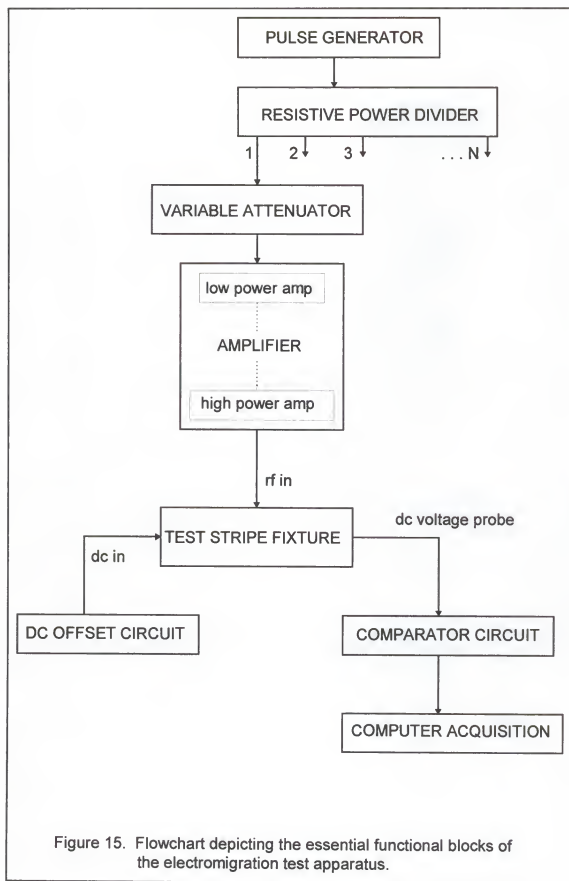
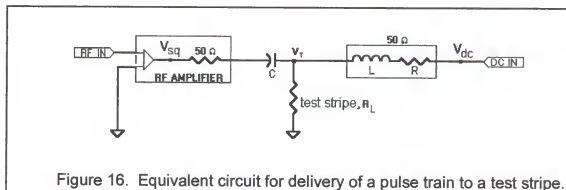


Figure 15. Flowchart depicting the essential functional blocks of the electromigration test apparatus.

Since this voltage depends on the stripe resistance, the circuit can be used as a sensor for the stripe resistance and can be set to "turn off" when it senses a resistance at or above the predefined "failure" resistance. The elapsed time indicator thus records the stripe "lifetime." The comparator/elapsed time indicator circuit only records the lifetime, it does not log the resistance versus time as the computer-based data acquisition system does.

The test stripes were kept at the desired ambient temperature by holding them in a temperature-regulated furnace. All circuitry remained outside the furnace, so the pulsed current had to be carried to the test stripes by way of coaxial cable. The cable was fed through the front panel of the furnace.

The RF amplifiers that are used to regain power on each branch do not operate as constant current sources or as constant voltage sources, so the pulse amplitude changes as stripe resistance changes. Figure 16 illustrates the effective circuit by which an AC-coupled squarewave and a DC offset are delivered to a test stripe so as to obtain a positive pulse train of peak voltage  $V_T$ .



The test stripe is represented by the resistor,  $R_L$ . The output of the RF amplifier behaves as though it is derived from a squarewave of constant peak-to-peak

voltage,  $V_{sq}$ , applied to a  $50\ \Omega$  output resistor. So, the squarewave that appears across the test stripe has a peak-to-peak voltage  $V_T$ , where

$$V_T = \frac{R_L}{R_L + 50} \times V_{sq} . \quad (30)$$

This squarewave arrives at  $R_L$  through the capacitor,  $C$ , so it is bidirectional. The DC offset circuit serves to raise the squarewave by an appropriate DC voltage to produce the desired unidirectional pulse. The DC offset voltage is derived from a constant voltage,  $V_{dc}$ , applied to an output resistance (composed of an inductor and a resistor) of  $50\ \Omega$ . This design keeps the baseline at zero as the stripe resistance changes during the course of a test. Since the peak pulse current changes over the course of a test, quoted test currents refer to current at time zero.

It is noteworthy that the peak pulse current does not remain constant as electromigration damage proceeds in the present test apparatus. It is more common, in practice, to apply a constant current. With a constant current, the areas of the test stripe that remain undamaged at any given moment experience the same current density that they experienced at the start of the test. Those localized areas where damage has occurred at any given moment probably show that damage in the form of decreased cross-sectional area. So, the current density increases at these locations quite severely. With the system used here, such a localized increase in current density still takes place, and the magnitude of this effect is expected to be significantly greater than the effect of

the decreasing current density in nondamaged areas. This issue is discussed more in the APPENDIX.

### Test Stripes

This work was meant to have implications directly applicable to industry. The electromigration test structure was therefore designed to be representative of an IC interconnection that could be found in practice. It was constructed by a leading U.S. manufacturer of integrated circuits, using standard CMOS process technologies. In addition to the standard Al(Cu) alloy, which was the primary conductive component, the test stripe incorporated a Ti/TiN barrier layer and a TiN anti-reflective coating. The cathode end of the stripe was contacted to an  $n^+$ -doped silicon well by way of a tungsten plug. Such a contact structure was discussed in the BACKGROUND, where it was characterized as a structure with important reliability implications for modern technologies.

The test stripe configuration is illustrated in Figure 17. It was 0.9  $\mu\text{m}$  wide and 300  $\mu\text{m}$  long. The thickness of the Al(Cu) layer was 0.6  $\mu\text{m}$ . The Ti/TiN barrier layer, which was placed below the Al(Cu) layer, was 0.07  $\mu\text{m}$  thick. The TiN anti-reflective coating, which was placed on top of the Al(Cu) layer, was less than 0.05  $\mu\text{m}$  thick.

Each test stripe was integrated, in conventional form, onto a silicon chip, which was then mounted in a dual in-line package (DIP). Each DIP was plugged into a panel on the inside of a temperature-regulated furnace. The pulsed test current was delivered through the panel to the DIP, and on to the test stripe by

way of standard IC bondwires attached to large bond pads at the ends of the stripe. The bond pads are depicted in Figure 17, as is the pulse polarity.

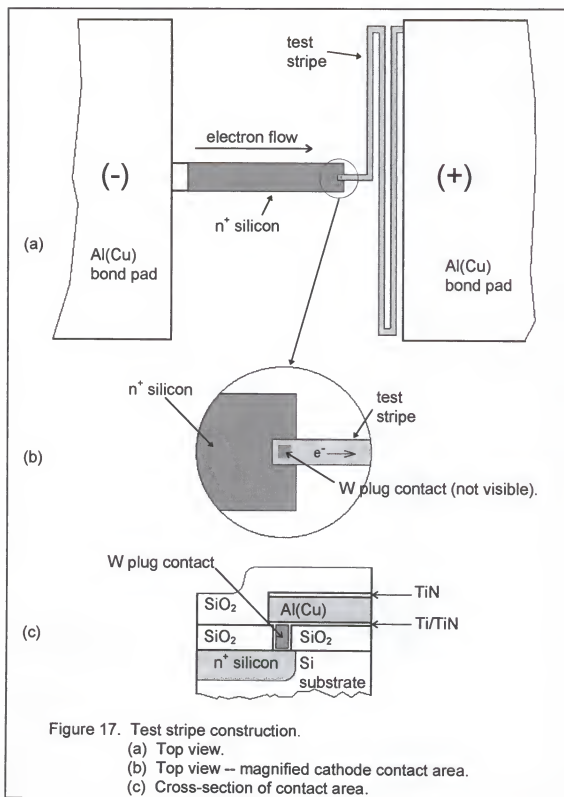


Figure 17. Test stripe construction.

(a) Top view.

(b) Top view -- magnified cathode contact area.

(c) Cross-section of contact area.

### Test Procedure

After loading a group of test stripes into the furnace, the temperature was raised to 100 °C. A program was then run whereby the temperature was raised further in 10 degree intervals, with resistance measurements being made at each interval, up to a final temperature of 200 °C. The resulting resistance versus temperature data could then be used to estimate any Joule heating that arises under test powering. After this preliminary step, the desired pulse conditions, as measured with a 6 GHz digitizing oscilloscope, were set up on the test stripes at 200 °C. A program was then started to take and log resistance measurements at 12-minute intervals for the duration of the test. This accumulated resistance versus time data forms the basis for all subsequent analysis and comparison. The lifetime of a test stripe can be defined as the test time needed for its resistance to increase by a certain percentage. Any such percentage may be agreed upon, so long as it is used consistently throughout all comparisons.

### Data Gathering and Analysis

The raw data was gathered in the form of stripe resistance ( $R$ ) versus time, but its interpretation as lifetime data requires that "failure" be defined as some percentage increase in stripe resistance. Such a percentage increase is more readily identifiable on a graph if the resistance divided by the starting resistance ( $R/R_0$ ) is plotted versus time rather than the resistance itself, so the



DAQ system was made to generate an R/Ro versus time file in addition to an R versus time file for each test stripe.

Any value of R/Ro can be used to define failure. Since an R/Ro versus time file was available for each sample at the conclusion of a test, the failure criterion could be defined at any time before or afterward. It was only necessary to make sure that any given test was run for a sufficient length of time that any particular R/Ro value that was likely to be decided on afterward was actually recorded in the R/Ro versus time file of every sample (or most of them).

Having the R/Ro versus time files in hand for a given test run, and having decided on a failure criterion, the time to failure could be determined for each test stripe of that run. The median of these failure times,  $t_{50}$ , was then estimated. This quantity was discussed in the BACKGROUND as a commonly used measure of electromigration reliability and basis of comparison between test variations.

The expected median time to failure can be estimated graphically. This starts by assuming (because it is usually true) that stripe failure times obey a lognormal distribution. With this assumption in mind, the failure times are ranked in ascending order and plotted according to rank on a probability axis. The time axis can be logarithmic, or it can be linear if the log-times are plotted. If a straight line is fitted to this plotted data, then  $t_{50}$  is given by the intersection of this line with the 50th percentile on the probability axis.

If it is true, however, that the failure times are distributed lognormally, the mean of the log-times is equal to the median of the log-times. So, if the mean of

the log-times is determined,  $t_{50}$  is the inverse log of that value. This is also a legitimate method for estimating  $t_{50}$ .

### Test Conditions

For all tests, the samples were held at an ambient temperature of 200 °C inside a temperature-regulated furnace. The starting pulse amplitude was 15 mA ( $j = 2.7 \times 10^6 \text{ A/cm}^2$ ) for all duty cycles and frequencies, and it was also 15 mA for the DC test. It was found that Joule heating causes an apparent temperature rise of ~ 5 degrees. The term "apparent" is used here because the estimated temperature rise was based on the current-induced increase of the total stripe resistance. This resistance rise was tacitly assumed to be uniform, even though it may very well be localized, and if it is localized, then the local increase in temperature is more than 5 degrees.

One way that a pulse train may be characterized is by frequency and duty cycle. Another is by pulse length (on-time) and pulse separation (off-time). One is equivalent to the other. A nomenclature was devised to identify each set of test conditions used in this work. This is illustrated through example, as follows, for the set of conditions labeled P133M50:

- "P" indicates pulsed current,
- "133M" indicates a frequency of 133 MHz,
- "50" indicates a duty cycle of 50%.

Table 1 is a list of the pulse treatments that were studied. A look at this table reveals that the test frequency was divided into three distinct ranges. The highest of these was on the order of 100 MHz. The middle range was on the

order of 1 MHz, and the lowest range was roughly 100 KHz. Duty cycles ranged from 33.3% to 100%. The duration of a test run depended heavily on the duty cycle. The shortest test was two weeks and the longest exceeded three months.

Table 1. Pulse treatments used for this study. Pulse trains are characterized by their frequency and duty cycle or by their pulse length ( $t_{on}$ ) and pulse separation ( $t_{off}$ ).

LABEL	FREQUENCY	DUTY CYCLE	$t_{on}$	$t_{off}$
P133M77	133 MHz	77%	5.775 ns	1.725 ns
P133M67	133 MHz	66.7%	5 ns	2.5 ns
P133M50	133 MHz	50%	3.75 ns	3.75 ns
P133M33	133 MHz	33.3%	2.5 ns	5 ns
P067M67	66.7 MHz	66.7%	10 ns	5 ns
P050M50	50.0 MHz	50%	10 ns	10 ns
P1_60M80	1.60 MHz	80%	500 ns	125 ns
P1_33M67	1.33 MHz	66.7%	500 ns	250 ns
P001M50	1 MHz	50%	500 ns	500 ns
P667K33	667 KHz	33.3%	500 ns	1000 ns
P667K67	667 KHz	66.7%	1000 ns	500 ns
P500K50	500 KHz	50%	1000 ns	1000 ns
P160K80	160 KHz	80%	5000 ns	1250 ns
P133K67	133 KHz	66.7%	5000 ns	2500 ns
P100K50	100 KHz	50%	5000 ns	5000 ns
P133K33	133 KHz	33.3%	2500 ns	5000 ns
P050K50	50 KHz	50%	10000 ns	10000 ns
DC	DC	100%	always on	never off

## RESULTS AND DISCUSSION

### Overview

The experiments that were performed in this study center primarily around the acquisition of electrical resistance data. Resistance change can be used as a convenient *in situ* indicator of the morphological progressions experienced by a test stripe during the course of an electromigration test. There are at least two possible approaches in the use of such data. The most common is to treat the stripe resistance as a measure of life status, for which a particular value of  $R/R_o$  indicates "failure." The median time to failure,  $t_{50}$ , is determined for each group of test subjects, and  $t_{50}$  becomes the measure by which various test treatments are compared. This is a common approach and is relied on heavily in this work. Another approach may be to evaluate the whole course of resistance change for each test stripe as it evolves over the duration of a test. In other words, the whole resistance versus time plot may be evaluated as a unit. If any particular feature in the plot can be correlated to specific morphological progressions, it may be used as a basis of comparison.

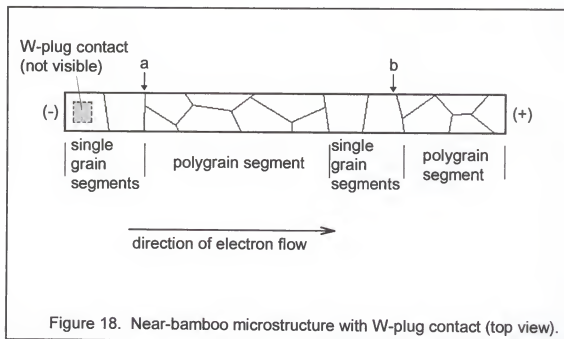
Correlation of specific damage features with  $R/R_o$  behavior and/or treatment conditions requires some kind of physical inspection of the test subjects. The goal may be visual evaluation, chemical analysis, or structure

analysis. The goal in this work was visual inspection, which was provided by optical microscopy and scanning electron microscopy (SEM).

### Resistance Plots and Optical Micrographs

Electrical resistance was monitored *in situ* only as a means to determine when a test had progressed sufficiently. The  $R/R_o$  information was downloaded and optical micrography was performed after the completion of each test run.

In evaluating the optical micrographs, the location of void formation is the most readily obtainable piece of information. It has been suggested by others that the tungsten plug contact will be the weak link in any interconnect structure that incorporates it. So, it is natural to look for any confirmation of this. Before expecting any such confirmation, however, it is useful to recall other relevant features of the test stripe that may influence failure behavior. In part, Figure 18 will be utilized for this purpose. The test stripes were  $0.9\ \mu\text{m}$  wide and  $0.6\ \mu\text{m}$



thick. They likely have near-bamboo grain structures similar to that depicted in Figure 18. This estimate was made in consideration of the stripe thickness and width, along with the knowledge that the grain size of a thin film is approximately equal to the thickness of the film.

A near-bamboo structure consists of a mixture of single grain segments and polygrain segments. If a test stripe would just happen to have a single grain segment over the tungsten contact, like that depicted in Figure 18, then material would have to migrate through the lattice of that segment for damage to occur at the contact. Such migration would be relatively slow, but the flux divergence at the contact interface would be severe and would encourage void formation. Of course, a polygrain segment may lay above the contact and might promote faster void formation. Significant structural gradients also exist at the upwind edges of the two polygrained segments (marked "a" and "b" in the figure). Grain boundary migration might lead to material depletion at these locations, as well, so it can be reasoned that damage need not be confined to the tungsten plug. The outcome should be determined by the sizes of the polygrain segments and the densities of grain boundaries in those segments, and whether a single grain segment or a polygrain segment lay above the contact.

Figure 19 is a top view, low magnification (~500X) optical micrograph of a test stripe. Its appearance is essentially the same as the depiction of Figure 17. It is included here as a frame of reference to the more highly magnified post-test micrographs that are presented shortly. The stripe is covered with a passivation coating, but it was not necessary to deprocess the chip in order to make optical

observations. Visible in Figure 19 are the serpentine test stripe, the  $n^+$ -silicon well to which the stripe makes contact, the two bond pads, and the foot of each bond wire lead. Recall that the  $n^+$  well is on a level below that of the stripe, and the stripe makes contact to it by way of a tungsten plug, which passes through a via in the dielectric (Figure 17(c)). In concurrence with Figure 17(a), the polarity of the applied current pulses was such that electron flow was from left to right in all experiments. Electromigration damage was therefore expected to take place somewhere near the left end of the stripe, near the tungsten contact.

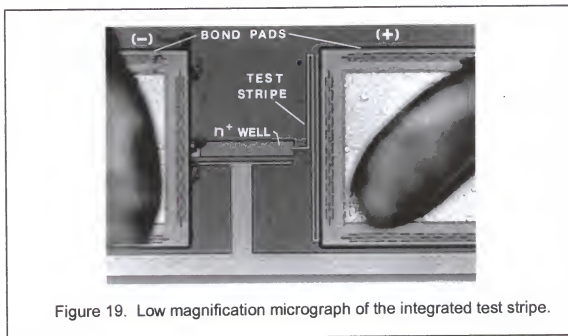


Figure 20 presents a number of histograms that depict the frequency of void occurrence according to position on the test stripe. The data for this figure were extracted from Figures 21 through 38, which contain, for each combination of pulse frequency and duty cycle, the post-test optical micrographs ( $\sim 1000\times$ ) and the corresponding  $R/R_o$  versus time plots for all of the tested stripes. Only

the cathode end of the test stripe is within the field of view in each micrograph, and the damage is pointed out by arrows. Occasionally, a tested stripe was not observable for one reason or another, so a few micrographs are missing. The damage histograms were generated by counting, for each predefined increment of distance from the cathode end, the number of test stripes for which damage was observed within that increment. Part (a) of Figure 20 defines the increments used, and Part (b) presents a cumulative count for all test stripes, from all stress treatments.

Figure 20(b) reveals that damage occurred most frequently within the 1st and 2nd increments. Evidently, the contact interface is, indeed, a limiting factor. Even so, some damage was observed several increments away from the contact. Parts (c) - (h) of Figure 20 display the normalized damage count versus distance from the cathode end for each of the test duty cycles -- 33%, 50%, 66.7%, 77%, 80%, and 100% (DC). The normalized count is, for each increment of distance, the number of damage counts registered in that increment divided by the total number of counts registered for the specified duty cycle, multiplied by 100 to obtain a percentage.

Two regimes are evident in Figure 20. Parts (f) - (h) show that damage is confined almost exclusively to the 1st and 2nd increments for duty cycles equal to and greater than 77%. Parts (c) - (e) show that the damage was more broadly distributed for duty cycles equal to and less than 66.7%. Every occurrence of damage beyond the 9th increment was found in the groups of stripes tested with a pulse duty cycle of 33%.



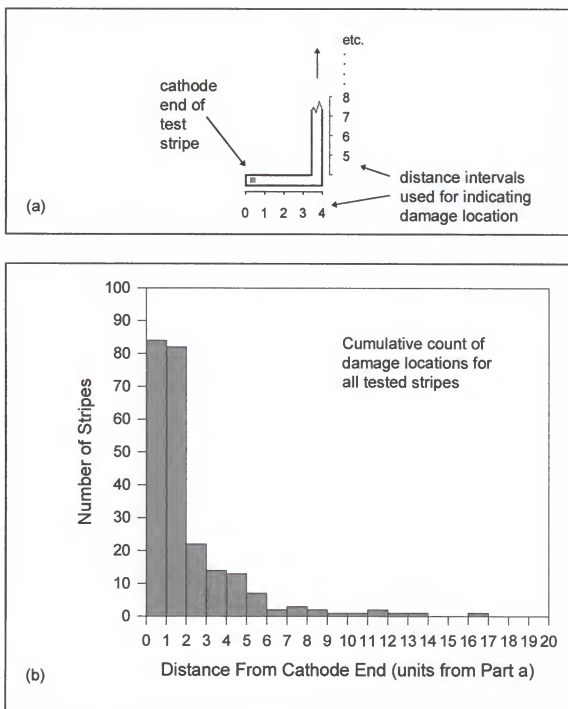


Figure 20. Location of test stripe damage.

- (a) Depiction of the cathode end of a test stripe and the distance intervals used to define damage location.
- (b) Cumulative count of damage observations for all tested stripes.

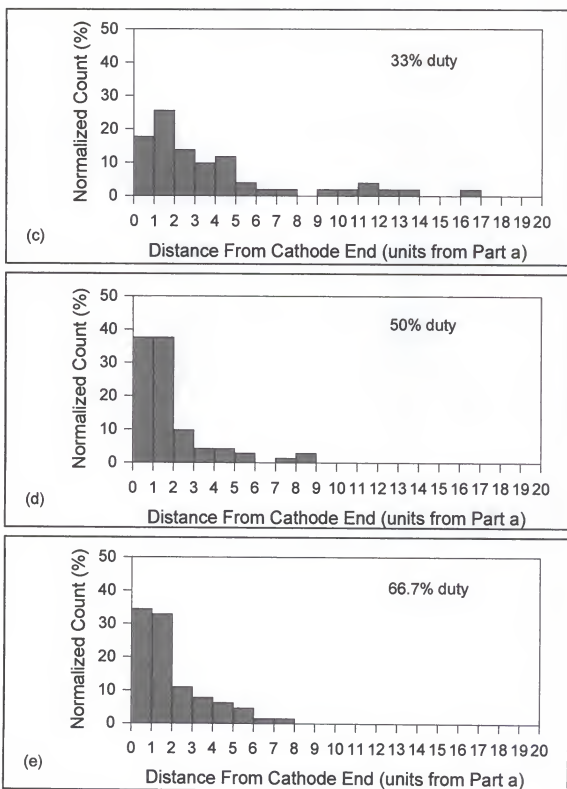


Figure 20 -- continued.

(c) Distribution of damage vs. position -- 33% duty cycle.

(d) Distribution of damage vs. position -- 50% duty cycle.

(e) Distribution of damage vs. position -- 66.7% duty cycle.

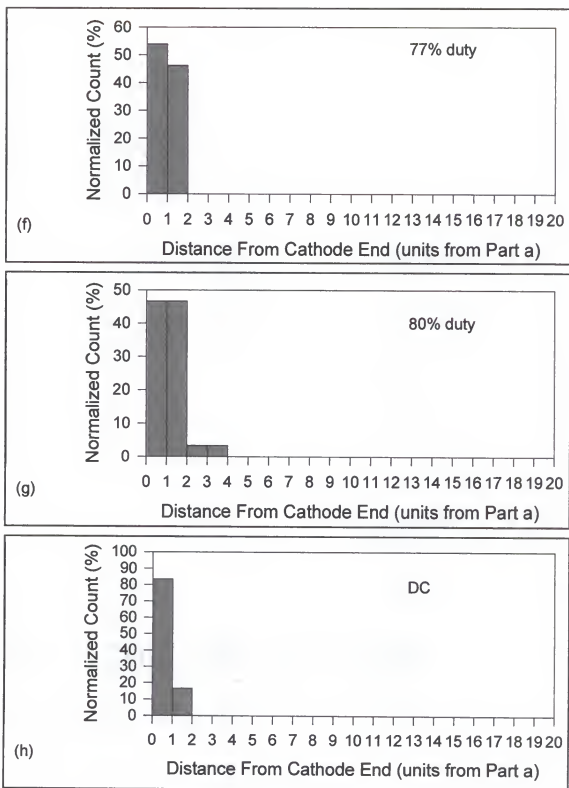


Figure 20 -- continued.

(f) Distribution of damage vs. position -- 77% duty cycle.

(g) Distribution of damage vs. position -- 80% duty cycle.

(h) Distribution of damage vs. position -- DC.

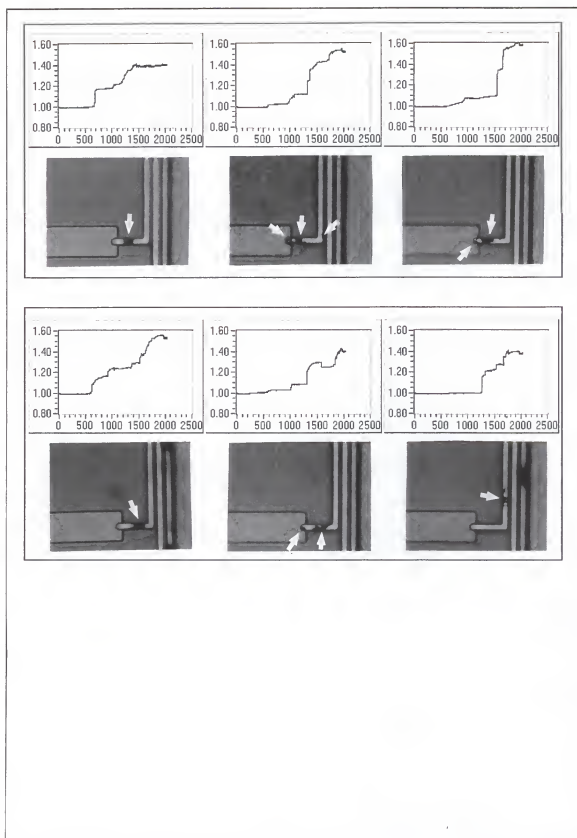


Figure 21. R/Ro vs. time (h) plots and optical micrographs for each test stripe of test lot P133K33 -- 133 KHz, 33.3% duty.

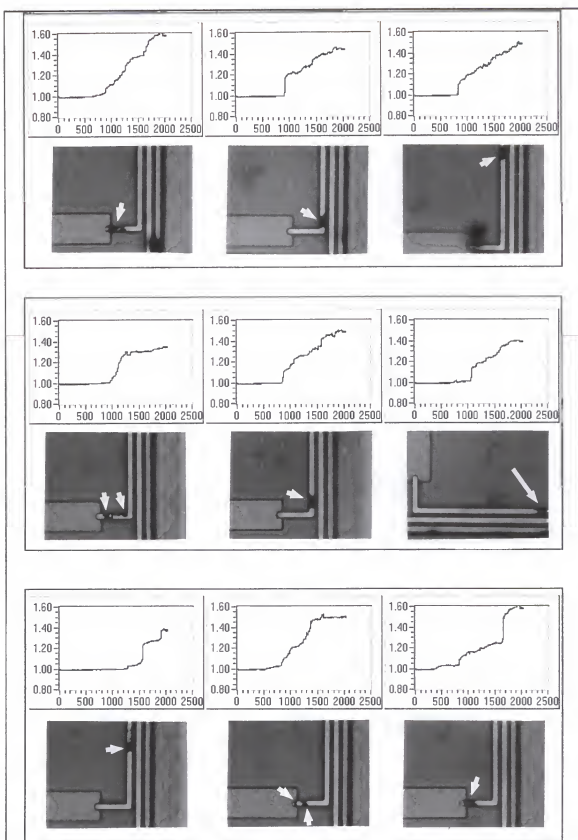


Figure 22. R/Ro vs. time (h) plots and optical micrographs for each test stripe of test lot P667K33 -- 667 KHz, 33.3% duty.

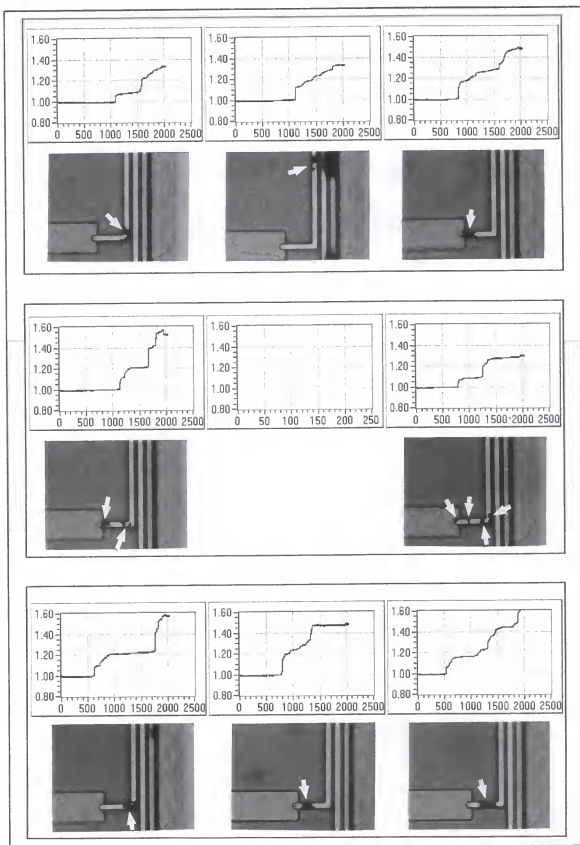


Figure 23. R/Ro vs. time (h) plots and optical micrographs for each test stripe of test lot P133M33 -- 133 MHz, 33.3% duty.

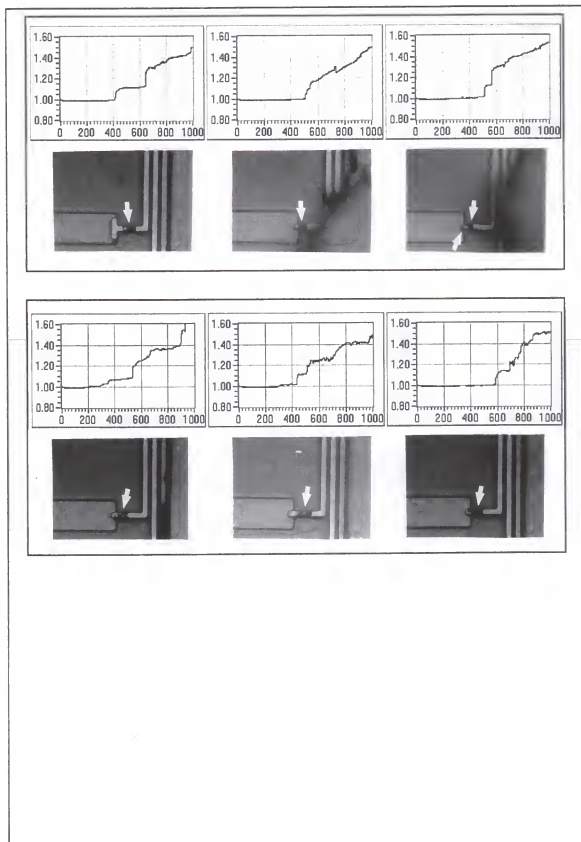


Figure 24. R/Ro vs. time (h) plots and optical micrographs for each test stripe of test lot P050K50 -- 50 KHz, 50% duty.

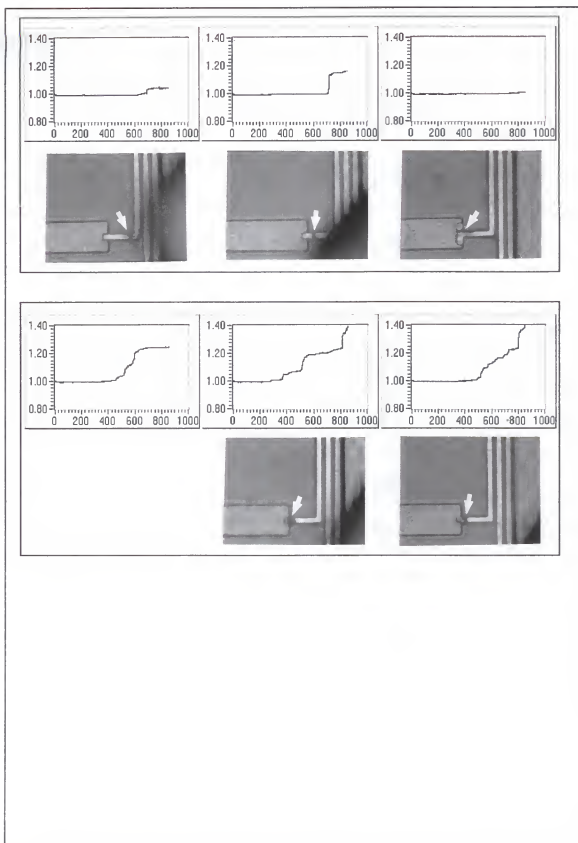


Figure 25.  $R/R_o$  vs. time (h) plots and optical micrographs for each test stripe of test lot P100K50 -- 100 KHz, 50% duty.



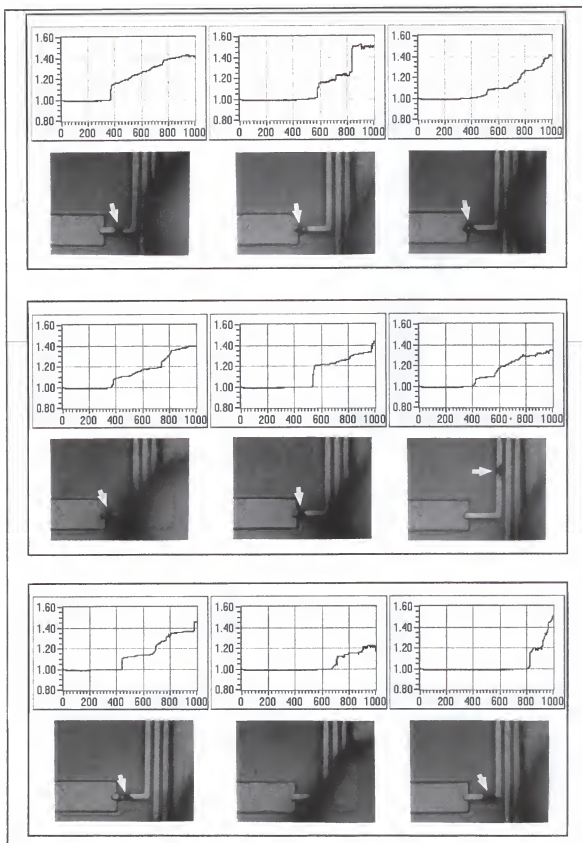


Figure 26. R/Ro vs. time (h) plots and optical micrographs for each test stripe of test lot P500K50 -- 500 KHz, 50% duty.

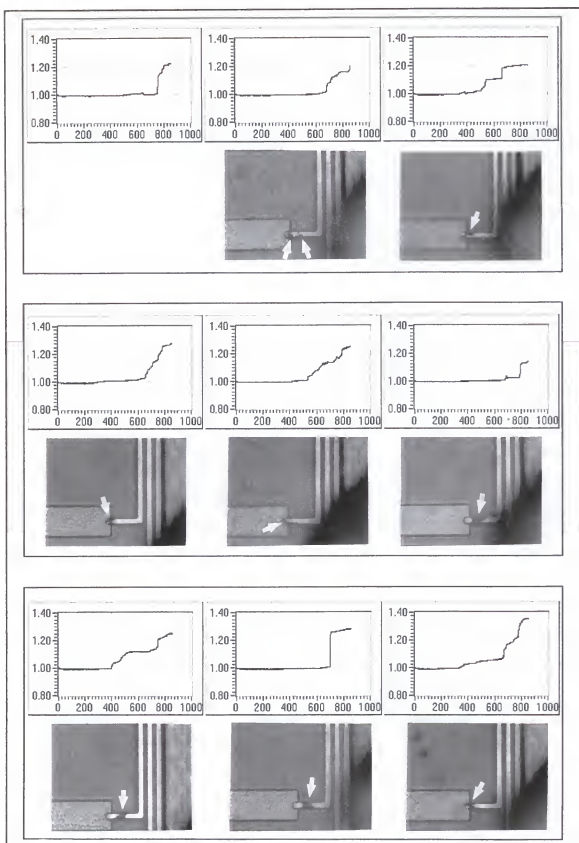


Figure 27. R/Ro vs. time (h) plots and optical micrographs for each test stripe of test lot P001M50 -- 1 MHz, 50% duty.

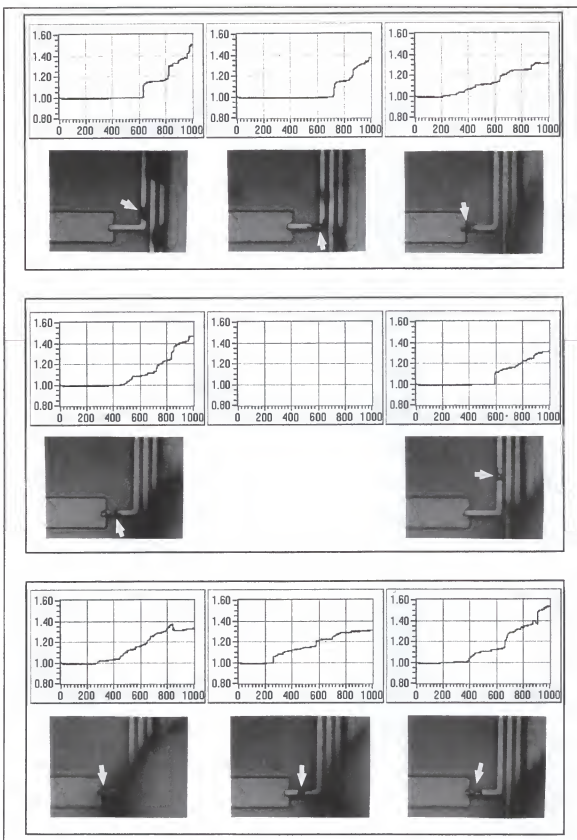


Figure 28. R/Ro vs. time (h) plots and optical micrographs for each test stripe of test lot P050M50 -- 50 MHz, 50% duty.

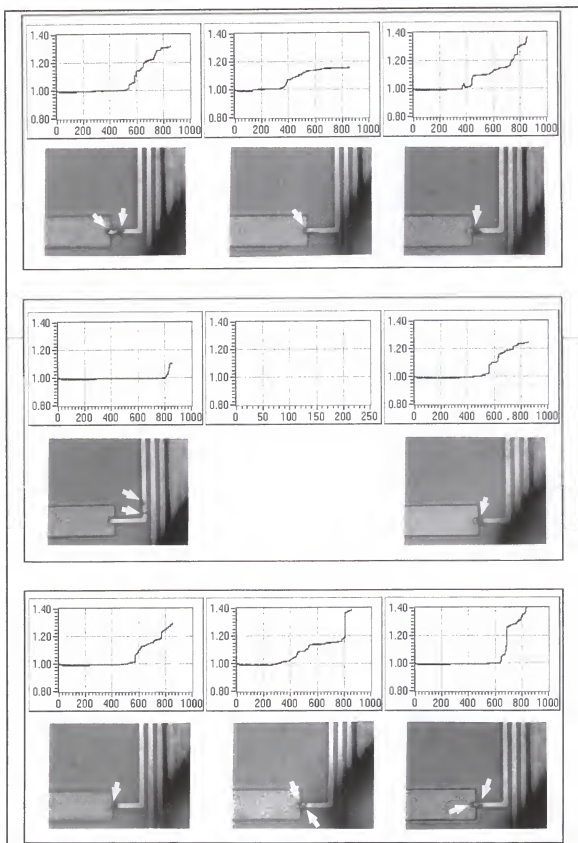


Figure 29. R/Ro vs. time (h) plots and optical micrographs for each test stripe of test lot P133M50 -- 133 MHz, 50% duty.

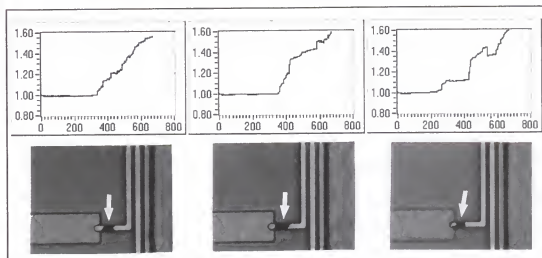
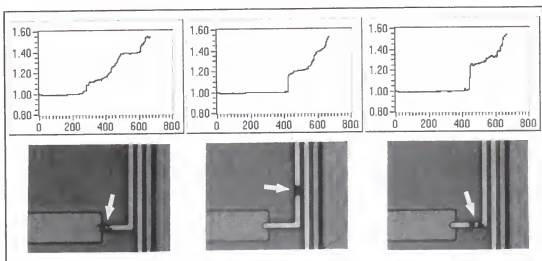


Figure 30. R/Ro vs. time (h) plots and optical micrographs for each test stripe of test lot P133K67 -- 133 KHz, 66.7% duty.

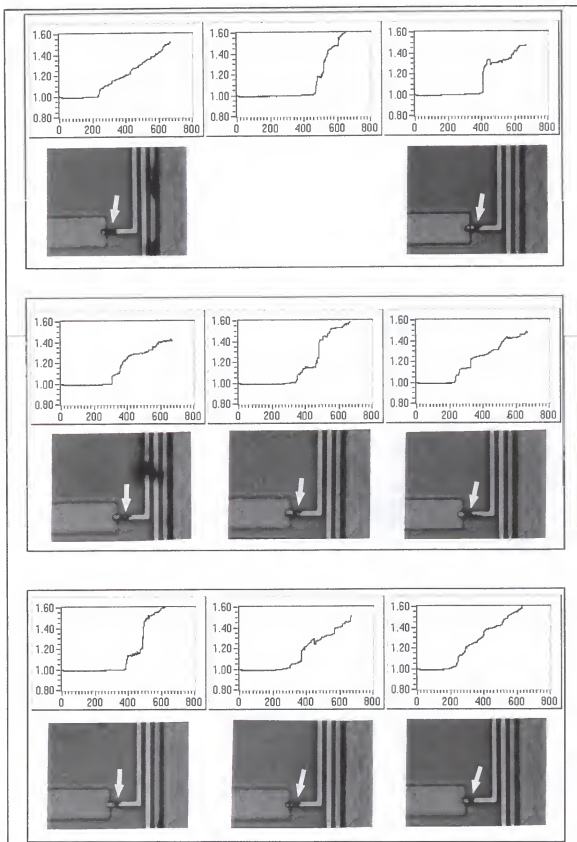


Figure 31. R/Ro vs. time (h) plots and optical micrographs for each test stripe of test lot P667K67 -- 667 KHz, 66.7% duty.

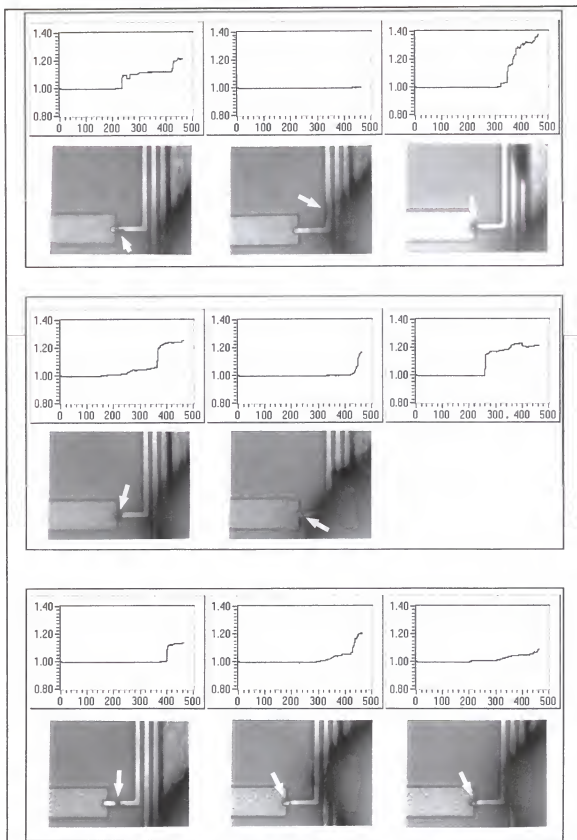


Figure 32. R/Ro vs. time (h) plots and optical micrographs for each test stripe of test lot P1\_33M67 -- 1.33 MHz, 66.7% duty.

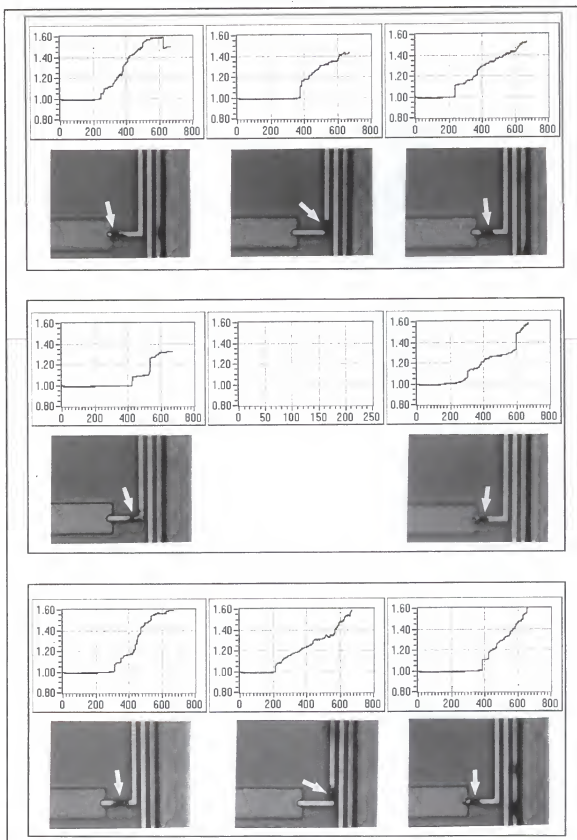


Figure 33. R/Ro vs. time (h) plots and optical micrographs for each test stripe of test lot P067M67 -- 67 MHz, 66.7% duty.



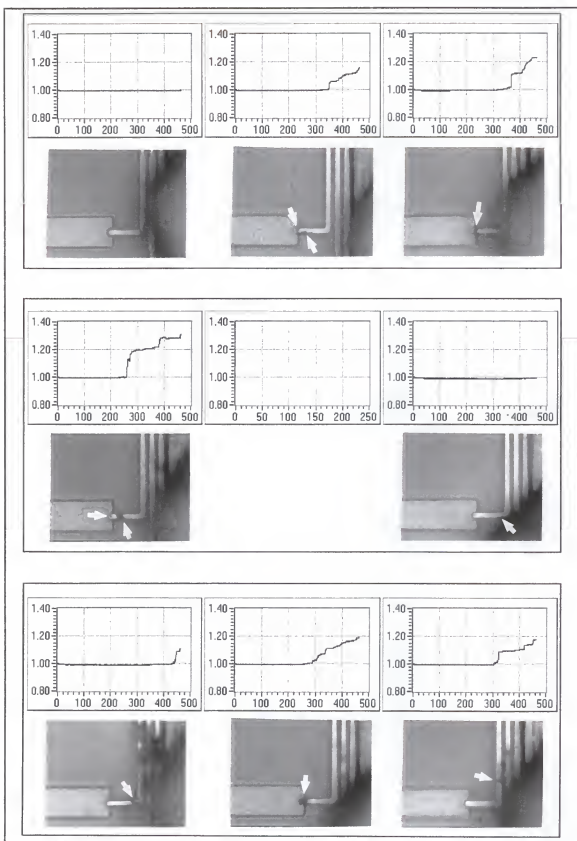


Figure 34. R/Ro vs. time (h) plots and optical micrographs for each test stripe of test lot P133M67 -- 133 MHz, 66.7% duty.

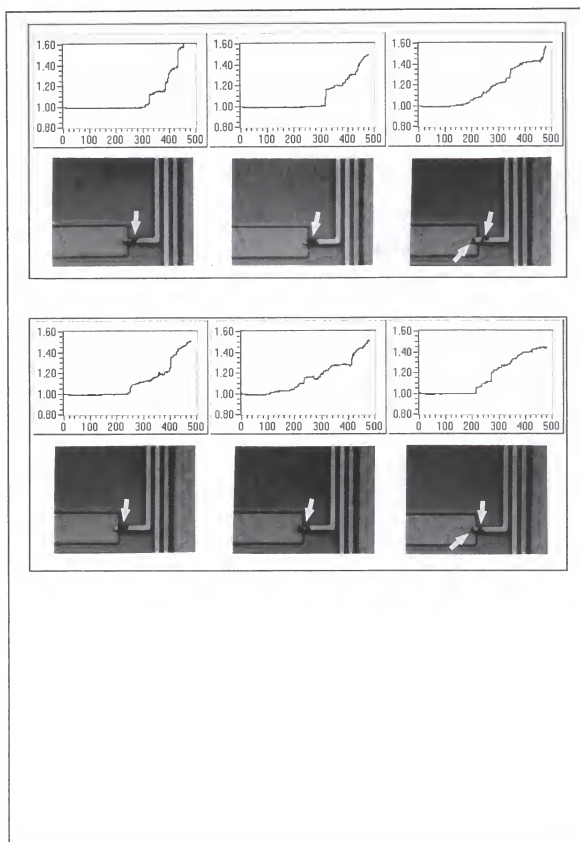


Figure 35. R/Ro vs. time (h) plots and optical micrographs for each test stripe of test lot P160K80 -- 160 KHz, 80% duty.

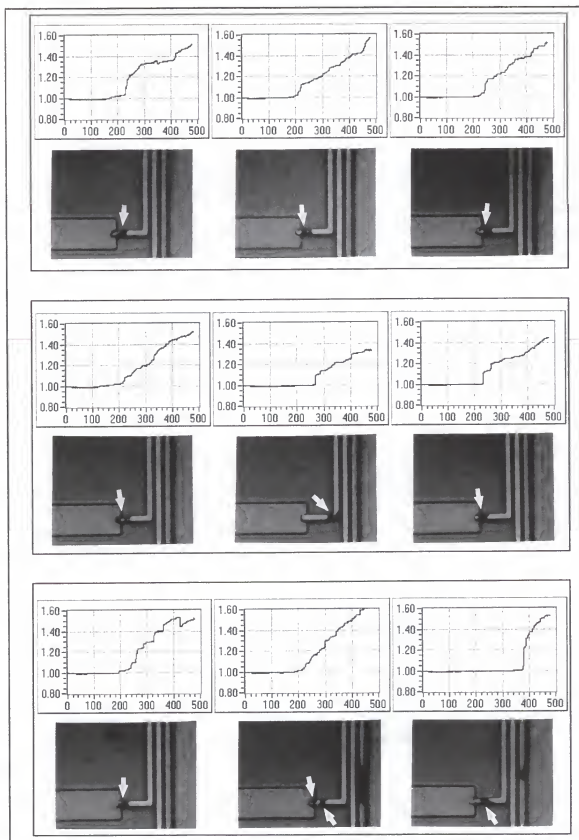


Figure 36. R/Ro vs. time (h) plots and optical micrographs for each test stripe of test lot P1\_60M80 -- 1.60 MHz, 80% duty.

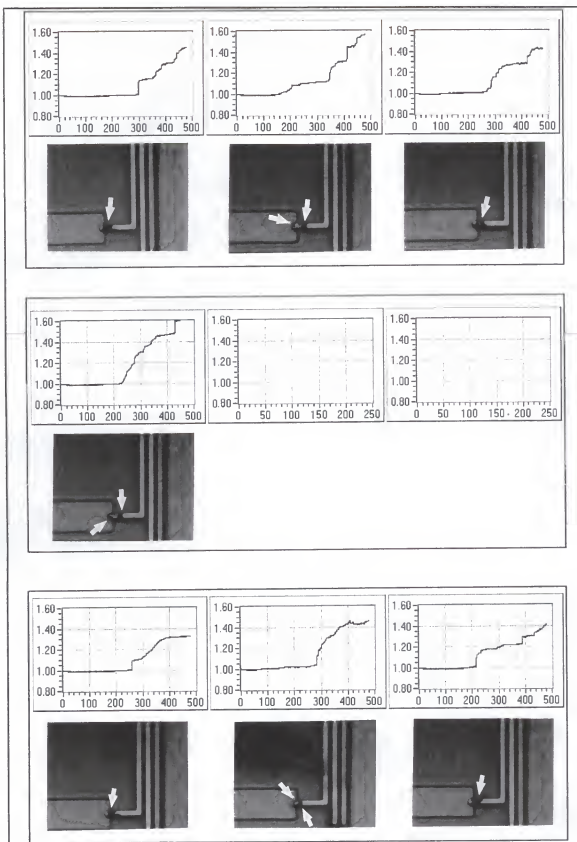


Figure 37. R/Ro vs. time (h) plots and optical micrographs for each test stripe of test lot P133M77 -- 133 MHz, 77% duty.

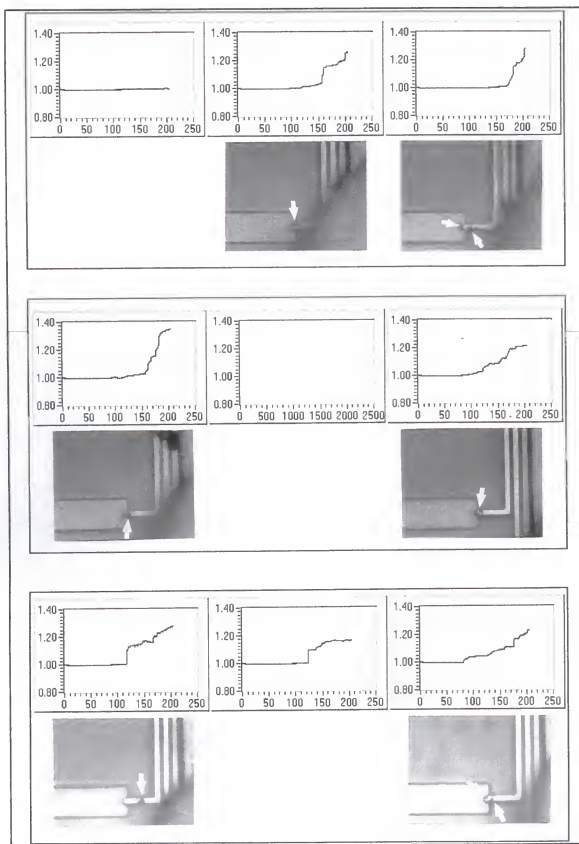


Figure 38. R/Ro vs. time (h) plots and optical micrographs for each test stripe of test lot DC -- DC.

The dependence of the damage location on duty cycle may be related to the near-bamboo grain structure of the stripes. The findings of Frankovic et al. lend support to this reasoning. Recall that their work was based on the concept of a critical stripe length, commonly called the "Blech length." The critical length is said to be the minimum stripe length, for a given current density, below which no net electromigration damage can be generated. They determined, for a given current density, that the Blech length increases with decreasing duty cycle. In changing the duty cycle from 100% to 25%, the critical length increased by a factor of 2.6.

The experiments of Frankovic et al. were performed with relatively wide test stripes, which most likely had a continuous network of grain boundaries. The Blech length was associated with the length of the entire stripe. With a near-bamboo grain structure, however, there should be a unique Blech length associated with each bamboo segment. For some test stripes, the first segment at the cathode end, be it a single grain segment or a polygrained segment, might happen to be longer than the Blech length for DC and large duty cycle pulses, but shorter than the Blech length for small duty cycle pulses. For DC and large duty cycles, then, damage would likely occur within this first segment, and it would usually occur at or very near the contact interface. With the smaller duty cycles, however, damage would not occur within this segment. A larger segment would need to be "found" somewhere down the length of the stripe.

Such behavior may account for the results depicted in Figure 20, but the critical lengths are not actually known. Frankovic et al. found critical lengths in

their experiments on the order of tens of micrometers. The current densities used in that study were around  $5 \times 10^5 \text{ A/cm}^2$ . The pulse amplitude of 15 mA used in the present work is equal to a current density of about  $2.7 \times 10^6 \text{ A/cm}^2$  in the stripe and about  $4 \times 10^6 \text{ A/cm}^2$  at the tungsten plug contact interface (the plug cross section was  $0.6 \mu\text{m} \times 0.6 \mu\text{m}$ ). Since  $j_l c$  is constant, other things being equal, a Blech length on the order of a few micrometers would not be out of the question for the present work, and the length increments defined in Figure 20 are about  $2.5 \mu\text{m}$ . Admittedly, it is not strictly correct to assume that other things are equal in comparing the two studies. For example, the test stripes used by Frankovic et al. were pure aluminum, whereas an aluminum-copper alloy was used in the present study. Their test temperature was the same ( $200^\circ\text{C}$ ). In any case, the above discussion offers a reasonable explanation for the results and reveals an interesting topic for future work.

The time that was required for post-test deprocessing of the samples for cross-sectional inspection prohibited such analysis on all stripes. Scanning electron micrographs were obtained in cross-section for a few stripes, however, and two are presented in Figure 39. The orientation of these micrographs is opposite to that of Figures 21 through 38, that is, the downwind direction is from right to left. The magnification was about 12000X.

Figure 39(a) reveals voiding above the tungsten contact, damage which would have been assigned to the 1st increment in Figure 20. In Figure 39(b), no damage can be seen at the tungsten plug, but some is evident farther downwind, within the 2nd and 3rd increments. An interesting feature of the depleted areas

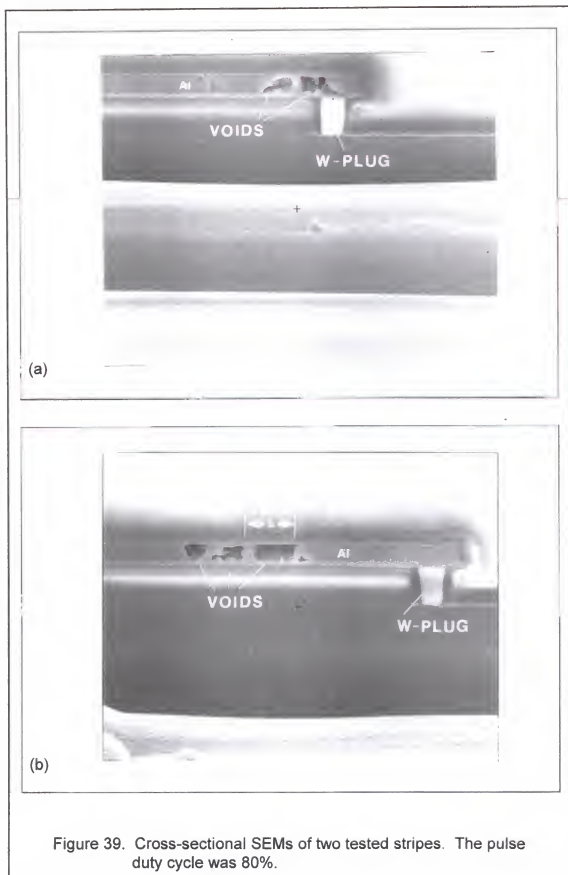


Figure 39. Cross-sectional SEMs of two tested stripes. The pulse duty cycle was 80%.



is their blocked appearance. Three such blocked areas are evident in Part (b), and their close spacing invites speculation on the Blech length. If the righthand edge of any given block is the upwind end of a bamboo segment, then it might be estimated that the length of the bamboo segment is equal to or less than the distance from its upwind edge to the upwind edge of the next block to the left. The Blech length, in turn, must be equal to or less than this measured distance, which is about  $1\text{ }\mu\text{m}$  for the distance,  $L$ , in Figure 39(b). The stripes pictured in Figure 39 were tested with a pulse duty cycle of 80%, a value for which the Blech length would be relatively small.

Two more cross-sectional SEMs are presented in Figure 40. These are more highly magnified ( $\sim 35000\times$ ) and center on the tungsten plug contact. The test current was DC, and it flowed from left to right in these pictures. In addition to the SEM, the corresponding top view optical micrograph and  $R/R_o$  versus time plot are included in each of Parts (a) and (b).

Part (a) reveals damage above the contact, and the  $R/R_o$  plot indicates an increase in resistance of about 7%. The optical micrograph shows a dark region just at the contact area, in agreement with the SEM. It is interesting to note the voiding that occurred at the left end of the test stripe, to the left of the current path. The migration of material from this region was not caused by the electron wind. Apparently, it was caused by the concentration gradient created by the electromigration-induced depletion of material directly above the contact.

Part (b) of Figure 40 shows a test stripe for which powering was shut down before the damage could proceed past the contact. The corresponding

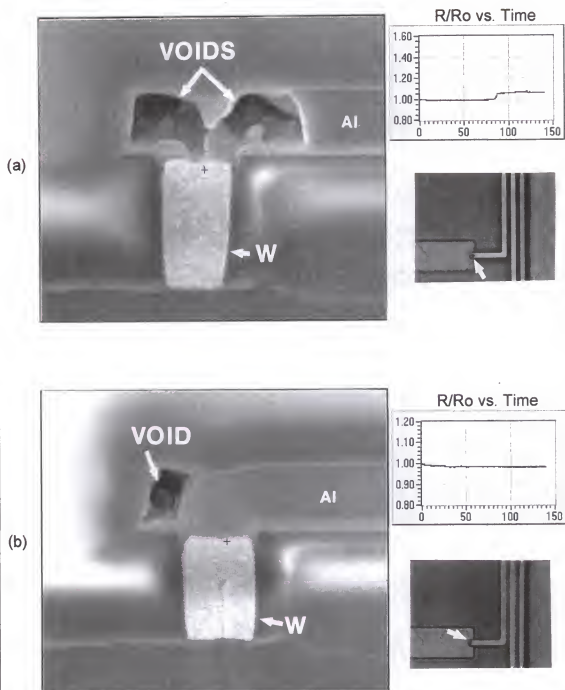


Figure 40. Cross-sectional SEMs of two tested stripes. The test current was DC.

(a) Damage above the tungsten contact.

(b) Damage at the leftmost edge, but not above the contact.

R/Ro plot shows, appropriately, no increase in resistance. The overhang of the interconnect around the contact provides a source of material that helps to delay failure. Such behavior is commonly observed in practice [71] and is an important consideration in IC miniaturization efforts that seek to eliminate such overhang.

There has been debate from time to time regarding the claim that lifetime enhancement could be caused by the relaxation of damage during the off times between pulses. The depletion of material from areas of contact overhang, like that depicted in Figure 40, is strong evidence for such a claim. It shows rather clearly that diffusion of material down an electromigration-induced concentration gradient may proceed at speeds comparable to the electromigration itself.

In addition to the optical micrographs, Figures 21 through 38 include the corresponding R/Ro versus time plots for each tested stripe. These plots may reveal something about the damage formation process. It is evident that R/Ro does not change smoothly over the course of a test run. The most consistent occurrence of this behavior is at the end of the so-called "incubation" period, which is the time during which copper is thought to be removed from a site of structural divergence. It is a common assumption that copper must be swept away from an area before the aluminum in that area is subject to migration. The stripe resistance may change very little during the incubation period, but it may rise rather rapidly when incubation has finished. Such behavior is displayed in the R/Ro plots of Figures 21 through 38. In addition to the initial jump in R/Ro, which occurs after a relatively long period of little or no change, sharp rises are also seen at later times. It is difficult to correlate any particular jump in R/Ro

with any particular damage site, but it might be estimated that the common observation of more than one damage site is evidence that each jump in  $R/R_o$  indicates the end of incubation at a different structural gradient.

### Lifetime Data

The standard quantitative basis for comparing electromigration behavior is  $t_{50}$ . It is this quantity that most models strive to predict. The concern here is the dependence of  $t_{50}$  on the frequency and the duty cycle of a pulsed stress current for a given temperature and pulse amplitude.

Figures 41 through 58 contain the raw data, extracted failure times, and lognormal failure plots for each of the 18 electrical stress treatments. Part (a) of each figure contains 6 to 9  $R/R_o$  versus time plots, one for each test stripe in that treatment lot. These plots are the same ones that were included with the optical micrographs, earlier. Part (b) of each figure is a table of the failure times, listed in ascending order for two failure criteria --  $R/R_o = 1.10$  and  $R/R_o = 1.20$ . These times were extracted from the plots of Part (a). The last column of the table, headed " $t_{50}$  (h)," contains the median failure time for each failure criterion. This median time was calculated by taking the logarithm of every failure time, finding the mean of these log-times, and computing the inverse logarithm of this mean. Such a method assumes, of course, that the failure times adhere to a lognormal distribution. Part (c) of each figure is a plot of the Part (b) failure times on a logarithmic time axis versus cumulative failure probability in percent.

Because failure times are assumed to be distributed lognormally, the plots given in Part (c) of each figure should indicate linearity. In fact, it is common to

estimate  $t_{50}$  for a group of failures by fitting a straight line to the given failure plot and finding the intersection of this line with the 50th percentile on the probability scale. Excellent linearity is often evident in Figures 41 through 58, but there are also many cases in which it would be difficult to fit, with confidence, a straight line to the data. The lack of consistent linearity is one reason that  $t_{50}$  was not estimated with this method, in addition to the fact that such a method does not provide the best estimate, anyway. The best estimate is given by the calculation described above.

The sometimes discontinuous behavior of the R/Ro data is reflected in the failure plots. It can be seen in many of the plots that the apparent slope for one R/Ro failure criterion is different from that for the other criterion. The data tend to merge at larger failure times, which reflects a tendency for the discontinuous jumps in R/Ro to be smaller for early failures than for late failures. Whenever a sample "lives" for a relatively long time, it is more likely to eventually experience a large jump in R/Ro. In such an instance, the failure time that is found using an R/Ro failure criterion of 10% may be essentially the same as that which is found using a criterion of 20%. Depending on whether one is primarily interested in early failures, median failures, or late failures, this behavior may be of significant practical concern regarding the selection of a failure criterion.

The apparent slope exhibited by a failure plot is essentially the standard deviation of the failure times. An estimate of the standard deviation, which can be performed graphically, is given by  $\log(t_{50}/t_{16})$ , but it is more appropriate to calculate it from its definition. It is normal practice to report the sample standard

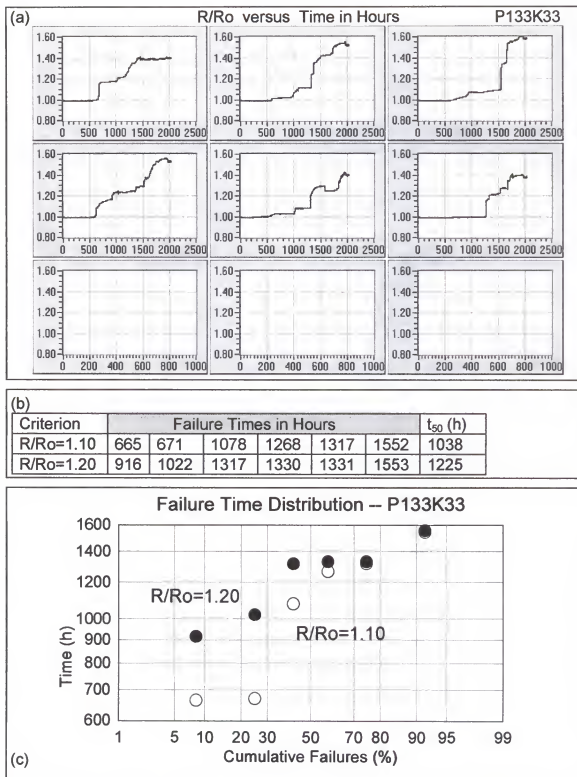


Figure 41. Data for sample lot P133K33 – 133 KHz, 33.3% duty cycle.  
 a) R/R<sub>0</sub> versus time plots for each of the 6 samples.  
 b) Failure times for the failure criteria R/R<sub>0</sub>=1.10 and R/R<sub>0</sub>=1.20.  
 c) Log-normal plot of failure times for each criterion.

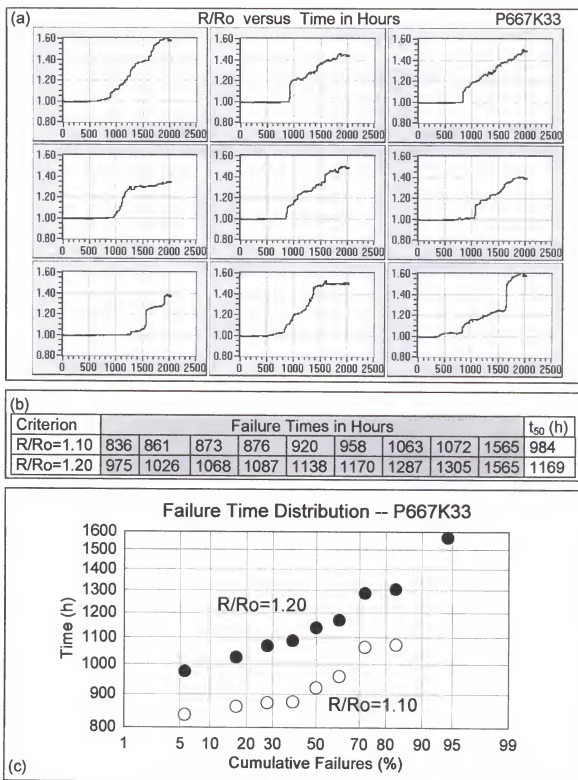


Figure 42. Data for sample lot P667K33 -- 667 KHz, 33.3% duty cycle.  
 a) R/R<sub>o</sub> versus time plots for each of the 9 samples.  
 b) Failure times for the failure criteria R/R<sub>o</sub>=1.10 and R/R<sub>o</sub>=1.20.  
 c) Log-normal plot of failure times for each criterion.

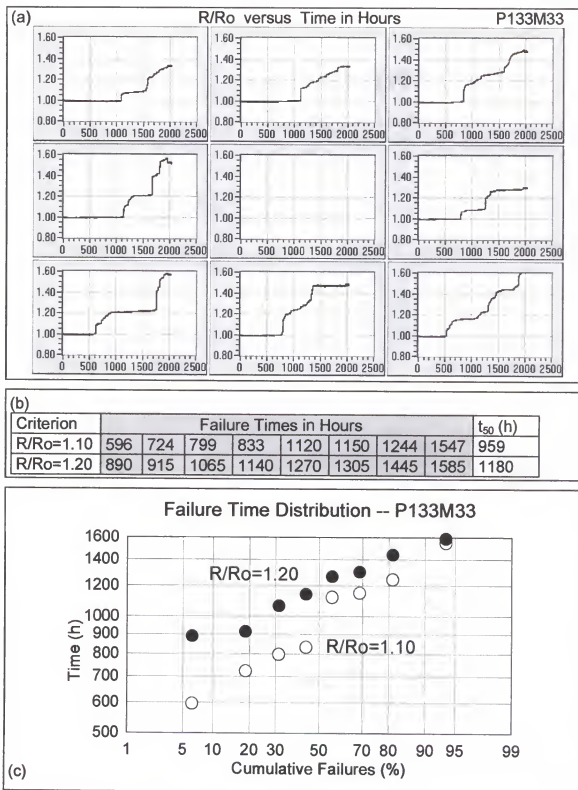


Figure 43. Data for sample lot P133M33 -- 133 MHz, 33.3% duty cycle.  
 a) R/R<sub>0</sub> versus time plots for each of the 8 samples.  
 b) Failure times for the failure criteria R/R<sub>0</sub>=1.10 and R/R<sub>0</sub>=1.20.  
 c) Log-normal plot of failure times for each criterion.



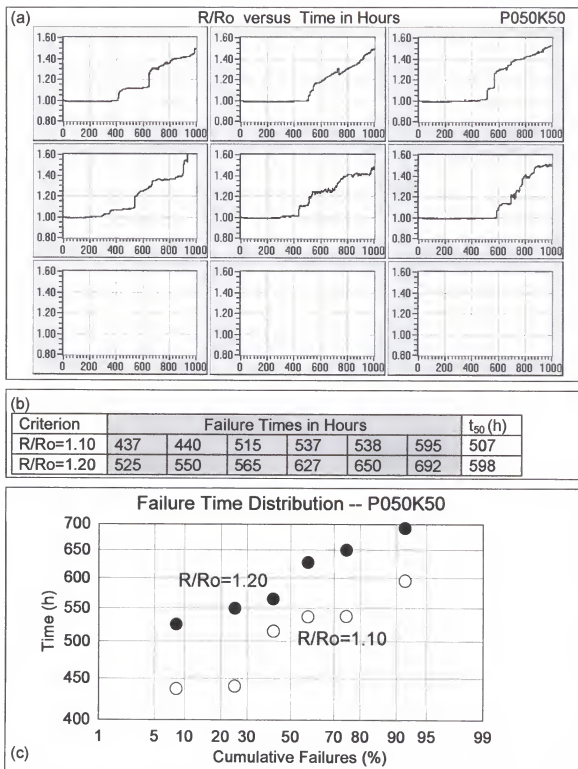


Figure 44. Data for sample lot P050K50 -- 50 KHz, 50% duty cycle.  
 a) R/R<sub>0</sub> versus time plots for each of the 6 samples.  
 b) Failure times for the failure criteria R/R<sub>0</sub>=1.10 and R/R<sub>0</sub>=1.20.  
 c) Log-normal plot of failure times for each criterion.

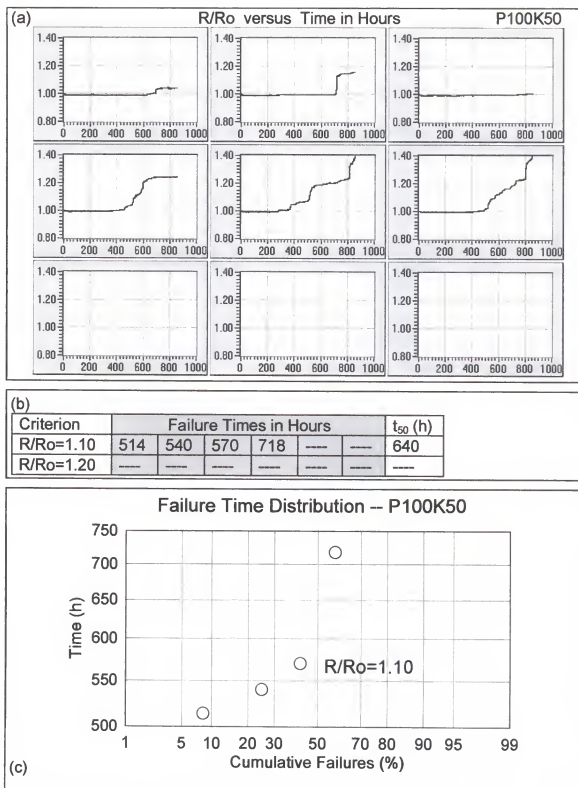


Figure 45. Data for sample lot P100K50 – 100 KHz, 50% duty cycle.  
 a) R/R<sub>o</sub> versus time plots for each of the 6 samples.  
 b) Failure times for the failure criteria R/R<sub>o</sub>=1.10 and R/R<sub>o</sub>=1.20.  
 c) Log-normal plot of failure times for the criterion R/R<sub>o</sub>=1.10.

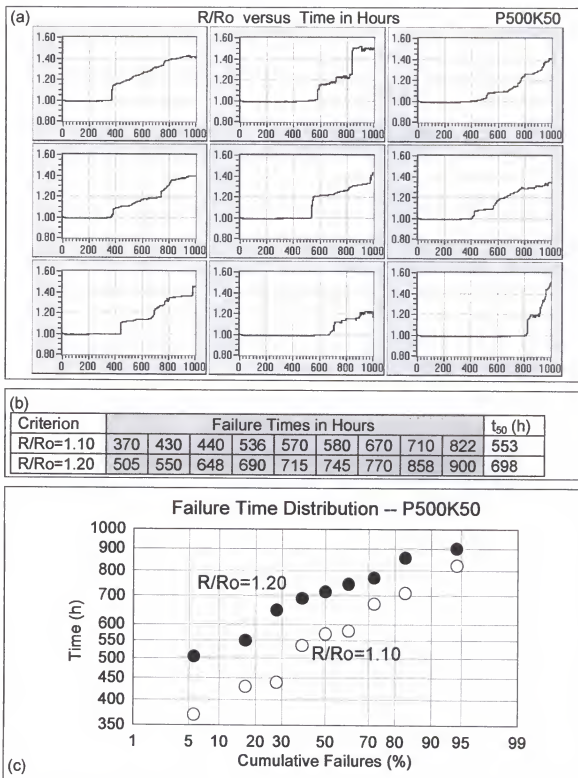


Figure 46. Data for sample lot P500K50 -- 500 KHz, 50% duty cycle.  
 a) R/R<sub>0</sub> versus time plots for each of the 9 samples.  
 b) Failure times for the failure criteria R/R<sub>0</sub>=1.10 and R/R<sub>0</sub>=1.20.  
 c) Log-normal plot of failure times for each criterion.

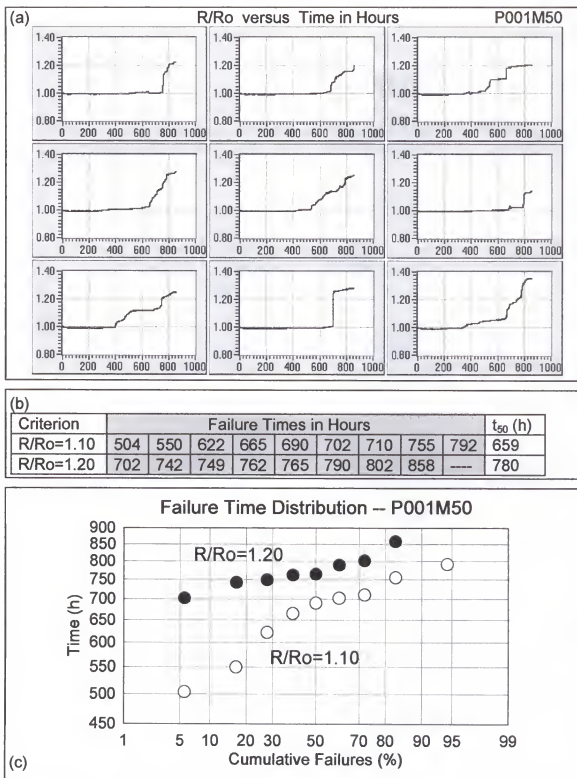


Figure 47. Data for sample lot P001M50 -- 1MHz, 50% duty cycle.  
 a) R/R<sub>0</sub> versus time plots for each of the 9 samples.  
 b) Failure times for the failure criteria R/R<sub>0</sub>=1.10 and R/R<sub>0</sub>=1.20.  
 c) Log-normal plot of failure times for each criterion.

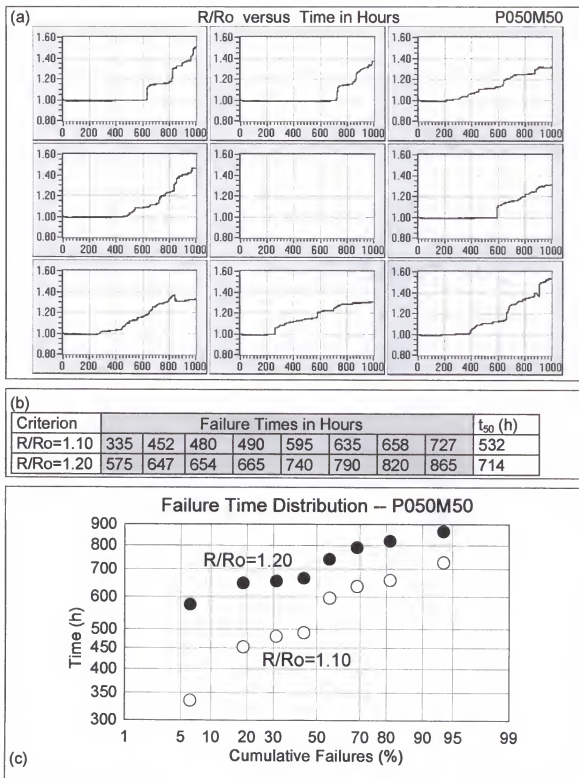


Figure 48. Data for sample lot P050M50 -- 50 MHz, 50% duty cycle.  
 a) R/R<sub>0</sub> versus time plots for each of the 8 samples.  
 b) Failure times for the failure criteria R/R<sub>0</sub>=1.10 and R/R<sub>0</sub>=1.20.  
 c) Log-normal plot of failure times for each criterion.

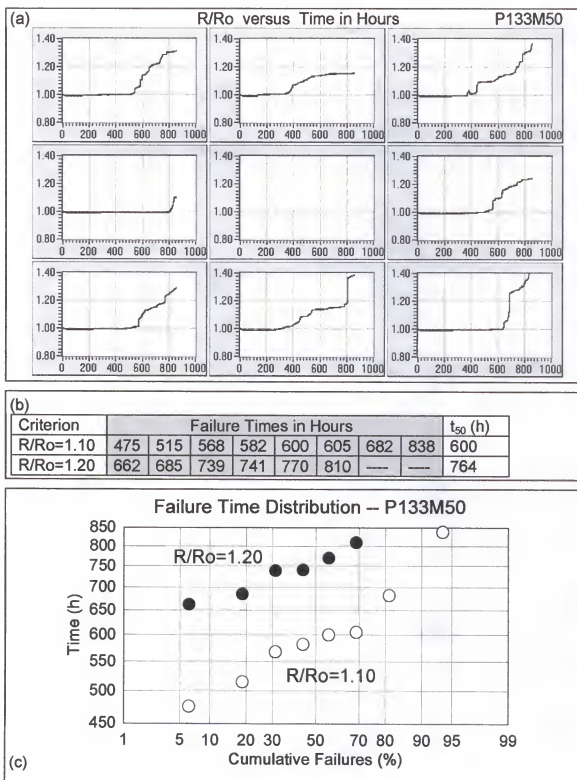


Figure 49. Data for sample lot P133M50 – 133 MHz, 50% duty cycle.  
 a) R/R<sub>0</sub> versus time plots for each of the 8 samples.  
 b) Failure times for the failure criteria R/R<sub>0</sub>=1.10 and R/R<sub>0</sub>=1.20.  
 c) Log-normal plot of failure times for each criterion.

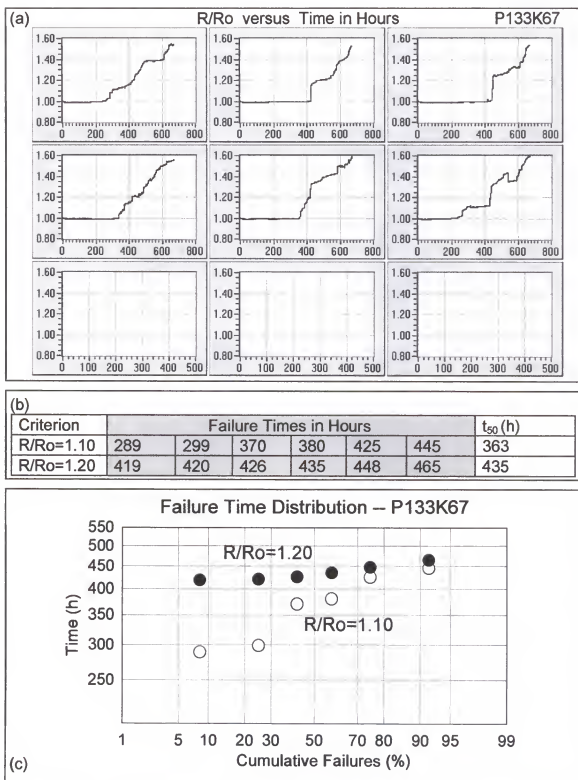


Figure 50. Data for sample lot P133K67 -- 133 KHz, 66.7% duty cycle.  
 a) R/Ro versus time plots for each of the 6 samples.  
 b) Failure times for the failure criteria R/Ro=1.10 and R/Ro=1.20.  
 c) Log-normal plot of failure times for each criterion.

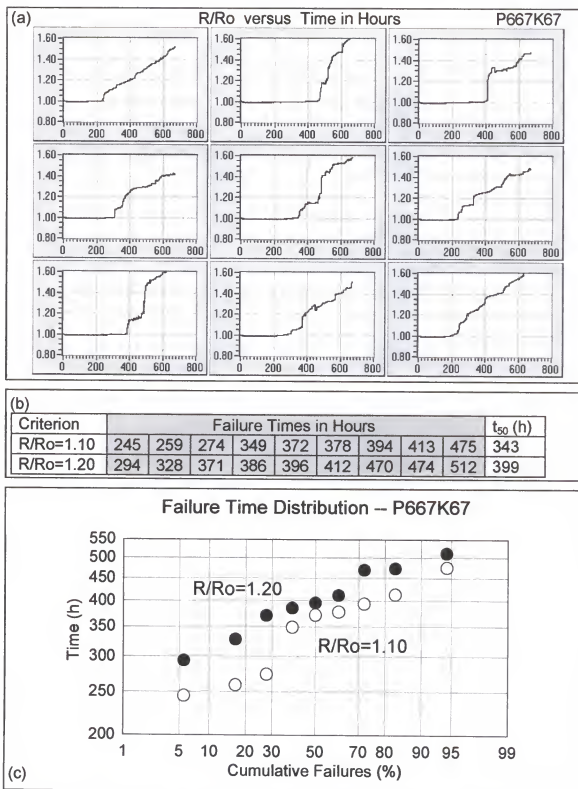


Figure 51. Data for sample lot P667K67 – 667 KHz, 66.7% duty cycle.  
 a) R/R<sub>0</sub> versus time plots for each of the 9 samples.  
 b) Failure times for the failure criteria R/R<sub>0</sub>=1.10 and R/R<sub>0</sub>=1.20.  
 c) Log-normal plot of failure times for each criterion.



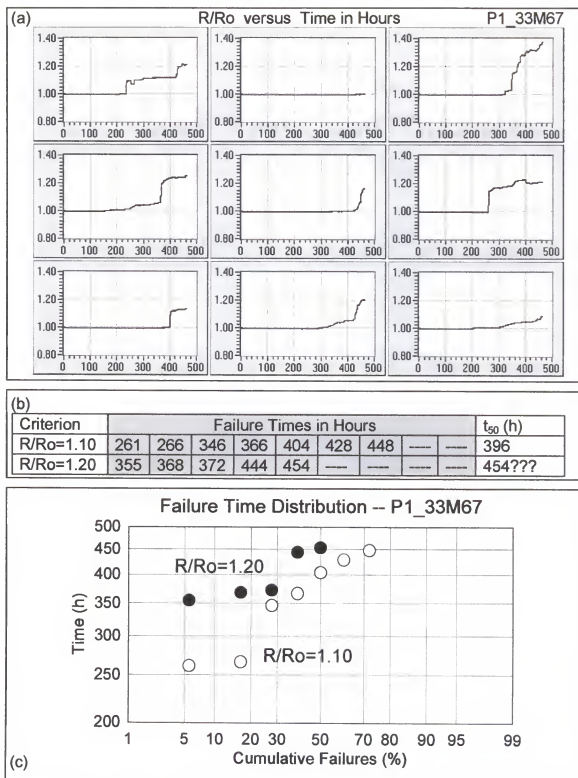


Figure 52. Data for sample lot P1\_33M67 -- 1.33 MHz, 66.7% duty cycle.  
 a) R/R<sub>0</sub> versus time plots for each of the 9 samples.  
 b) Failure times for the failure criteria R/R<sub>0</sub>=1.10 and R/R<sub>0</sub>=1.20.  
 c) Log-normal plot of failure times for each criterion.

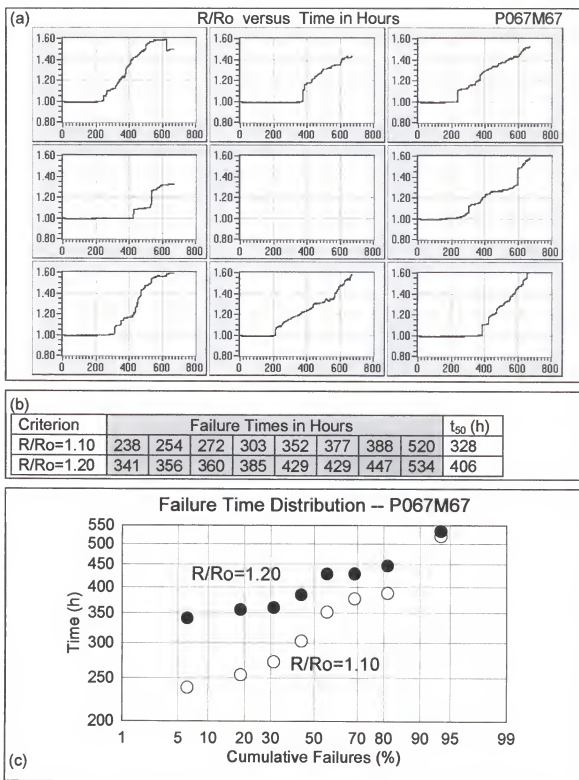


Figure 53. Data for sample lot P067M67 -- 66.7 MHz, 66.7% duty cycle.  
 a) R/R<sub>0</sub> versus time plots for each of the 8 samples.  
 b) Failure times for the failure criteria R/R<sub>0</sub>=1.10 and R/R<sub>0</sub>=1.20.  
 c) Log-normal plot of failure times for each criterion.

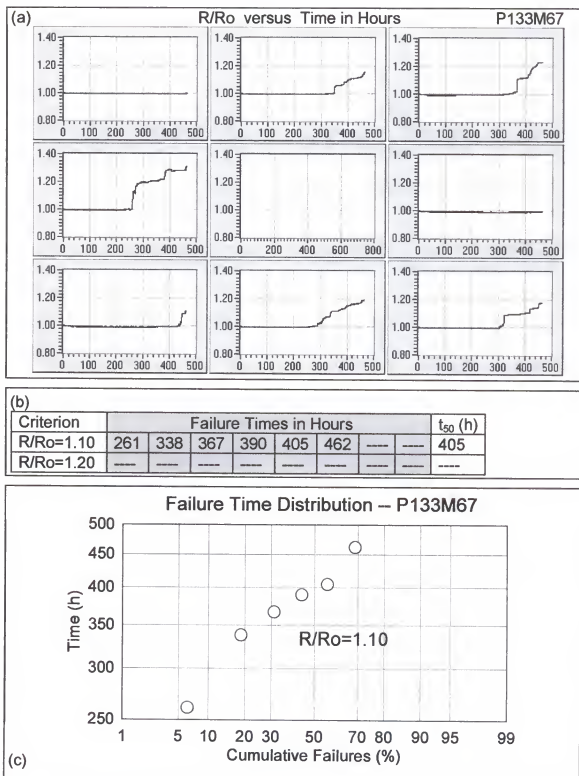


Figure 54. Data for sample lot P133M67 -- 133 MHz, 66.7% duty cycle.  
 a) R/R<sub>0</sub> versus time plots for each of the 8 samples.  
 b) Failure times for the failure criteria R/R<sub>0</sub>=1.10 and R/R<sub>0</sub>=1.20.  
 c) Log-normal plot of failure times for the criterion R/R<sub>0</sub>=1.10.

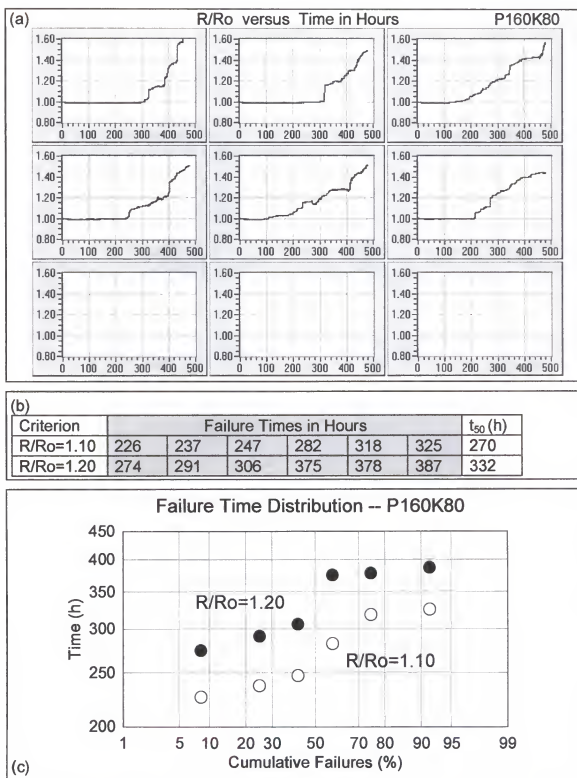


Figure 55. Data for sample lot P160K80 -- 160 KHz, 80% duty cycle.  
 a) R/R<sub>0</sub> versus time plots for each of the 6 samples.  
 b) Failure times for the failure criteria R/R<sub>0</sub>=1.10 and R/R<sub>0</sub>=1.20.  
 c) Log-normal plot of failure times for each criterion.

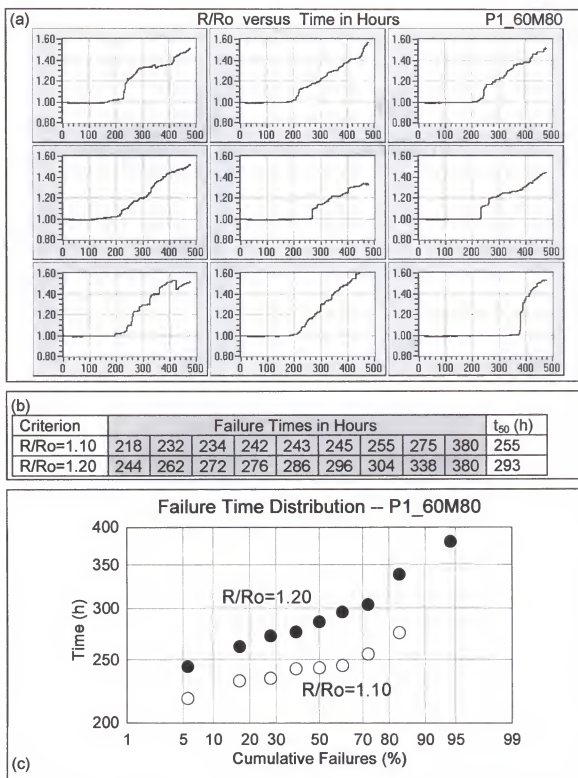


Figure 56. Data for sample lot P1\_60M80 – 1.60 MHz, 80% duty cycle.  
 a) R/R<sub>0</sub> versus time plots for each of the 9 samples.  
 b) Failure times for the failure criteria R/R<sub>0</sub>=1.10 and R/R<sub>0</sub>=1.20.  
 c) Log-normal plot of failure times for each criterion.

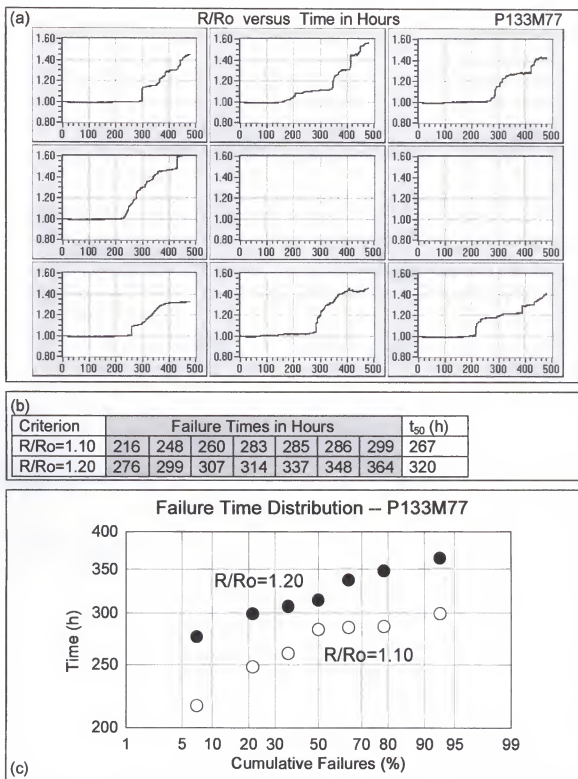


Figure 57. Data for sample lot P133M77 -- 133 MHz, 77% duty cycle.  
 a) R/R<sub>0</sub> versus time plots for each of the 7 samples.  
 b) Failure times for the failure criteria R/R<sub>0</sub>=1.10 and R/R<sub>0</sub>=1.20.  
 c) Log-normal plot of failure times for each criterion.

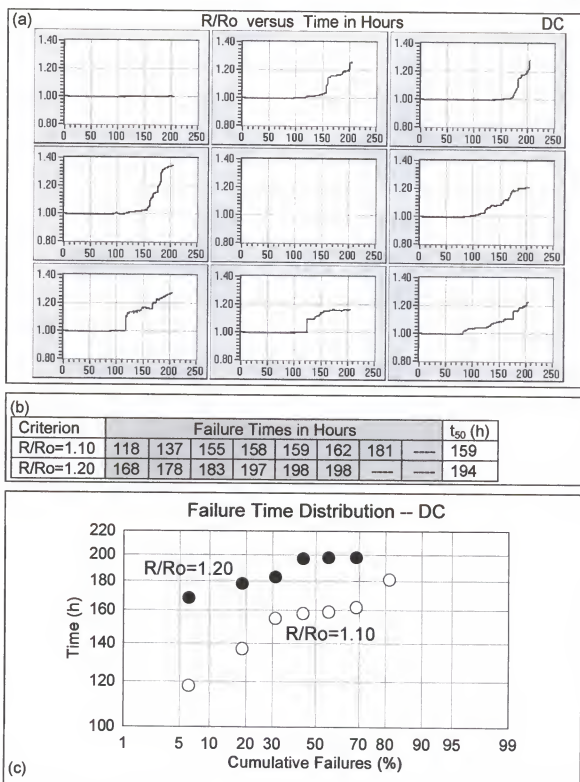


Figure 58. Data for sample lot DC -- DC, 100% duty cycle.  
 a) R/Ro versus time plots for each of the 8 samples.  
 b) Failure times for the failure criteria R/Ro=1.10 and R/Ro=1.20.  
 c) Log-normal plot of failure times for each criterion.

deviation in addition to  $t_{50}$ , because the degree of spread about  $t_{50}$  is a significant factor in estimates of reliability. The standard deviation was calculated for the  $R/R_o = 1.10$  failure times (actually, the logarithms of the failure times) from each test lot, and the results are summarized in Table 2. Since the primary goal of this study was to determine the roles of pulse duty cycle and pulse frequency, any dependence of the standard deviation on these variables would be of particular interest. No dependence is evident. However, the values are smaller than those typically found by other researchers [59], who have reported standard deviations around 0.2 to 0.4. The uniformity of the samples and/or the control of the stress conditions was apparently quite good.

Table 2. Standard deviation of the logarithms of the failure times (failure criterion  $R/R_o = 1.10$ ) for each test lot.

Sample Lot	Std. Dev. (of log-times)
P133K33	0.1642
P667K33	0.0876
P133M33	0.1433
P050K50	0.0562
P100K50	0.0881
P500K50	0.1162
P001M50	0.0658
P050M50	0.1135
P133M50	0.0778
P133K67	0.0811
P667K67	0.1024
P1_33M67	0.1252
P067M67	0.1170
P133M67	0.1148
P133M77	0.0511
P160K80	0.0706
P1_60M80	0.0731
DC	0.0732
	0.0956 AVERAGE



### Relationships Between Lifetime, Pulse Frequency and Duty Cycle

We want to know how pulse frequency and duty cycle (or  $t_{on}$  and  $t_{off}$ ) affect the life of an interconnect when it is subjected to a pulsed stress current. In this work, test stripe life has been characterized by the median time to failure,  $t_{50}$ , for a group of test structures. The data that were detailed in Figures 41 through 58 included, for 18 treatments, the individual times to failure and the median times to failure for each of two failure criteria,  $R/R_o=1.10$  and  $R/R_o=1.20$ . Figures 59 through 66 present those  $t_{50}$  data ( $R/R_o = 1.10$ ) with respect to the various pulse treatments. The error bars in these figures indicate 90% confidence intervals. Again, the furnace temperature (200 °C) and the pulse amplitude (15 mA) were the same for all tests.

Figure 59, which displays  $t_{50}$  versus duty cycle for the fixed frequency of 133 MHz, shows, as expected, an increasing lifetime with decreasing duty cycle. Since  $t_{50}$  from the DC experiment was 159 hours (Figure 58), the on-time model predicts that  $t_{50} = 159/d$ , where  $d$  is the duty cycle expressed as a fraction. The average current density model predicts that  $t_{50} = 159/d^2$ . These relationships are displayed in the figure. Recall that the use of the name "average current density model" in connection with a  $1/d^2$  dependence involves a tacit assumption that  $t_{50}$  is proportional to  $1/j^2$  where  $j$  is the current density. It is seen that the average current density model is a reasonably appropriate predictor of  $t_{50}$  for duty cycles equal to and greater than 50%. For a duty cycle of 33.3%, however, the actual  $t_{50}$  was somewhat less than that predicted by the average current density model. The model predicts more lifetime enhancement than was actually observed. The

observed  $t_{50}$  is still significantly enhanced, however. It is almost a factor of two larger than the  $t_{50}$  that is predicted by the on-time model.

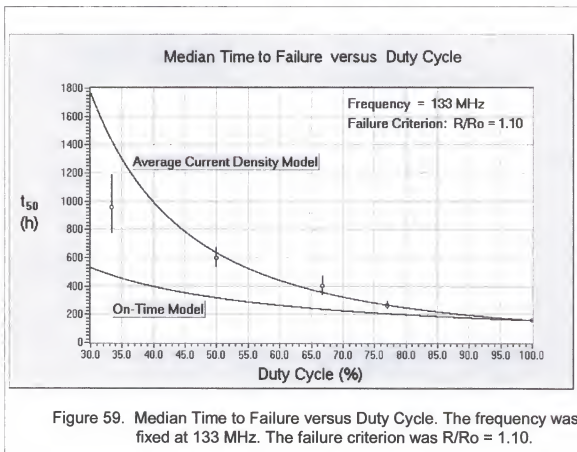


Figure 60 is similar in nature to Figure 59, but it shows the response of  $t_{50}$  when the pulse on time (pulse length) was held constant at 500 ns and the off time (the time between pulses) was varied from 125 ns to 1000 ns. This range of on/off times is equivalent to a range of duty cycles from 80% to 33.3%, and an approximate frequency of 1 MHz. Again, the experimental data are seen to fall rather close to the prediction of the average current density model, except for the point at an off time of 1000 ns, where there is a significant deviation toward a less enhanced lifetime. This data point represents a duty cycle of 33.3%, so the

behavior shown is equivalent to that displayed in Figure 59, for which the pulse frequency was roughly two orders of magnitude larger.

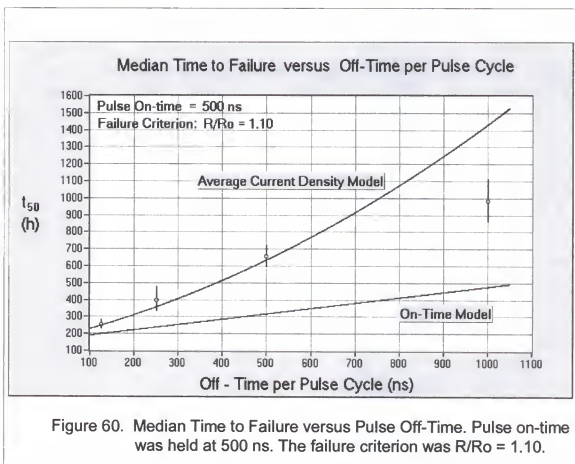
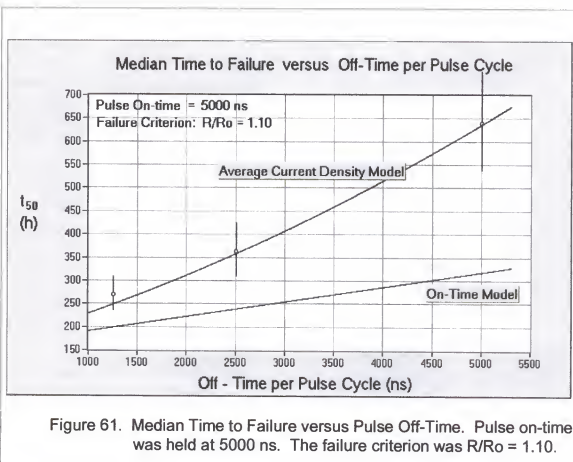
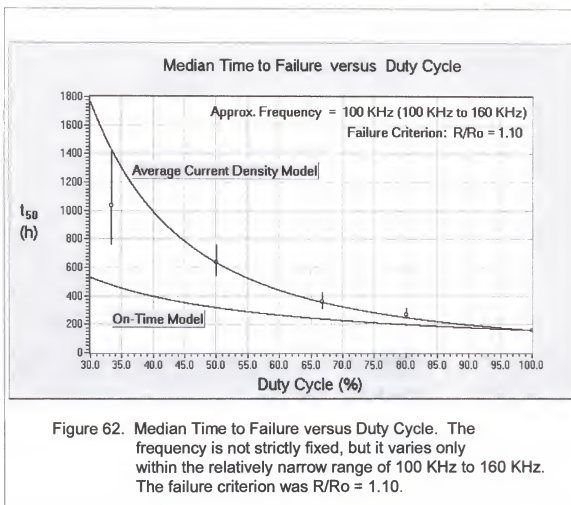


Figure 61 presents the dependence of  $t_{50}$  on the pulse off time for a fixed on time of 5000 ns. A data point was not obtained for an off time of 10,000 ns, which would correspond to a 33.3% duty cycle. But, the three points that are included lay fairly close to the average current density model, just as the three equivalent points in Figure 60 do. The on-time/off-time combinations that were included in Figure 61 represent a range of frequencies (100 KHz to 160 KHz) near 100 KHz.



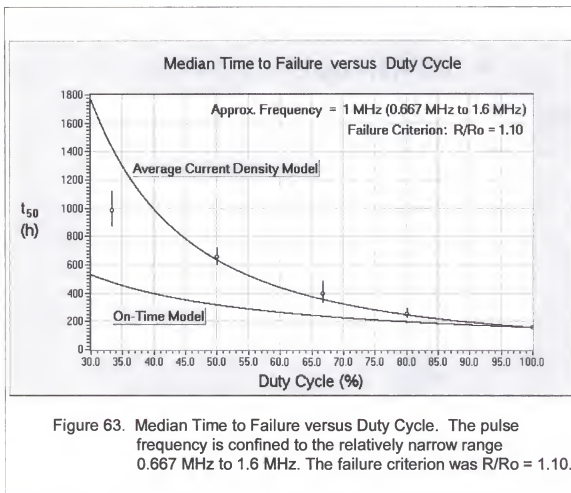
An experiment was performed in the frequency range represented in Figure 61 at a duty cycle of 33.3%, but it was not included in the figure, because it did not fit into the fixed on time, variable off time format. The on time for the experiment was 2500 ns and the off time was 5000 ns, which corresponds to a pulse frequency of 133 KHz. The  $t_{50}$  from this experiment may still be presented with the data of Figure 61 if  $t_{50}$  is plotted versus duty cycle without regard to the frequency or the on time and off time. This can be justified by assuming, for the moment, that the frequency does not significantly influence  $t_{50}$ , and that even if it does happen to have a small influence, it should not be noticeable over a small range of frequencies such as 100 KHz to 160 KHz. Figure 62 shows such a plot.



Again, a deviation from the average current density model is revealed for a duty cycle of 33.3%, just as it was with the other two pulse frequencies.

It is useful to redisplay the data of Figure 60 in the  $t_{50}$  versus duty cycle format, as well, so that all three orders of frequency are represented in the same context. This is again done with the assumption that a small frequency variation is of no significant consequence. The plot is given in Figure 63. A deviation from the average current density model is expected, and is observed, for a duty cycle of 33.3%.

Figures 62 and 63 were presented with the temporary assumption that  $t_{50}$  is not strongly dependent on frequency. It is advisable, then, to inspect the data



to determine the validity of such an assumption. Figures 64, 65, and 66 present  $t_{50}$  data for fixed duty cycles and variable frequency. The duty cycle was fixed at 33.3% for Figure 64, 50% for Figure 65, and 66.7% for Figure 66. Error bars are included again as 90% confidence intervals. Predictions of  $t_{50}$  from the on-time model and the average current density model appear as horizontal lines in these figures. There is a statistical spread inherent in these predictions, because they

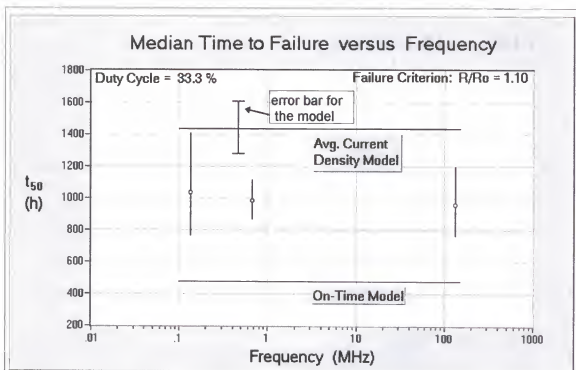


Figure 64. Median Time to Failure versus Frequency. The duty cycle is fixed at 33.3%. The failure criterion was  $R/R_o = 1.10$ .

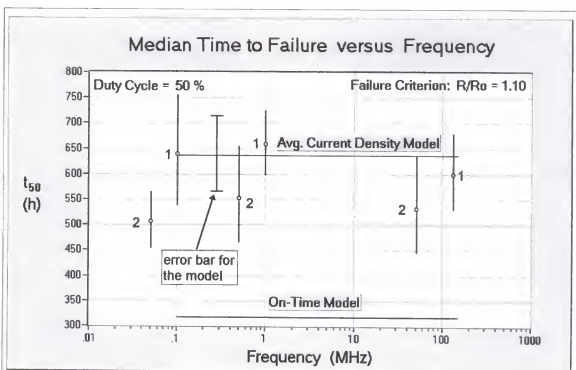
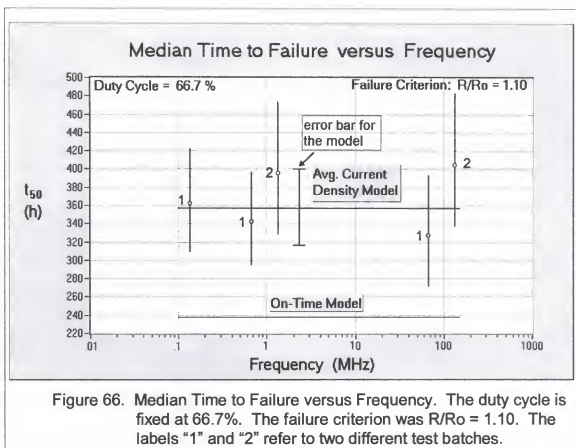


Figure 65. Median Time to Failure versus Frequency. The duty cycle is fixed at 50%. The failure criterion was  $R/R_o = 1.10$ . The labels "1" and "2" refer to two different test batches.



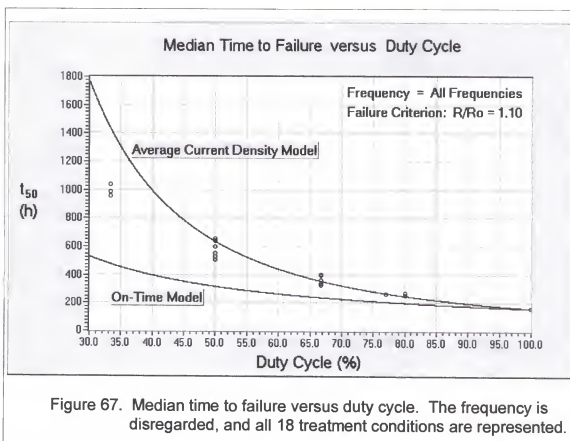
are based on the experimental  $t_{50}$  from the DC test. It is appropriate, then, to include confidence intervals around them. An error bar is included with the average current density prediction in each figure. One was not included in Figures 59 through 63, just for the sake of clarity.

The most certain observation that can be drawn from these results is that the experimental  $t_{50}$  values obtained for a duty cycle of 33.3% fall about midway between the two models, whereas the data are distributed about the average current density prediction for duty cycles of 50% and 66.7%. This is, of course, the same trend that was revealed in previous figures. Each of Figures 65 and 66 includes results from two different test batches. The data points are labeled "1"



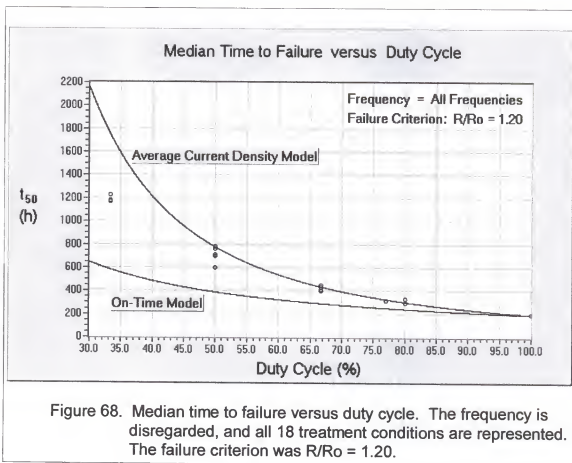
or "2", depending on whether they were obtained from the first batch or the second batch. The data within each batch are fairly consistent, but there is a noticeable difference between them. In Figure 65, for example, test batch #1 yielded data quite close to the average current density prediction, but batch #2 yielded smaller  $t_{50}$ 's. Similar behavior is evident in Figure 66, except that #2 yielded noticeably larger  $t_{50}$ 's than did #1.

If the batch-to-batch variation in the data for duty cycles of 50% and 66.7% is taken into consideration, then no specific frequency dependence is evident. The duty cycle is certainly the variable of most importance. It is useful, then, to display every data point from all pulse treatments on one plot versus duty cycle. This is done in Figure 67. Except for the separation between test



batches at 50%, the data are quite tightly clustered at each duty cycle and vary primarily according to the duty cycle.

The lifetime analysis reported in Figures 59 through 67 was based on the failure criterion  $R/R_o = 1.10$ . Of course, another criterion could have been used. Figures 41 through 58 did include  $t_{50}$ 's for the failure criterion  $R/R_o = 1.20$ , so it is worthwhile to present these data as a function of duty cycle, and this is done in Figure 68. There is one less data point at 50%, and also at 66.7%, in this



figure, compared to Figure 67, because an insufficient number of test stripes reached the condition  $R/R_o = 1.20$  to make an estimate of  $t_{50}$  for two of the 18 treatments. In any event, the results are similar, and the conclusions are the

same as those connected with Figure 67. The test stripe lifetime was enhanced significantly over the prediction of an on-time model for every pulse treatment, enhancement was more pronounced the lower the duty cycle, and the average current density model was a good predictor of  $t_{50}$  for duty cycles greater than 50%. At 50%, the results from one test batch agreed well with this model, but those of a second batch indicated less enhancement. The  $t_{50}$ 's for a duty cycle of 33.3% were somewhat less enhanced than the average current density prediction.

### Further Discussion

It has been demonstrated that the on-time model does not provide an accurate picture of pulsed current electromigration behavior in the range of frequencies from 100 KHz to 133 MHz. The consistent observation of lifetime enhancement confirms that either less damage is inflicted during each current pulse than would be inflicted by an equal length of DC time and/or some sort of damage recovery occurs during the time between pulses. The view of Towner and van de Ven, and that of Brooke, as well, suggested the former. That is, they believed that the atoms "experience" an average of the pulsed stressing current. The findings of their work, as well as the frequent reports in the literature that the average current density model is an accurate predictor of  $t_{50}$ , might lend support to this view. Other reports in the literature and the results of this work suggest, however, that deviations from the average current density model are common.

The models of Clement, Maiz, and Dwyer predict a  $1/d^2$  dependence, which is usually considered to be one and the same as an average current

density dependence, but they are based on idealized treatments of vacancy supersaturation and relaxation rather than an "experienced" current concept. These models include various simplifications, such as the assumption of a uniform matrix or an infinite test stripe length, in order to render a tractable treatment. There is no reason, without such simplifications, to expect a  $1/d^2$  dependence in all practical circumstances.

The treatment given by Wu and McNutt acknowledges this fact through a more generalized assessment. Recall that they developed the expression

$$t_{50}(\text{pulsed}) = \left( \frac{F_r}{d} \right) \cdot t_{50}(\text{DC}), \quad (27)$$

where  $d$  was the duty cycle and  $F_r$  was called the "damage relaxation factor."

The damage relaxation factor was defined as

$$F_r = 1 + \left( \frac{\tau_d}{\tau_r} \right) \cdot \left( \frac{1}{d} - 1 \right), \quad (28)$$

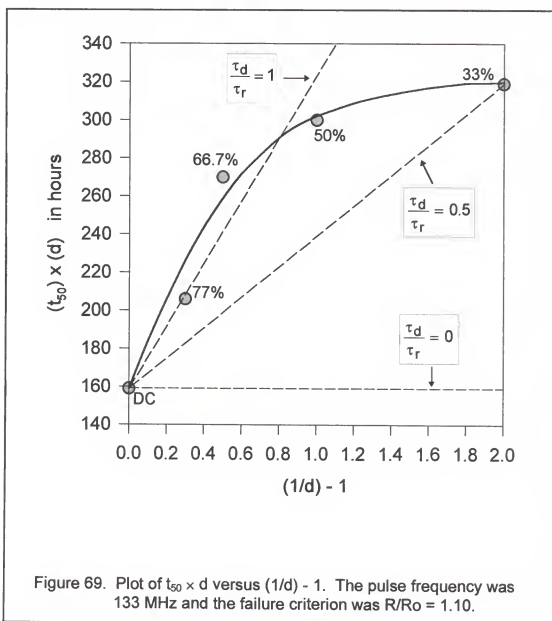
where  $\tau_d$  was a characteristic time constant associated with the rate of damage generation by a DC stressing current and  $\tau_r$  was an equivalent time constant for damage relaxation. Both  $\tau_d$  and  $\tau_r$  were assumed to be much larger than the on and off times of the pulsed current. Combination of these equations gives

$$t_{50}(\text{pulsed}) \cdot d = t_{50}(\text{DC}) \cdot \frac{\tau_d}{\tau_r} \cdot \left( \frac{1}{d} - 1 \right) + t_{50}(\text{DC}). \quad (31)$$

The degree of lifetime enhancement is associated with the ratio  $\tau_d/\tau_r$ , and  $\tau_d/\tau_r$  is probably affected by several influences, such as the local microstructure, the local composition, current density [97], and thermal transients, to name a few.

With  $\tau_d/\tau_r$  being a constant, a plot of  $[t_{50}(\text{pulsed}) \times d]$  versus  $[(1/d) - 1]$  should produce a straight line according to this relation, and  $\tau_d/\tau_r$  can be extracted from its slope. Equation (31) expresses a  $1/d^2$  dependence when  $\tau_d/\tau_r$  happens to be equal to one and a  $1/d$  dependence when  $\tau_d/\tau_r$  is equal to zero.

Figure 69 is a plot of  $[t_{50} \times d]$  versus  $[(1/d) - 1]$  for the 133 MHz results. Each point is labeled with its corresponding duty cycle. If the data points are



assumed to reflect a continuous functional dependence, then the solid curve may represent such a dependence. This curve has no meaning in the present context, however, because  $\tau_d/\tau_r$  is defined as a constant, and the associated straight line must go through the DC data point. It is apparent that Figure 69 reveals at least two regimes. One of these is displayed by the data points for duty cycles of 77%, 66.7%, and 50%, because it could be estimated that these fall around the dashed line for a  $\tau_d/\tau_r$  ratio equal to one. The other is associated with the data point for 33%, which falls on the dashed line for a  $\tau_d/\tau_r$  equal to 0.5.

This analysis is not meant to suggest that Equation (31) can represent two different straight lines at the same time. The interpretation is that the 33% point lay on a line that represents a DC-referenced  $\tau_d/\tau_r$  of 0.5, and the other points fall about a line that represents a DC-referenced  $\tau_d/\tau_r$  of 1. The failure of the data to fall along a single straight line just means that some additional factor is at work, and this factor apparently undergoes a transition somewhere between duty cycles of 50% and 33%.

The usefulness of Figure 69 is derived from its explicit quantification of the degree of lifetime enhancement in terms of the relative rates of damage and recovery. For example, the data of Figure 59 indicate that  $t_{50}$  is halfway between the on-time prediction and the average current density prediction for a duty cycle of 33%. In the context of Figure 69,  $\tau_d/\tau_r = 0.5$  is also halfway between these two predictions, that is, 0.5 is halfway between zero and one.

The deviation from  $\tau_d/\tau_r = 1$  that is exhibited for a duty cycle of 33.3% could arise from any physical influence that changes  $\tau_d$ ,  $\tau_r$ , or both  $\tau_d$  and  $\tau_r$ .

One readily envisioned example of such an influence involves the temperature excursions that are often associated with pulsed current stressing. When the pulse amplitude is large enough and the pulse on times are long enough, a significant rise in the stripe temperature may be experienced on each pulse, and the temperature might even reach the steady state DC value. In addition, the temperature might be allowed to drop back to that of the ambient during the off times between pulses if they are long enough. If the amount of Joule heating is severe, then the temperature fluctuation may be quite large. The relatively low temperature during the off times, compared to that during the on times, would result in a value of  $\tau_d/\tau_r$  that is smaller than it would be if there were no temperature fluctuations. In fact,  $\tau_d/\tau_r$  may approach zero, which is the value for an on-time dependence of  $t_{50}$  on duty cycle.

The experiments that were performed in this study did not involve extreme Joule heating, and, in addition, the pulse frequencies were too high to allow any significant temperature fluctuations. This latter contention is especially true for the pulse frequency of 133 MHz, which is why it was chosen for Figure 69. Some other effect was operating in these experiments.

Other possible sources of influence on  $\tau_d/\tau_r$  are current density, local microstructure, and local chemical composition, but the pulse amplitude was the same and the samples were presumed to be identical for all pulse treatments. There is no fundamental correlation between these factors and the pulse duty cycle or frequency. But, a possible effective correlation between duty cycle and microstructure was identified earlier. It was suggested that an increase in the

Blech length with decreasing duty cycle sometimes causes the electromigration damage process to "select" an alternate site away from the cathode contact if the first bamboo segment at the contact happens to be too short. So, it might be said that the local microstructure does effectively depend on the duty cycle.

With this reasoning, it could be contended that damage occurs in bamboo segments that are, on average, longer for small duty cycles than they are for large duty cycles. A given accumulation of damage produces a damage gradient that depends inversely on the segment length. Since the rate of recovery should be proportional to the damage gradient, recovery should be slower (larger  $\tau_r$ ) for longer segments. If so, the effective value of the ratio  $\tau_d/\tau_r$  would be smaller for small duty cycles than it is for large duty cycles, and this is just the type of behavior displayed in Figure 69.

The possible relationship between damage location and the amount of lifetime enhancement (or  $\tau_d/\tau_r$ ) can be further investigated by examining all of the results for  $d = 50\%$ . Recall that there was a noticeable spread in  $t_{50}$  between the two separate groups of data points that were gathered from the two different test batches (Figure 65). The  $t_{50}$  data for one group, batch #1, fell about the average current density model, but the data for the second group, batch #2, were shifted toward less enhancement. The connection between lifetime enhancement and damage location may be further assessed, then, independent of the duty cycle.

The histograms of Figure 70 present the normalized damage count versus distance from the cathode for a duty cycle of 50%. These data are the same as those that were presented in Figure 20 (d), except that they have been divided



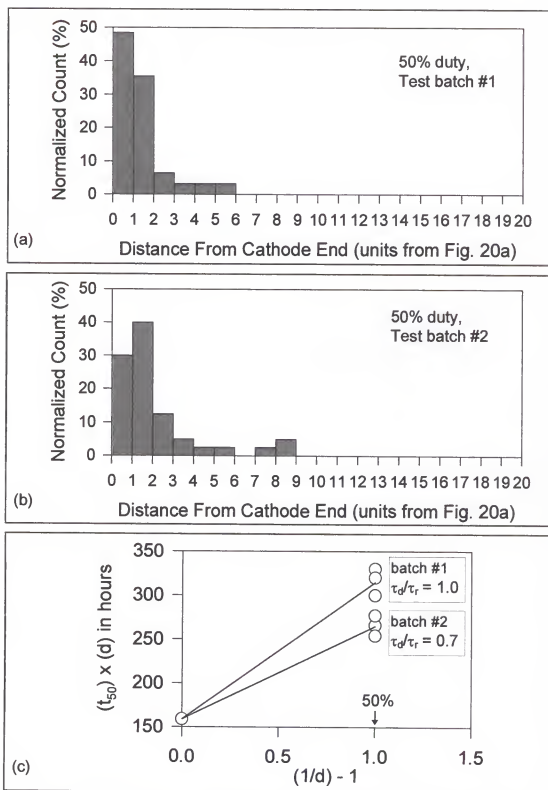


Figure 70. Distribution of damage versus position -- 50% duty cycle.

(a) Test batch #1.

(b) Test batch #2.

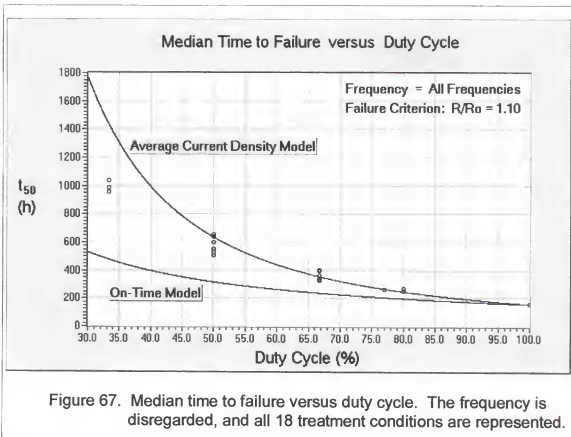
(c) Estimation of  $\tau_d/\tau_r$  for each batch.

between Parts (a) and (b) according to test batch. Part (a) represents batch #1, and Part (b) represents batch #2. A shift of damage away from the cathode is evident for batch #2, relative to #1. Part (c) shows the estimations of  $\tau_d/\tau_r$  for the two batches -- about 1.0 for batch #1 and 0.7 for batch #2. There seems, once more, to be a correlation between damage location and  $\tau_d/\tau_r$ , such that  $\tau_d/\tau_r$  is smaller with increasing incidence of downwind damage. This might again be explained in terms of the Blech length. The duty cycle would not, in this case, be the reason for the variation in Blech length, however, and a suggestion for an alternative cause is difficult to offer. There may have been some nonuniformity in the samples according to which part of the source wafer they were taken from.

The generalized treatment of lifetime enhancement in terms of  $\tau_d/\tau_r$  is effective in explaining the results of this study. It seems that a dependence of  $t_{50}$  on  $1/d^2$  ( $\tau_d/\tau_r = 1.0$ ) can be taken as a fundamental reference point that holds up for many cases, but sometimes breaks down when additional physical influences are present. The "additional physical influence" that was acting in the present study appears to be the microstructure of the test stripes. A near-bamboo grain structure may be responsible for the interaction between duty cycle, damage location, and degree of lifetime enhancement.

## SUMMARY AND CONCLUSION

The central purpose of this work was to determine how the reliability ( $t_{50}$ ) of IC interconnections depends on the duty cycle and the frequency of a pulsed stress current, with special emphasis on very high frequencies -- up to 133 MHz. The concentration on very high frequencies grew out of a technological need, as well as a desire to contribute such information to the literature, which holds few reports for frequencies greater than 1 MHz. Figure 67 provides a succinct view of the results, so it is repeated here.



It was found that lifetime enhancement was substantial over the entire range of frequencies and did not depend on the frequency in any specific way. Enhancement was more pronounced, in absolute terms, the smaller the duty cycle, but the widely touted average current density model overestimated the lifetime somewhat at the smallest duty cycle tested – 33.3%. Whenever pulsed currents are in consideration, IC miniaturization can certainly be pursued more aggressively than an on-time prediction would allow, but care should be taken in extending the average current density model to low duty cycles. Unique factors related to the specific metallization scheme in question may ultimately determine the actual behavior.

One possible “unique factor” that was identified in the present study was the increased incidence of damage at downwind locations for small duty cycles. By referencing the work of Frankovic et al., it was suggested that a Blech length effect could be the cause of this behavior if it were assumed, as it often is, that a unique Blech length is associated with each segment of a near-bamboo grain structure. The segment over the tungsten plug contact might sometimes be too short for any net damage to occur there, and such a condition would arise more frequently the larger the Blech length, that is, the smaller the duty cycle. When damage is prevented at the tungsten contact, it must “find” a longer segment farther downwind.

A correlation was also noted between the amount of  $t_{50}$  enhancement and the incidence of downwind damage. This would appear, on the surface, to be a direct reflection of the duty cycle dependence described above, but it was not

observed exclusively with duty cycle variations. It was also observed between two different batches of samples tested with a duty cycle of 50%. The batch for which  $t_{50}$  enhancement was smaller revealed an increased incidence of damage downwind, compared to the other, for which enhancement was larger. The explanation was again given in terms of Blech lengths, along with the use of a generic construct ( $\tau_d/\tau_r$ ) from Wu and McNutt. The ratio,  $\tau_d/\tau_r$ , was introduced, where  $\tau_d/\tau_r = 1.0$  corresponded to the average current density model and  $\tau_d/\tau_r = 0$  corresponded to the on-time model. Presumably,  $\tau_r$  increases with the length of the bamboo segment being damaged, which is larger, on average, the larger the Blech length. The estimated value of  $\tau_d/\tau_r$  was about 0.5 for a 33.3% duty cycle and about 1.0 for duty cycles above 50%. At 50%,  $\tau_d/\tau_r$  was about 0.7 for one test batch (less enhancement) and about 1.0 for the other (more enhancement).

The use of a concept such as  $\tau_d/\tau_r$  relies on the assumption that lifetime enhancement is caused by a backflow of material (or vacancies) during the off times between pulses. This is contrary to an “experienced” current view, that has been supported by some researchers. It was seen, however, through direct experimental observation (Figure 40), that diffusion of material may proceed down an electromigration-induced concentration gradient at a speed comparable to the electromigration itself.

Several models (e.g. those of Maiz, Clement, and Dwyer) predict that  $t_{50}$  should fundamentally be proportional to  $1/d^2$ . This may be correct, other things being equal, but additional influences can play a role. A microstructure-induced Blech length effect might be the additional influence in the present work.

Other observations were worth noting. First, the  $R/R_0$  versus time plots showed that the test stripe resistance often increased in discontinuous bursts rather than one gradual rise. This was assumed to be evidence of multiple damage sites, each requiring a different incubation period. Multiple damage sites were indeed observed in the micrographs. Second, there was no apparent dependence of the standard deviation of the failure times on pulse duty cycle or frequency. The standard deviations were smaller, however, than those normally found by other researchers.

Some of the conclusions that were offered here are a simple reflection of the data. Others are based on additional analysis, which provided reasonable explanations for the results, but also revealed interesting topics for future work. The next chapter addresses this thought.

## SUGGESTIONS FOR FUTURE WORK

While a number of interesting conclusions were derived from this study, further investigations would be worthwhile. For example, there is room to expand the range and the quantity of stress conditions tested. Such an effort would represent a simple continuation of the path followed here. An alternate direction could be taken as well, by pursuing other topics that are suggested by the present findings.

It was determined that lifetime enhancement is a pervasive element of pulsed electromigration at all high and very high frequencies up to 133 MHz. This is an important finding, but it would be useful to push toward even higher frequencies, possibly as high as 1 GHz. The primary obstacle would be the difficulty of delivering a 1 GHz pulse waveform to a test stripe and faithfully monitoring the electromigration response.

The dependence of  $t_{50}$  on the duty cycle was not predicted well by the average current density model at the smallest duty cycle tested -- 33.3%. An explanation was offered for this finding, but it is still necessary to investigate smaller duty cycles, perhaps as small as 5%. Long test times would be required to perform these experiments, however, and this may discourage such efforts.

The Blech length effect that was offered as a reason for the increased incidence of downwind damage at small duty cycles should be confirmed with a

systematic study. Such work might involve the fabrication of special test stripes, which have a bamboo grain structure with precisely controlled segment lengths. First, the association of a unique Blech length with each bamboo segment could be confirmed by determining whether the threshold current density depends on the segment length for a constant total stripe length. The segment lengths could then be systematically varied in an attempt to identify any possible effect on the location of damage. The duty cycle - Blech length relationship introduced by Frankovic et al. might also be investigated.

Any dependence of  $t_{50}$  on the bamboo segment length could be identified in the same setup. A decreasing  $t_{50}$  with increasing segment length would justify the explanation that was given for the deviations of  $t_{50}$  from the average current density prediction.

It would be useful to visually observe the damage process as it occurs. The discontinuous progression of  $R/R_0$  might be more thoroughly explained from the results. *In situ* chemical analysis would provide even more information, particularly with respect to the movement of copper and its role in the behavior of  $R/R_0$  versus time. However, such work would probably be outside the arena of pulsed electromigration concerns, unless the pulse duty cycle or frequency would happen to affect the mode by which  $R/R_0$  changes.

Suggestions for future work are a natural outgrowth of any research project. They may sometimes be as important as the conclusions themselves.



## APPENDIX

### Test Apparatus

#### Summary

The purpose of this appendix is to provide specific details of the circuitry that was constructed for this work. It is included as a documentation of circuit schematics and to provide more detailed descriptions of circuit functions than those provided in the main body of the dissertation. Figure 15 is presented again, on the next page, as a guide to the major circuit functional blocks. Each block is now discussed.

#### Pulse Generator

Test waveforms originate from a commercial pulse generator whose output can be controlled with regard to frequency, duty cycle, and pulse amplitude. It was not possible, however, to design a single distribution circuit to accommodate the full range of test frequencies specified in this work, partly because the gain bandwidth of a given amplifier is usually limited to some frequency range and partly because the selection of such components as coupling capacitors and blocking inductors depends on the frequency. As such, the full range of frequencies which may be available from any given pulse generator is not necessarily deliverable to the sample on any given channel.

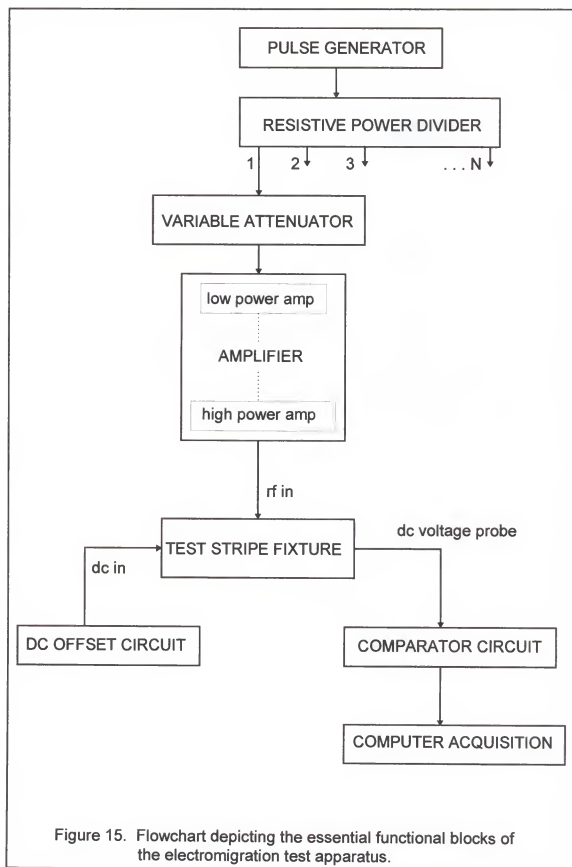
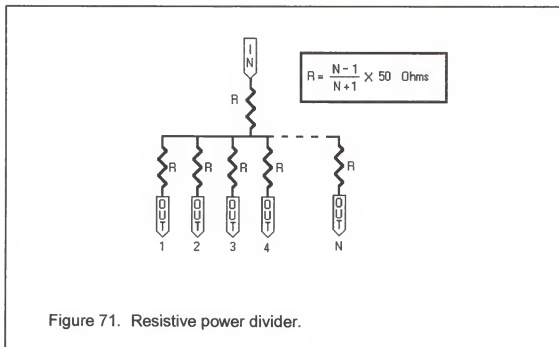


Figure 15. Flowchart depicting the essential functional blocks of the electromigration test apparatus.

The 24 channels have, therefore, been divided into three subsets, the circuitry for each one being designed for and dedicated to a particular frequency range. Each group is supplied by its own pulse generator.

### Power Divider

Test waveforms have to be distributed to multiple channels, which is the purpose of a power divider. Reactive dividers would distribute the signal with less power loss, but they are expensive and have frequency limitations. Resistive power dividers were chosen because they are not so expensive and they work well across a wide frequency range if small surface mount resistors are used. Figure 71 depicts a resistive divider which divides the signal into N branches. The values of the resistors, R, are all the same. The transmission cables used here have a characteristic impedance of 50  $\Omega$ . In order to satisfy



the impedance-matching requirement, then, the value of  $R$  must be chosen so that  $50\ \Omega$  is "seen" looking into the divider from both directions, assuming that the "OUT" of each branch feeds into a  $50\ \Omega$  input impedance and the "IN" comes from a  $50\ \Omega$  output impedance. Power losses can be recovered later with the appropriate amplifiers.

### Variable Attenuator

Each channel has a voltage variable attenuator, which is used to adjust the amplitude of the waveform on that channel, independent from the other channels. This is needed, even in the case that the same pulse amplitude is desired on every channel, because it is unlikely that the signals on all of the channels will reach their respective test stripes with identical amplitudes. Each branch will likely differ slightly from the other branches because the transmission line lengths will not be identical and the amplifier gain will vary slightly from branch to branch, among other things. The variable attenuator is also required, of course, in the case that a different pulse magnitude is desired on each channel. The circuit is shown in Figure 72.

### Amplifier

Power is lost in the resistive divider and in the attenuator, so an amplifier(s) may be required to deliver a waveform of sufficient magnitude to the sample. Operational amplifiers, because of their versatility, would be a logical choice for this application. A  $1 \times 10^7\ \text{A/cm}^2$  pulse repeated at a rate of 100 MHz with a 15% duty factor is difficult to achieve, however, with any but the most

expensive op-amps, so a wideband RF amplifier (Motorola, CA5915) was found to handle this part of the job. The associated circuit is presented in Figure 73. This particular amplifier has a maximum output power of 1W and a gain of +15dB with a bandwidth up to 1200 MHz on the high end. The low end of the

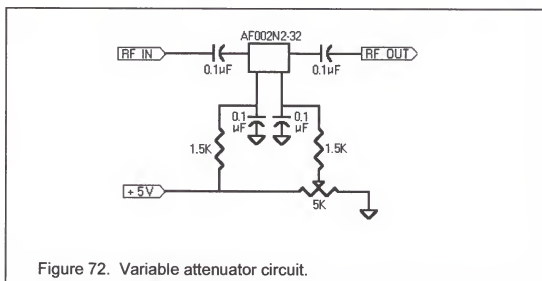


Figure 72. Variable attenuator circuit.

gain bandwidth occurs at about 50 MHz, however, so a different amplifier (Motorola, MHW591) is used from this frequency down to about 1 MHz. The frequency range at and below 1 MHz can be handled with inexpensive operational amplifiers (Analog Devices, AD846). It is useful in some cases to first recover just that power which was lost in the power dividers and the attenuators before sending the signal on to the high power amplifiers. Low power MMIC amplifiers (Avantek, MSA -1105) are used for this purpose, so the "AMPLIFIER" box of Figure 15 contains this "low power amp" in addition to one of the other three "high power amps" (CA5915, MHW591, or AD846). Each of the three frequency ranges just mentioned is assigned to its own dedicated group of channels, as described earlier in the "Pulse Generator" section.

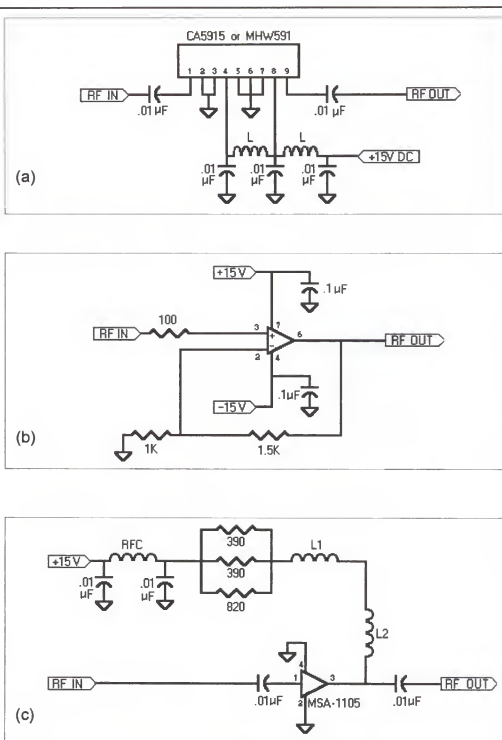


Figure 73. Amplifier circuits.

- (a) Amplifier circuit for the CA5915 and MHW591.
- (b) Operational amplifier (AD846) circuit.
- (c) Low power amplifier (MSA-1105) circuit.

### DC Offset Circuit

The RF amplifier circuits and the attenuator circuits used in this system provide an AC coupled output, that is, they do not transmit any DC component which may have been present on the input waveform. The output is bidirectional, so, if a unidirectional, positive current pulse is desired, for example, then a DC offset current must be added to the output of the amplifier. A circuit is provided for this purpose, and the schematic is given in Figure 74. It is essentially an adjustable constant voltage source, and there is one of these "voltage sources" for each channel. The circuit drives a DC current through a

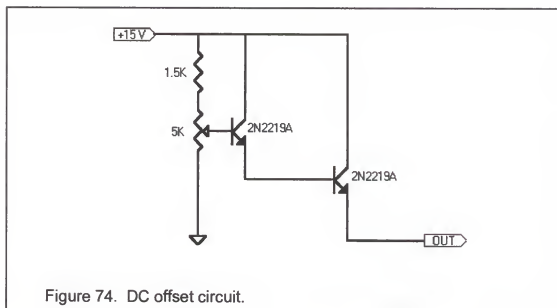
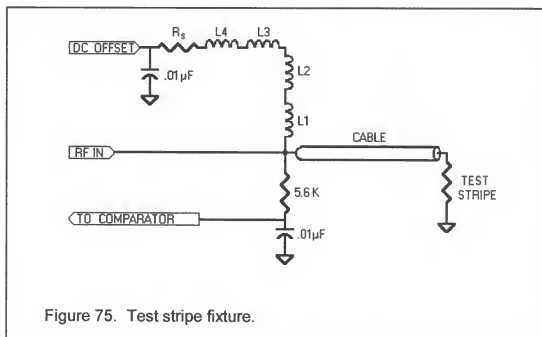


Figure 74. DC offset circuit.

series resistor, a series inductance, and into the test stripe, which are all part of the so-called "test stripe fixture," depicted in Figure 75. The "OUT" terminal of Figure 74 feeds into the "DC OFFSET" terminal of the test stripe fixture. It also feeds the "dc in" line of Figure 15. More about the test stripe fixture will be discussed shortly. The DC offset current is added to the bidirectional pulse

waveform coming from the amplifier ("RF in," Figs. 15 and 75), and, by changing the sign and the magnitude of the DC current, the waveform can be shifted up or down to produce a positive pulse train, a negative pulse train, or anything in between.

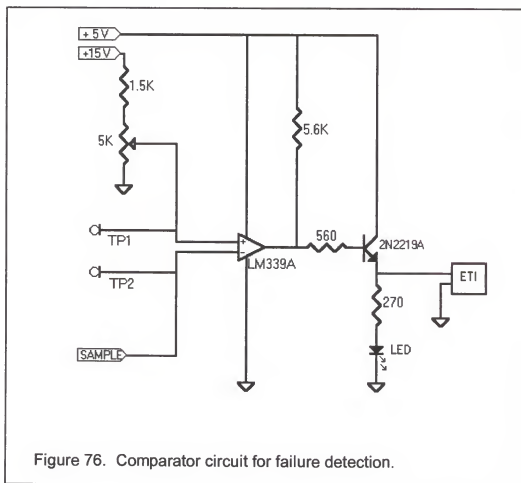


### Comparator Circuit

This circuit is revealed in Figure 76, and is part of the first generation failure detection scheme. One of the inputs to the LM339A comparator is connected to the test stripe fixture through a 5.6 K $\Omega$  current-blocking resistor, and acts to sample the DC level on the stripe, which is just equal to the offset voltage. Since the offset voltage is produced (see the previous section) by dividing the output of a constant voltage source between a series resistance (resistor plus inductor) and the test stripe, the offset voltage depends on, and changes with, the resistance of the stripe. Specifically, the offset voltage rises



as the stripe resistance rises. The other input to the LM339A is connected to another adjustable voltage source. The offset voltage is "compared" to this "trip voltage" by the comparator. The result of this comparison determines the comparator's output voltage, which is 5 V so long as the offset voltage is less than the trip voltage, and is zero if the offset voltage exceeds the trip voltage. Using the fact that the offset voltage depends on the stripe resistance, the trip voltage can be set equal to that offset voltage which corresponds to the failure



resistance as determined from the failure criterion (a 10% increase in resistance, for example). The pre-failure 5 V output of the comparator is used to light an

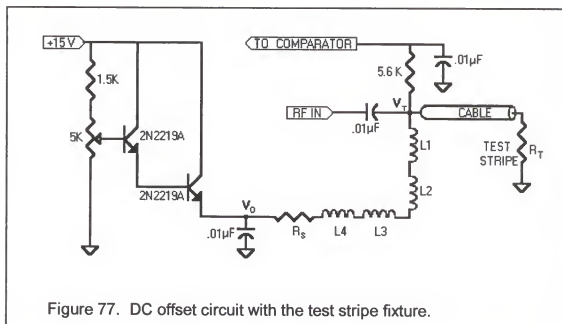
LED and to drive an elapsed time indicator (ETI). When the offset voltage exceeds the trip voltage, that is, when the sample "fails," the comparator output voltage goes to zero. The LED goes out, providing quick visual confirmation of a failure, and the ETI stops running, thus recording the lifetime.

### Computer acquisition

With the appropriate voltage measurements, a calculation of the sample stripe resistance can be made while the stripe is under test. If these voltages are logged periodically over the course of the test, a plot of resistance versus time may be obtained, and this is exactly what is done with the computer-based data acquisition (DAQ) system. A 64 channel plug-in board with DC voltage inputs is used in conjunction with a personal computer. Under the direction of an appropriate program, the 48 voltages which are required to calculate the resistances of the 24 test stripes are acquired by the board at short intervals, the resistances are calculated, and a resistance versus time file is generated. The file can later be manipulated and plotted for display.

The determination of test stripe resistance can be made *in situ* while the stripes are under test by making use of the offset circuit arrangement. The method can be described with reference to Figure 77, which shows the test stripe fixture together with the offset circuit. The current that goes through the 5.6 K $\Omega$  resistor to the comparator circuit is negligible compared to the offset current. Also, no DC goes through the RF coupling capacitor. It is essentially true, then that all of the current supplied by the offset circuit goes through the test stripe. If the total resistance of  $R_s$ ,  $L_4$ ,  $L_3$ ,  $L_2$ , and  $L_1$  is known (call it

$R_{\text{series}}$ ), and if it is known that this resistance stays constant during the test (the variability is very small, in fact), then the resistance of the test stripe,  $R_T$ , can be calculated from  $V_T$ ,  $V_O$ , and  $R_{\text{series}}$ . The voltages  $V_T$  and  $V_O$  can, of course, be measured with a digital voltmeter if a quick check is needed, but most data



acquisition (DAQ) is done automatically through the computer interface. The DAQ system makes the required voltage measurements at regular time intervals, and it automatically calculates and logs the stripe resistances at these intervals. The calculation of stripe resistance,  $R_T$ , is given by

$$R_T = \frac{V_T \cdot R_{\text{series}}}{V_O - V_T} \quad \text{in } \Omega. \quad (32)$$

The series resistance,  $R_{\text{series}}$ , although its variation is small, is not strictly constant. It varies slightly with the local temperature, so a simple means of compensating for this variation was devised by calibrating the temperature

dependence of  $R_{\text{series}}$  for each channel to that of a reference resistance. The DAQ program incorporates this calibration into the voltage measurements.

### Test stripe fixture

The test stripe, which is akin to an integrated circuit interconnect, is patterned onto a silicon chip by methods used in standard IC lithography and wafer processing, the chip is mounted in a dual in-line package (DIP) and each end of the test stripe is wired to a pin on the DIP. For testing, the DIP is plugged into one of the specially constructed high-temperature receptacles that are arranged on a panel inside a temperature-regulated furnace. Each receptacle connects a DIP-packaged test stripe to the external circuitry via a  $50\ \Omega$  coaxial cable. Again, the test stripe fixture was depicted in Figure 75, and it contains the series inductors and the series resistor into which the offset circuitry is driven, as well as the current-blocking, high-valued resistor to which the comparator circuit is connected.

### Use of the Comparator

The life status of the test stripes may be continuously indicated and the eventual time to failure may be recorded through the comparator-based detection scheme. This function was introduced earlier. Although the computer DAQ system, which was added as an upgrade, makes the use of this feature unnecessary, it can be useful when quick visual checks of the test status may be desired during the course of a test.

The use of this feature goes as follows. The starting DC offset voltage  $V_T$ , and the starting stripe resistance are first determined for each test channel. It is assumed that  $V_O$  stays constant during the test (a fairly accurate assumption), and a calculation is made to determine that value of  $V_T$  which corresponds, for example, to a 10% increase in stripe resistance or whatever increase has been chosen as the failure criterion. The comparator "trip" voltage is set to this value in order to record the time of failure with the ETI. The LEDs will stay on so long as  $V_T$  is less than the trip voltage, that is, so long as the test stripes have not yet failed.

#### Further Discussion of Design and Procedure

It has already been explained that this apparatus uses a constant DC voltage,  $V_O$ , to drive the offset current to the test stripe through a series resistance. The resulting dependence of the offset voltage,  $V_T$ , on the stripe resistance is the basis for the stripe resistance calculation. The resistance could be monitored just as well, however, by maintaining a constant offset current, because the DC voltage across the stripe would depend on the stripe resistance in this case, also. The main reason for choosing the present design relates back to the primary purpose of the offset circuit, which is to shift the AC coupled RF pulse waveform up or down, so as to obtain a pulse train of the desired polarity. The RF amplifiers employed here, and also the pulse generators for that matter, have a  $50\ \Omega$  output impedance and therefore are intended to drive a  $50\ \Omega$  load. This situation is depicted in Figure 78.  $V_O$  is the open circuit output voltage of the amplifier, and  $V_T$  is the voltage across the load.

It is determined from voltage divider analysis that  $V_T$  changes, and so the peak-to-peak magnitude of the waveform changes, as  $R_L$  changes. The offset voltage must change in like manner, so that the waveform remains DC shifted by the correct amount to maintain a unidirectional pulse or whatever was set up at

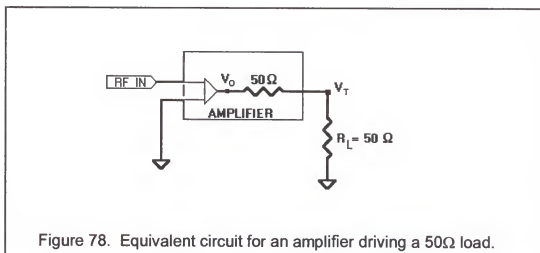


Figure 78. Equivalent circuit for an amplifier driving a 50Ω load.

the start of the experiment. As such, it is required that the DC offset circuit also deliver a constant voltage,  $V_o$ , which is driven across a series resistance equal to  $R_s + R_{L4} + R_{L3} + R_{L2} + R_{L1}$ , as depicted in Figure 77. The series resistance is to the offset circuit as the output impedance is to the amplifier, so if this resistance is 50 Ω, then the correct DC shift is maintained as  $R_L$  deviates from 50 Ω.

The preceding discussion shows that the present design does not provide the often used constant current test conditions. This is more or less important depending on whether the failure criterion calls for a small or large resistance increase and how rapidly the resistance change occurs. Since it is usually assumed that electromigration is accompanied by local dimensional changes, a constant current does not really provide a constant current density. So the use

of a constant current is not particularly consistent with the usual models (Black's equation) that are employed, anyway. A constant voltage provides a constant current density if the change in resistance is due solely to a uniform change in the cross-section and the resistivity remains constant. It may not be fair to assume that the local resistivity remains constant, however, and electromigration damage does not typically show as a uniform change in cross-section. It most often shows up as small, localized changes. When the test stripes are very long compared to the damage area, the local changes in cross-section are much greater than the change in resistance would indicate under the assumption that these changes are actually taking place uniformly over the length of the test stripe. The present setup provides something in between constant current and constant voltage, but even so, the local current density rises severely during the damage process. The current density in the nondamaged areas will decrease, but this decrease is fairly small relative to the increase at the damage sites. In the end, it is probably unimportant whether the electrical stress condition is constant current, constant voltage, or something in between.

## REFERENCES

1. Verhoeven, J., *Metallurgical Reviews*, 8(31), 311 (1963).
2. Huntington, H. B. in Diffusion in Solids: Recent Developments, edited by A. S. Nowick, and J. J. Burton (Academic Press, New York, NY, 1975) pp. 303-352.
3. Sorbello, R. S. in Electro- and Thermo-transport in Metals and Alloys, edited by R. E. Hummel and H. B. Huntington (AIME, New York, NY, 1977) pp. 2-19.
4. d'Heurle, F. M. and Ho, P. S. in Thin Films: Interdiffusion and Reactions, edited by J. M. Poate, K. N. Tu, and J. W. Mayer (Wiley-Interscience, New York, NY, 1978) pp. 243-303.
5. Kwok, T. and Ho, P. S. in Diffusion Phenomena in Thin Films and Microelectronic Materials, edited by D. Gupta and P. S. Ho (Noyes, Park Ridge, NJ, 1988) pp. 369-431.
6. Christou A. (editor), Electromigration and Electronic Device Degradation (Wiley-Interscience, New York, NY, 1994) all pp.
7. Hummel, R. E., *International Materials Reviews*, 39(3), 97 (1994).
8. Huntington, H. B. and Grone, A. R., *J. Phys. Chem. Solids*, 20, 76 (1961).
9. Black, J. R., *Proc. IEEE*, 57(9), 1587 (1969).
10. Black, J. R., *IEEE Trans. Electron Dev.*, ED-16(4), 338 (1969).
11. d'Heurle, F. M., *Metallurgical Transactions*, 2, 683 (1971).
12. Agarwala, B. N. in Proc. 13th Int. Reliability Physics Symp. (IEEE, 1975) p. 107.
13. Schafft, H. A., Grant, T. C., Saxena, A. N., and Kao, C. in Proc. 23rd Int. Reliability Physics Symp. (IEEE, 1985) p. 93.



14. Venables, J. D. and Lye, R. G. in Proc. 10th Int. Reliability Physics Symp. (IEEE, 1972) p. 159.
15. Sigsbee, R. A. in Proc. 11th Int. Reliability Physics Symp. (IEEE, 1973) p. 301.
16. Shatzkes, M. and Lloyd, J. R., J. Appl. Phys., 59(11), 3890 (1986).
17. Hummel, R. E., Physica Status Solidi (a), 107, K175 (1988).
18. Black, J. R. in Proc. 12th Int. Reliability Physics Symp. (IEEE, 1974) p. 142.
19. Hummel, R. E. and Geier, H. J., Thin Solid Films, 25, 335 (1975).
20. Blech, I. A. and Kinsbron, E., Thin Solid Films, 25, 327 (1975).
21. Tai, K. L. and Ohring, M., J. Appl. Phys., 48, 36 (1977).
22. Gangulee, A. and d'Heurle, F. M., Scripta Met., 7, 1027 (1973).
23. Park, C. W. and Vook, R. W., Appl. Phys. Lett., 59, 175 (1991).
24. Attardo, M. J. and Rosenberg, R., J. Appl. Phys., 41, 2381 (1970).
25. Hummel, R. E., DeHoff, R. T., and Geier, H. J., J. Phys. Chem. Solids, 37, 73 (1976).
26. Spitzer, S. M. and Schwartz, S. S., IEEE Trans. Electron Dev., 16, 348 (1969).
27. Blech, I. A. and Meieran, E. S., J. Appl. Phys., 40, 485 (1969).
28. Berenbaum, L., J. Appl. Phys., 42, 880 (1971).
29. Weise, J., Thin Solid Films, 13, 169 (1972).
30. Black, J. R. in Proc. 6th Int. Reliability Physics Symp. (IEEE, 1968) p. 148.
31. Oliver, C. B. and Bower, D.E. in Proc. 8th Int. Reliability Physics Symp. (IEEE, 1970) p. 116.
32. Learn, A. J., Appl. Phys. Lett., 19, 272 (1971).
33. Gangulee, A., J. Appl. Phys., 45, 3749 (1974).

34. Hummel, R. E. and Malone, D. W. in Materials Reliability Issues in Microelectronics, edited by J. R. Lloyd, F. G. Yost, and P. S. Ho (Mater. Res. Soc. Proc. 225, Pittsburgh, PA, 1991) p. 67.
35. Agarwala, B. N., Patnaik, B., and Schnitzel, R., J. Appl. Phys., 39, 1487 (1972).
36. Hummel, R. E. in Electro- and Thermo-transport in Metals and Alloys, edited by R. E. Hummel and H. B. Huntington (AIME, New York, NY, 1977) p. 93.
37. Rosenberg, R., J. Vac. Sci. Technol., 9(1), 263 (1972).
38. Li, P., Yapsir, A. S., Rajan, K., and Lu, T-M., Appl. Phys. Lett., 54, 2443 (1989).
39. Knorr, D. B., Rodbell, K. P., and Tracy, D. P. in Materials Reliability Issues in Microelectronics, edited by J. R. Lloyd, F. G. Yost, and P. S. Ho (Mater. Res. Soc. Proc. 225, Pittsburgh, PA, 1991) p. 21.
40. Rodbell, K. P., Knorr, D. B., and Tracy, D. P. in Materials Reliability in Microelectronics II, edited by C. V. Thompson and J. R. Lloyd (Mater. Res. Soc. Proc. 265, Pittsburgh, PA, 1992) p. 107.
41. Knorr, D. B., Rodbell, K. P. in Materials Reliability in Microelectronics II, edited by C. V. Thompson and J. R. Lloyd (Mater. Res. Soc. Proc. 265, Pittsburgh, PA, 1992) p. 113.
42. Vaidya, S. and Sinha, A. S., Thin Solid Films, 75, 253 (1981).
43. Nix, W. D., Metallurgical Transactions, 20A, 2217 (1989).
44. Blair, J. C., Ghate, P. B., Haywood, C. T., Appl. Phys. Lett., 17(7), 281 (1970).
45. Gangulee, A. and d'Heurle, F. M., Thin Solid Films, 16, 227 (1973).
46. Pierce, J. M. and Thomas, M. E., Appl. Phys. Lett., 39(2), 165 (1981).
47. d'Heurle, F. M. and Ames, I., Appl. Phys. Lett., 16, 80 (1970).
48. Chisholm, M. F., Aaron, D. B., Wiley, J. D., and Perepezko, J. H., Appl. Phys. Lett., 53(2), 102 (1988).

49. Ames, I., d'Heurle, F. M., and Horstmann, R. E., IBM J. Res. Develop. 14, 461 (1970).
50. Learn, A. J., J. Electronic Materials, 3, 531 (1974).
51. van Gurp, G. J., Appl. Phys. Lett., 19, 476 (1971).
52. Agarwala, B. N., Berenbaum, L., and Peressini, P., J. Electronic Materials, 3, 137 (1974).
53. Agarwala, B. N., Digiacomio, G., and Joseph, R. R., Thin Solid Films, 34, 165 (1976).
54. Berenbaum, L. and Rosenberg, R. in Proc. 9th Int. Reliability Physics Symp. (IEEE, 1971) p. 136.
55. d'Heurle, F. M., Ainslie, N. G., Gangulee A., and Shine, M. C., J. Vac Sci. Technol., 9, 289 (1972).
56. d'Heurle, F. M., Gangulee, A., Aliotta, C. F., and Ranieri, V. A., J. Electronic Materials, 4, 497 (1975).
57. d'Heurle, F. M., Gangulee, A., Aliotta, C. F., and Ranieri, V. A., J. Appl. Phys., 46, 4845 (1975).
58. Agarwala, B. N., Attardo, M. J., and Ingraham, A. P., J. Appl. Phys., 41, 3954 (1970).
59. Schafft, H. A., Staton, T. C., Mandel, J., and Shott, J. D., IEEE Trans. Electron Dev., ED-34, 673 (1987).
60. English, A. T., Tai, K. A., and Turner, P. A., J. Appl. Phys., 45, 3757 (1974).
61. Scoggan, G. A., Agarwala, B. N., Peressini, P. P., and Brouillard, A. in Proc. 13th Int. Reliability Physics Symp. (IEEE, 1975) p. 151.
62. Kwok, T. in Proc. 26th Int. Reliability Physics Symp. (IEEE, 1988) p. 185.
63. Kinsbron, E., Appl. Phys. Lett., 36(12), 968 (1980).
64. Iyer, S. S. and Ting, C. Y., IEEE Trans. Electron Dev., ED-31, 1468 (1984).
65. Vaidya, S., Sheng, T. T., and Sinha, A. K., Appl. Phys. Lett., 36(6), 464 (1980).

66. Ainslie, N. G., d'Heurle, F. M., and Wells, O. C., Appl. Phys. Lett., 20(4), 173 (1972).
67. Blech, I. A., J. Appl. Phys., 47(4), 1203 (1976).
68. Matsuoka, F., Iwai, H., Hama, K., Itoh, H., Nakata, R., Nakakubo, T., Maeguchi, K., and Kanzaki, K., IEEE Trans. Electron Dev., 37, 562 (1990).
69. Tao, J., Young, K. K., Pico, C. A., Cheung, N. W., and Hu, C., IEEE Trans. Electron Dev., 12(12), 646 (1991).
70. Hu, C.-K., Small, M. B., Rodbell, K. P., Stanis, C., Mazzeo, N., Blauner, P., Rosenberg, R., and Ho, P. S. in Materials Reliability in Microelectronics III edited by K.P. Rodbell, W.F. Filter, H. J. Frost, and P. S. Ho (Mater. Res. Soc. Proc. 309, Pittsburgh, PA, 1993) p. 111.
71. Kawasaki, H., Lee, C., and Yu, T.-K., Thin Solid Films, 253, 508 (1994).
72. Hu, C.-K., Thin Solid Films, 260, 124 (1995).
73. Shacham-Diamand, Y., MRS Bulletin, XX(11), 78 (1995).
74. Kim, C., Selister, S. I., Morris, Jr., J. W. in Materials Reliability in Microelectronics III, edited by K.P. Rodbell, W.F. Filter, H. J. Frost, and P. S. Ho (Mater. Res. Soc. Proc. 309, Pittsburgh, PA, 1993) p. 127.
75. Oates, A. S. and Barr, D. L., J. Electronic Materials, 23(1), 63 (1994).
76. English, A. T., Tai, K. L., and Turner, P. A., Appl. Physics Letters, 21, 397 (1972).
77. Rosenberg, R. and Ohring, M., J. Appl. Phys., 42(13), 5671 (1971).
78. Blech, I. A. and Herring, C., Appl. Phys. Lett., 29(3), 131 (1976).
79. Davis, J. R., Proc. IEE, 123(11), 1209 (1976).
80. Miller, R. J. in Proc. 16th Int. Reliability Physics Symp. (IEEE, 1978) p. 241.
81. Kinsbron, E., Melliar-Smith, C. M., and English, A. T., IEEE Trans. Electron Dev., ED-26(1), 22 (1979).
82. Schoen, J. M., J. Appl. Physics, 51(1), 508 (1980).

83. Arzigian, J. S. in Proc. 21st Int. Reliability Physics Symp. (IEEE, 1983) p. 32.
84. Wu, C. J. and McNutt, M. J. in Proc. 21st Int. Reliability Physics Symp. (IEEE, 1983) p. 24.
85. English, A. T. and Kinsbron, E., J. Appl. Phys., 54(1), 275 (1983).
86. Towner, J. M. and van de Ven, E. P. in Proc. 21st Int. Reliability Physics Symp. (IEEE, 1983) p. 36.
87. Brooke, L. in Proc. 25th Int. Reliability Physics Symp. (IEEE, 1987) p. 136.
88. Lloyd, J. R. and Koch, R. H. in Proc. 25th Int. Reliability Physics Symp. (IEEE, 1987) p. 161.
89. Lloyd, J. R. and Koch, R. H., Appl. Phys. Lett. 52(3), 194 (1988).
90. Harrison, J. W., IEEE Trans. Electron Dev., 35(12), 2170 (1988).
91. Suehle, J. S. and Schafft, H. A. in Proc. 27th Int. Reliability Physics Symp. (IEEE, 1989) p. 229.
92. Liew, B. K., Cheung, N. W., and Hu, C. in Proc. 27th Int. Reliability Physics Symp. (IEEE, 1989) p. 215.
93. Maiz, J. A. in Proc. 27th Int. Reliability Physics Symp. (IEEE, 1989) p. 220.
94. Hatanaka, K., Noguchi, T., and Maeguchi, K. in Symposium on VLSI Technology: Digest of Technical Papers (IEEE and JSAP, 1989) p. 19.
95. Hummel, R. E. and Hoang, H. H., J. Appl. Physics, 65(5), 1929 (1989).
96. Liew, B. K., Cheung, N. W., and Hu, C., IEEE Trans. Electron Dev. 37(5), 1343 (1990).
97. Suehle, J. S. and Schafft, H. A. in Proc. 28th Int. Reliability Physics Symp. (IEEE, 1990) p. 106.
98. Liew, B. K., Fang, P., Cheung, N. W., and Hu, C. in Proc. 28th Int. Reliability Physics Symp. (IEEE, 1990) p. 111.
99. Tao, J., Young, K. K., Pico, C. A., Cheung, N. W., and Hu, C., IEEE Electron Dev. Lett., 12(12), 646 (1991).

100. Kwok, T., Kaufman, R., and Davari, B. in Materials Reliability Issues in Microelectronics, edited by J. R. Lloyd, F. G. Yost, and P. S. Ho (Mater. Res. Soc. Proc. 225, Pittsburgh, PA, 1991) pp. 85-89.
101. Clement, J. J., J. Appl. Phys. 71(9), 4264 (1992).
102. Clement, J. J. in Materials Reliability in Microelectronics II, edited by C. V. Thompson and J. R. Lloyd (Mater. Res. Soc. Proc. 265, Pittsburgh, PA, 1992) pp. 57-63.
103. Tao, J., Young, K., Cheung, N., and Hu, C. in Proc. 30th Int. Reliability Physics Symp. (IEEE, 1992) p. 338.
104. Li, Z., Bauer, C. L., Mahajan, S., and Milnes, A. G., J. Appl. Phys., 72(5), 1821 (1992).
105. Hinode, K., Furusawa, T., and Homma, Y. in Proc. 30th Int. Reliability Physics Symp. (IEEE, 1992) p. 205.
106. Castaño, E. and Maiz, J., Microelectron. and Reliab., 33(8), 1189 (1993).
107. Baldini, G. L., Scorzoni, A., and Tamarri, F., Microelectron. and Reliab., 33(11/12), 1841 (1993).
108. Ting, L. M., May, J. S., Hunter, W. R., and McPherson, J. W. in Proc. 31st Int. Reliability Physics Symp. (IEEE, 1993) p. 311.
109. Tao, J., Cheung, N., and Hu, C., IEEE Trans. Electron Dev., 41(4), 539 (1994).
110. Pierce, D. G., Snyder, E. S., Swanson, S. E., and Irwin, L. W. in Proc. 32nd Int. Reliability Physics Symp. (IEEE, 1994) p. 198.
111. Ohfuji, S. and Tsukada, M., J. Appl. Phys, 78(6), 3769 (1995).
112. Frankovic, R., Bernstein, G. H., and Clement, J. J. in Materials Reliability in Microelectronics VI, edited by W. F. Filter, J. J. Clement, A. S. Oates, R. Rosenberg, and P. M. Lenahan (Mater. Res. Soc. Proc. 428, Pittsburgh, PA, 1996) p. 109.
113. Frankovic, R., Bernstein, G. H., and Clement, J. J., IEEE Electron Dev. Lett., 17(5), 244 (1996).

114. Verbruggen, A. H., van den Homberg, M. J. C., Kalkman, A. J., Kraayeveld, J. R., Willemsen, A. W.-J., and Radelaar, S. in Materials Reliability in Microelectronics VI, edited by W. F. Filter, J. J. Clement, A. S. Oates, R. Rosenberg, and P. M. Lenahan (Mater. Res. Soc. Proc. 428, Pittsburgh, PA, 1996) p. 121.
115. Tao J., Chen, J. F., Cheung, N. W., and Hu, C., IEEE Trans. Electron Dev., 43(5), 800 (1996).
116. Tao J., Chen, J. F., Cheung, N. W., and Hu, C. in Proc. 34th Int. Reliability Physics Symp. (IEEE, 1996) p. 180.
117. Dwyer, V. M., IEEE Trans. Electron Dev., 43(6), 877 (1996).

## BIOGRAPHICAL SKETCH

David Wayne Malone was born on May 30, 1962, in Cincinnati, Ohio, and was raised in Melbourne, Florida. He attended Melbourne High School from 1977 to 1980, and upon graduation, he pursued further education in the field of engineering. While in attendance at the University of Florida, David obtained practical experience with Occidental Chemical Company, White Springs, FL, and Harris Corporation, Melbourne, FL, through the Cooperative Education program. He received his bachelor's degree in materials science and engineering from the University of Florida in May of 1987. David returned to the University of Florida in 1988 to pursue graduate studies and to perform research under the supervision of Professor Rolf E. Hummel. He investigated novel techniques of thin film deposition, as well as pulsed current electromigration. He received his master's degree in May of 1992 and his doctoral degree in May of 1997.



I certify that I have read this study and that in my opinion it conforms to acceptable standards of scholarly presentation and is fully adequate, in scope and quality, as a dissertation for the degree of Doctor of Philosophy.



Rolf E. Hummel, Chairman  
Professor of Materials Science  
and Engineering

I certify that I have read this study and that in my opinion it conforms to acceptable standards of scholarly presentation and is fully adequate, in scope and quality, as a dissertation for the degree of Doctor of Philosophy.



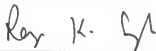
Robert T. DeHoff  
Professor of Materials Science  
and Engineering

I certify that I have read this study and that in my opinion it conforms to acceptable standards of scholarly presentation and is fully adequate, in scope and quality, as a dissertation for the degree of Doctor of Philosophy.



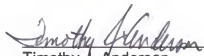
Robert M. Park  
Professor of Materials Science  
and Engineering

I certify that I have read this study and that in my opinion it conforms to acceptable standards of scholarly presentation and is fully adequate, in scope and quality, as a dissertation for the degree of Doctor of Philosophy.



Rajiv K. Singh  
Associate Professor of Materials  
Science and Engineering

I certify that I have read this study and that in my opinion it conforms to acceptable standards of scholarly presentation and is fully adequate, in scope and quality, as a dissertation for the degree of Doctor of Philosophy.

  
Timothy J. Anderson  
Professor of Chemical  
Engineering

This dissertation was submitted to the Graduate Faculty of the College of Engineering and to the Graduate School and was accepted as partial fulfillment of the requirements for the degree of Doctor of Philosophy.

May, 1997

  
Winfred M. Phillips  
Dean, College of Engineering

\_\_\_\_\_  
Karen A. Holbrook  
Dean, Graduate School